5-2018

Quantifying Aqueous Plutonium Using Hybrid Extractive Scintillation Resins

Amruta Balappa Pujari
Clemson University, apujari@g.clemson.edu

QUANTIFYING AQUEOUS PLUTONIUM USING HYBRID EXTRACTIVE SCINTILLATION RESINS

A Thesis
Presented to
the Graduate School of
Clemson University

In Partial Fulfillment
of the Requirements for the Degree
Master of Science
Environmental Engineering and Earth Sciences

---

by
Amruta Balappa Pujari
May 2018

Accepted by:
Dr. Timothy A. DeVol, Committee Chair
Dr. Brian A. Powell
Dr. Scott M. Husson

ABSTRACT

Hybrid extractive scintillating resins (HESR) were developed for uptake and detection of aqueous plutonium (Pu). These resins consist of titanium dioxide (TiO_2), which is responsible for Pu uptake, embedded in the scintillating resin. The scintillating resin emits light when excited by alpha radiation from plutonium which can be detected with a photomultiplier tube (PMT). Two main approaches were used for preparing these resins; first, incorporating inorganic compounds after polymerization: post-polymerization methods (HESR-I) and second, incorporating inorganic compounds before polymerization: pre-polymerization method (HESR-II). The physical characterization of HESR was done using thermogravimetric analysis (TGA), scanning electron microscopy (SEM) and energy-dispersive X-ray spectroscopy (EDX). Batch uptakes for aqueous plutonium-238 (+5 oxidation state) were performed. For a contact time of 1440 minutes, the highest fraction Pu sorbed was 0.71±0.10 with corresponding conditional K_D of 1×10^3 mL g^{-1} for HESR-II, containing 57% of TiO_2 by weight (HESR-II(57)), of the size 106-212 μm. The corresponding plutonium detection efficiency was 96%. Pseudo first-order rate model and pseudo second-order rate model were used for analyzing the kinetic data for sorption of Pu on HESR-II. Rate order was calculated as 1.5 with respect to plutonium concentration and overall rate constant was 2.4×10^9 mol^{-1} s^{-1} using pseudo second-order model. HESR-II(57) displays linear Pu detection response and a calculated minimum detectable concentration of Pu^{5+} is 0.38 Bq L^{-1} for batch cell setup. The hybrid extractive scintillating resins were developed for monitoring plutonium contamination in groundwater and surface water.

DEDICATION

To all the species that have gone extinct due to human exploitation and the ones yet to.

To all the species affected by 150 million metric tons of plastic in the oceans and the ones yet to.

To all the species starving and suffering due to diminishing polar ice and the ones yet to.

To all the species that were left homeless due to deforestation and the ones yet to.

To all the species that suffocated due to oil spills and the ones yet to.

To all the species that have experienced pain due to poaching, animal farming and human negligence and the ones yet to.

To all the humans around the world who are striving to make a difference for better and the ones yet to.

ACKNOWLEDGMENTS

I would like to thank Dr. Timothy A. DeVol for giving me this opportunity to be a part of this project. I would also like to acknowledge and thank my committee members Dr. Scott M. Husson and Dr. Brian A. Powell for their constant feedback and guidance. My deepest gratitude towards Dr. Seliman, Dr. Bliznyuk, Dr. Duval and William Fullmer for constant support throughout in and outside the laboratory. Many thanks to my dearest friends who constantly supported me during my stay at Clemson. I cannot thank my family enough for supporting me follow my dreams 9000 miles away from home. This work was supported by the Defense Threat Reduction Agency, Basic Research Award #HDTRA1-12-1-0012, to Clemson University.

TABLE OF CONTENTS

Page

Table of Contents (Continued)

Page

LIST OF TABLES

Table **Page**

List of Tables (Continued)

Table **Page**

LIST OF FIGURES

Figure **Page**

List of Figures (Continued)

Figure **Page**

List of Figures (Continued)

Figure **Page**

List of Figures (Continued)

Figure **Page**

List of Figures (Continued)

Figure **Page**

CHAPTER 1

INTRODUCTION

Ionizing radiation originates either from naturally occurring radionuclides in the environment or due to human activities. Plutonium-238 and ^{239}Pu are the most commonly occurring among 20 identified Pu isotopes in the environment (Keith, 2010). Plutonium-238 ($t_{1/2}$ = 87.7 years, specific activity= 6.3×10^{11} Bq/g) was first synthesized in 1940 by bombarding uranium-238 (^{238}U) with deuterons (Silva & Nitsche, 1995). Plutonium-239 ($t_{1/2}$ = 2.4 x 10^4 years, specific activity= 2.3×10^9 Bq/g) was first synthesized by bombarding ^{238}U with neutrons (Katz, 2006). Plutonium-239 is an attractive isotope for use in nuclear weapons because of fifty percent higher fission cross section compared to previously used nuclear fuel ^{235}U (Katz, 2006). Plutonium-238 is not feasible for nuclear weapons due to high heat output (Silva & Nitsche, 1995). Plutonium-238 is a major source of power in satellites and spacecrafts as the decay heat corresponds to 560 watts/kg and neutron generation value of 2600 neutrons/g-sec (Silva & Nitsche, 1995).

The global stockpile of separated Pu was 505 MT as of 2014 (Mian & Glaser, 2015). A major proportion of this stockpile was created in civilian programs and less than fifty percent of the accounted stockpile was produced for nuclear weapons. There exists 130,000 weapon-equivalents of separated Pu stockpile globally (Mian & Glaser, 2015). One weapon-equivalent corresponds to 3 kg of weapons-grade Pu or 5 kg of reactor-grade Pu (Mian & Glaser, 2015). **Figure 1.1** shows the global stockpile of separated Pu. The amount of separated Pu has increased since the end of the cold war. Countries such as

Pakistan and India are still producing weapons-grade Pu that has resulted in an overall increase in Pu stockpile (Mian & Glaser, 2015).

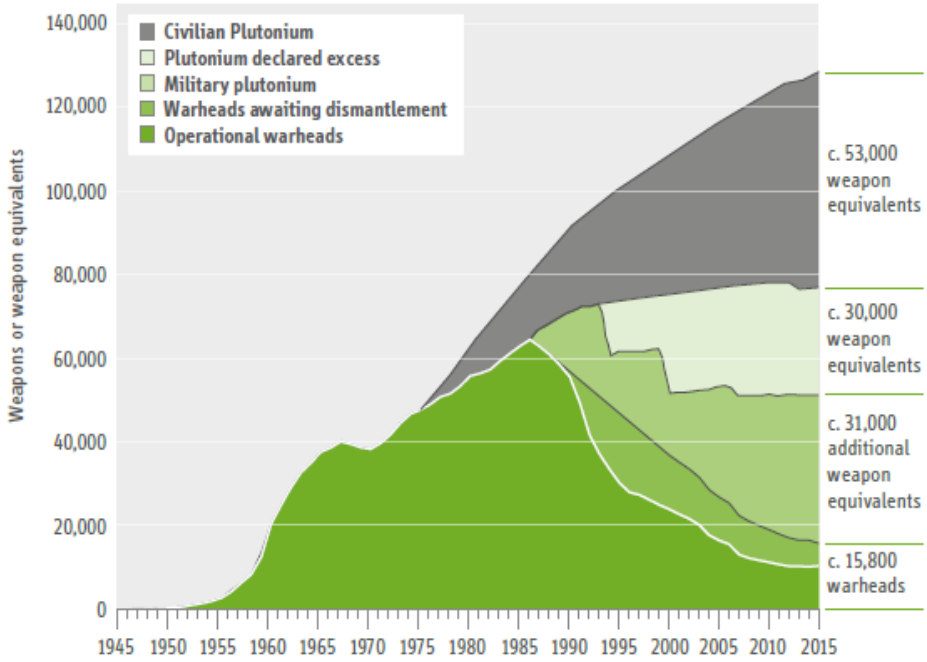

Figure 1.1. *Global separated plutonium stockpile* (Mian & Glaser, 2015)
Reprinted with the permission from Creative Commons

Figure 1.2 shows the separated Pu stockpile in different nations until the end of 2014. There is an uncertainty on the order of 10-30% in the military stockpile declared by Russia, Pakistan, Israel, India, China, and France. The United States and Russia have the largest stockpiles of weapons-grade Pu. Russia, United Kingdom, and France have the largest amount of reactor grade Pu. The United States currently owns 30.8 MT of excess weapons-grade Pu. The mixed oxide (MOX) facility that was planned to be constructed in Savannah River site, would be producing the MOX fuel from the present excess Pu to power nuclear reactors for power generation. The construction is currently halted (Mian &

Glaser, 2015). United States Waste Isolation Pilot Plant (WIPP), which is in the state of New Mexico, holds an estimate of 4.1 MT of Pu (Mian & Glaser, 2015).

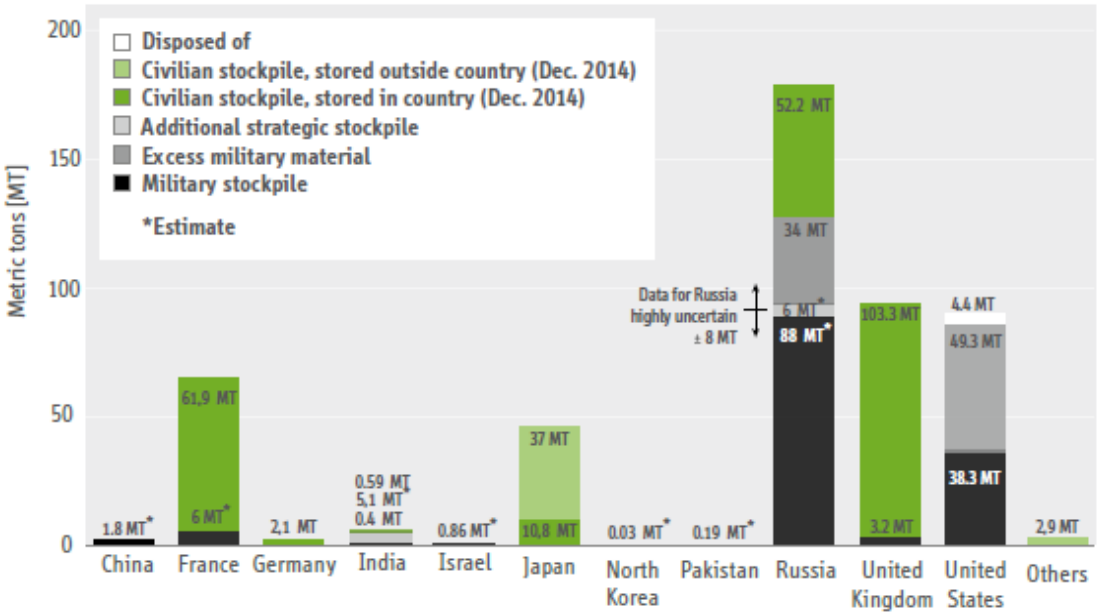

Figure 1.2. *Global separated plutonium stockpile in major countries* (Mian & Glaser, 2015) *Reprinted with permission from Creative Commons*

Environmental Protection Agency (EPA) currently regulates the National Priorities List (NPL) sites and rigorous cleanup activities have been emphasized. Agency for Toxic Substances and Disease Registry, in the year 2010, reported plutonium contamination in 16 NPL sites (Keith, 2010). There has been no recent update in the information of Pu contamination in NPL sites. Plutonium isotopes can be released into the environment from nuclear weapons testing, disposal of nuclear waste, accidents or nuclear weapons production facilities (Keith, 2010). About 500 million gallons of highly radioactive and toxic waste was generated during recovery of Pu through chemically processing uranium (Crowley & Ahearne, 2002). There was an additional 450 billion gallons of process liquid

created accompanying Pu recovery (Crowley & Ahearne, 2002). U.S. Department of Energy reports contaminated solid waste of 76000 cubic meters contaminated with Pu and another 1.2 million cubic meters of buried low-level solid waste at Hanford site (Crowley & Ahearne, 2002).

Plutonium fallout due to weapon testing, waste disposal, the release of effluent and accidents have resulted in the introduction of Pu into natural waters (Mahara & Kudo, 1995). In 1969, due to the failure in a waste transfer line, there was a release of 300 Ci (1×10^{13} Bq) ^{238}Pu at Mound Plant, Ohio (Hanson, 1980). The plant has discharged 0.5 Ci (2×10^{10} Bq) activity of ^{238}Pu into the river that is located near the plant site since its installation (Keith, 2010). In 1964, a satellite that was powered by a ^{238}Pu radioisotope thermoelectric generators (RTGs) failed during the rocket launch. The satellite contained 17 kilocuries of ^{238}Pu, amounting to 12.3 kg (Krey, 1967). About eighty-eight percent of this total inventory was accounted after tracking the Pu in the stratosphere. Twenty percent of this accounted inventory was documented to have been transported into the Northern Hemisphere and the residual eighty percent exists in the Southern Hemisphere (Krey, 1967).

The decay rate per unit mass of ^{238}Pu is much higher than other Pu isotopes and corresponds to higher disintegration for the given mass of the isotope. The higher specific activity of ^{238}Pu causes higher biological damage for the same amount of Pu uptake via a specific exposure pathway (Keith, 2010). If ingested, Pu which penetrates the intestine wall accumulates in bones and liver (Goldman et al., 1991).

Plutonium, when released in aqueous environments, can react through four major processes: colloid formation, complexation, precipitation and sorption (Silva & Nitsche, 1995). In most of the cases, radioactive contaminants are dispersed over a large area and trace concentration is present in the environment posing a threat to living organisms. The maximum contaminant level (MCL) with respect to gross alpha-emitting radionuclides set by the United States Environmental Protection Agency for drinking water is 0.56 Bq/L (EPA, 2000). Hence, sophisticated detection techniques are required to identify aqueous Pu contamination.

This research study aims at synthesis and characterization of hybrid extractive scintillating resin for simultaneous extraction of aqueous Pu(V) and its detection using scintillation technique. A novel method where titanium dioxide embedded in organic polymer matrix was used as Pu sorbent from aqueous solutions and Pu detection was accomplished using scintillation method. The main objective of this research was to develop resin for inexpensive and portable Pu sensor that could be utilized for environmental monitoring of Pu contamination in natural waters.

CHAPTER 2

BACKGROUND

2.1 Origin of plutonium

Natural fission reactions in the uranium deposits at Oklo and Bagombe mines produced Pu because of neutron capture by isotopes of uranium (Gauthier et al., 1996). An estimated 2.5 MT of Pu was produced in these deposits that eventually has decayed over the past 2 billion years (Cowan, 1976). Only very minute traces of naturally produced Pu are present in the environment today. Most of the Pu that exists in the environment today is due to human activities.

Plutonium, named after the planet Pluto, was synthesized for the first time at University of California Berkeley by Glenn Seaborg, Edwin McMillian, Joseph Kennedy, and Arthur Wahl in 1940/41 (Katz, 2006). Manhattan Project started in 1942 was the beginning of manmade Pu production on a large scale. Plutonium-239 is the primary Pu isotope used in nuclear weapons. Plutonium-239 was synthesized from neutron capture process of ^{238}U producing ^{239}U. Uranium-239 rapidly undergoes beta decay into ^{239}Np that further beta decays into ^{239}Pu (Crowley & Ahearne, 2002). While ^{239}Pu was used in nuclear weapons, ^{238}Pu was utilized in powering the satellite's RTGs for space mission by NASA (Goldman et al., 1991) (Rinehart, 2001). The radioactive decay from plutonium-238 is converted to electricity keeping the satellite functional in space. These are considered extremely reliable when solar power can no longer be harnessed by the satellite as it moves into outer space. **Figure 2.1** depicts the major Pu formation pathways. (n, γ) denotes a

neutron adsorption process and (β^-) denotes a beta decay process. The shaded boxes depict significant isotopes undergoing neutron-induced fission.

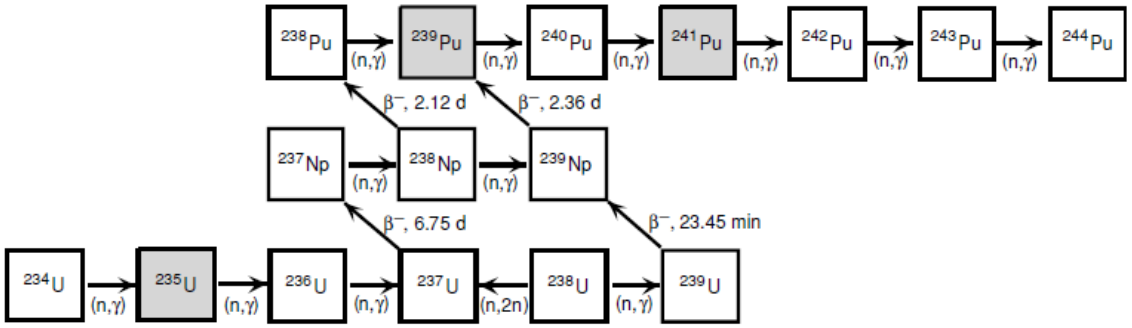

Figure 2.1. *Pathways for formation of plutonium* (Katz, 2006)
Reprinted with the permission of Springer Nature

Hanford site in Washington and Savannah River site in South Carolina were the sources of Pu while Oak Ridge site in Tennessee was the source of enriched uranium for manufacturing nuclear weapons (Crowley & Ahearne, 2002). There existed three reactors and two plants for chemical processing to manufacture Pu at Hanford during World War II. Due to the growing demands for Pu, six nuclear reactors and three plants for chemical processing were built at Hanford with an addition of two processing plants and five nuclear reactors at Savannah River site after the war (Crowley & Ahearne, 2002). From the total of 45 years of radioisotope production in the United States, an estimate of 103 MT of weapons-grade Pu was documented in both Savannah River site and Hanford site where Pu was formerly produced (Crowley & Ahearne, 2002). An estimate of 67 MT of Pu was synthesized from 97000 MT of uranium at Hanford site.

2.2 Physicochemical properties of plutonium

Plutonium has an outer electronic configuration of $[Rn]7s^25f^6$ with melting and boiling point of 640 °C and 3228 °C, respectively (Katz, 2006). The early research of Pu identified two of its phases: α and β. α phase at ambient temperature is brittle with a density of 20 g/cc and β phase is a high-temperature soft phase with a density of 16 g/cc. With time, other phases were identified: γ, δ and ε. **Figure 2.2** gives the detailed analysis of the transition of the pure Pu properties along with the phases as a function of temperature (Mitchell et al., 2004). As shown in the figure the electrical resistivity, an intrinsic property of the given substance to resist current flow, of α phase Pu increases substantially between -240 to -200 ºC and then decreases steadily until it reaches 100 ºC. The electrical resistivity drops at 100 ºC during the transition into β phase and stays closely constant through γ phase up to 300 ºC. While transition into δ phase the resistivity drops suddenly followed by constant trend up to 440 ºC and then gradually increases with the transition into ε phase. Tensile strength, tendency to resist breakage under tension, shows an overall decrease through the phases with an increase in temperature. Dilation, the difference in the volume per unit volume, showed an overall increase with a sudden

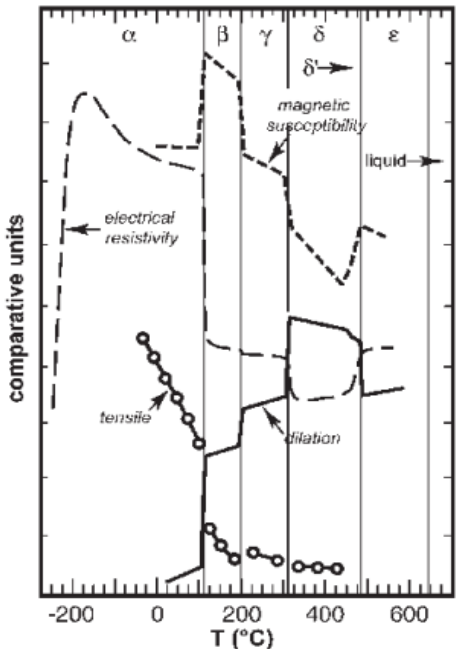

Figure 2.2. *Properties of Pu and phase transition as a function of temperature* (Mitchell et al., 2004)

Reprinted with the permission of Surface Science Reports.

increase at 100 ºC. After the sudden increase in dilation at 300 ºC there exists an overall decrease until 500 ºC.

Plutonium has twenty radioactive isotopes varying from mass number 228 to 247 that have been characterized (Katz, 2006). A few of the major isotopes are summarized in **Table 2.1**.

Table 2.1. *Major plutonium isotopes and associated properties* (Katz, 2006)

Isotope	Half-life	Decay method	Production method
^{238}Pu	87.7 yr	α	^{238}U
^{239}Pu	2.411×10^4 yr	α	^{239}Np daughter
^{240}Pu	6.561×10^3 yr	α	multiple and capture
^{241}Pu	14.35 yr	β > 99.99% α $2.45\text{x}10^{-3}$ %	multiple and capture
^{242}Pu	3.75×10^5 yr	α	multiple and capture

Chemistry of Pu in aqueous solution is very complex and unique. Plutonium in aqueous solution exists either in +3, +4, +5 or +6 oxidation states which can also simultaneously exist in groundwater because of the very close redox potential, of 1 volts, and the kinetics associated with rapid interconversion (Katz, 2006). In surface water systems with pH higher than 6.5 and a positive activity of electrons (Eh), +4, +5 and +6 states are common. In highly acidic and non-complexing environment, Pu in +3 and +4 states exist in the hydrated form as $Pu^{3+}_{(aq)}$ and $Pu^{4+}_{(aq)}$, respectively. Plutonium in +5 and +6 states has an enormous positive charge associated with the cation and form $PuO^{+}_{2(aq)}$ and $PuO^{2+}_{2(aq)}$ ions, respectively. Heptavalent Pu is unstable in an acidic environment and in alkaline conditions it forms $PuO_4(OH)^{3-}_{2(aq)}$ by forming coordination with hydroxide

ions (Katz, 2006). The Pu undergoes hydrolysis in the following order: $Pu^{4+}_{(aq)}$ > $PuO^{2+}_{2(aq)} \approx Pu^{3+}_{(aq)} > PuO^{+}_{2(aq)}$. Higher the ion charge/size ratio higher is the tendency for ions to readily hydrolyze. Pu(V) only hydrolyzes in basic pH. Pu(V) disproportionates into Pu(IV) and Pu(IV) states. Sometimes under special conditions, it forms into Pu(III) state. These disproportionation reactions in moderate acidic environments are not considered very favorable (Katz, 2006). The overall disproportionation reaction is given by **Equation 2.1**,

$$2PuO_2^+ + 4H^+ \leftrightarrow Pu^{4+}\ PuO_2^{2+} + 2H_2O \qquad \textit{Equation 2.1}$$

Plutonium readily forms complexes with organic ligands such as fulvate, formate, citrate, acetate, humate, lactate, oxalate and tartrate, and with inorganic ligands such as carbonate, chloride, hydroxyl, nitrate, sulfate, bromide and fluoride (Crane et al., 2015). **Figure 2.3** display the Eh-pH relationship of different oxidation states of Pu (Ewing, 2015).

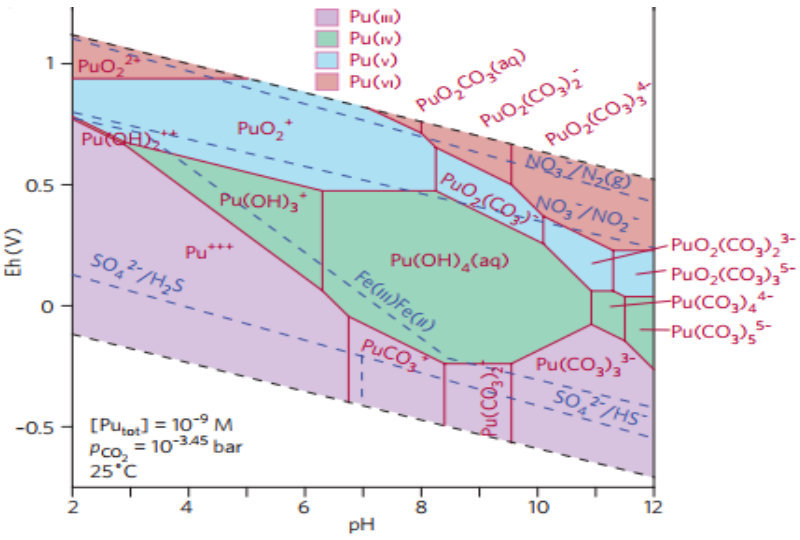

Figure 2.3. *Speciation of plutonium* (Ewing, 2015)

Reprinted with the permission of Springer Nature

2.3 Plutonium uptake studies

The oxidation state of Pu reduces from +5 to +4 when sorbed to a surface depending on solution Eh and pH values (Marsac et al., 2015). This reduction mechanism has been explained by: (1) Disproportionation of Pu(V) species resulting in reduction, (2) occurrence of trace reductants in the form of impurities on the surface, (3) reduction due to radiolysis by particles, or (4) electron shuttering process (Zavarin et al., 2012). Sorption of Pu(IV) is studied to be thermodynamically more favorable than Pu(V) which is proposed as the driving force of the reduction. Zavarin et al. in their study concluded that the slow uptake for of Pu(V) on calcite surface was due to the slow surface-mediated reduction of sorbed Pu(V) to Pu(IV). Hence, the rate controlling step for adsorption was the surface-mediated reduction (Zavarin et al., 2005).

<u>Pu sorption to montmorillonite</u>

Pu(V) sorption studies on montmorillonite were performed by (Begg et al., 2013). The concentration of Pu ranging from 10^{-6} to 10^{-16} M was measured by different analytical techniques such as liquid scintillation counting, accelerator mass spectrometry, and mass spectrometry. It was observed that 80% to 95% of Pu(IV) was sorbed to montmorillonite in the duration of one hour. Sorption of Pu(V), in contrast, was

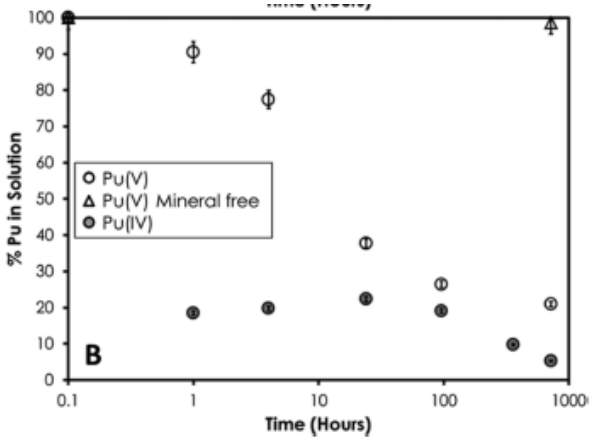

Figure 2.4. *Sorption of Pu(IV) and Pu(V) on montmorillonite* (Begg et al., 2013)

Reprinted with the permission of American Chemical Society

observed to be initially slow with 10% to 15% of Pu sorbed in first one hour as depicted in **Figure 2.4**, where the initial Pu concentration was 10^{-9} M. This trend of faster initial uptake of Pu(IV) and slower uptake of Pu(V) has been noticed on other minerals such as goethite and calcite (Keeney-Kennicutt et al., 1985). The slower uptake trend of Pu(V) was explained by the slower reduction rate to Pu(IV) on the mineral surface. K_D values for Pu(V) uptake by montmorillonite ranged from 1970 mL/g to 6700 mL/g.

Pu sorption to goethite

Pu(IV) and Pu(V) sorption studies were performed using goethite at pH varying from 2 to 10 (Sanchez et al., 1985). It was observed that Pu(IV) had much faster sorption to the goethite surface than Pu(V). While Pu(IV) reached equilibrium within a duration of one hour, Pu(V) did not reach equilibrium even after the contact duration of 20 days. Sorption of Pu(IV) was noted to be optimum in the pH range of 3 to 5 but for Pu(V) the range lies between 5 to 7. There is an expected shift in adsorption edge for Pu(V) at higher contact duration because of the gradual reduction of Pu(V) to Pu(IV) on the surface of goethite. It was seen that Pu(V) state is stable in aqueous solution and remains in the same oxidation state but behaved differently once sorbed to goethite surface which was explained by radiolysis or disproportionation reaction. It was proposed that Pu(V), when sorbed to the surface of goethite, was reduced slowly by water to +4 state. The slow initial adsorption of Pu(V) was explained by the relatively low hydrolysis tendency. Further sorption measurement of both these Pu oxidation states in the presence of high carbonate concentration showed a reduction in Pu sorption to the surface of goethite. It was shown with the increase in alkalinity above 3000 mg/L would result in the formation of Pu-CO_3

complexes resulting in a decrease of Pu sorption to the mineral. K_D values or associated details to calculate K_D were not reported.

Plutonium sorption to titanium dioxide

Phases of titanium dioxide are rutile, anatase, brookite, and cotunnite. Rutile and anatase are tetragonal systems while brookite is a rhombohedral system. The densities of rutile and anatase are 4.24×10^6 g/m^3 and 3.83×10^6 g/m^3, respectively (Diebold, 2003). Cotunnite is synthesized at high pressures (Diebold, 2003). The small black balls in **Figure 2.5** represent titanium atoms in the lattice and larger white balls represent oxygen atoms. TiO_2 is known to oxidize the metals sorbed to its surface. The behavior of plutonium on titanium surface is still not known completely but all the oxidation states are assumed to be converted to +4 (Diebold, 2003).

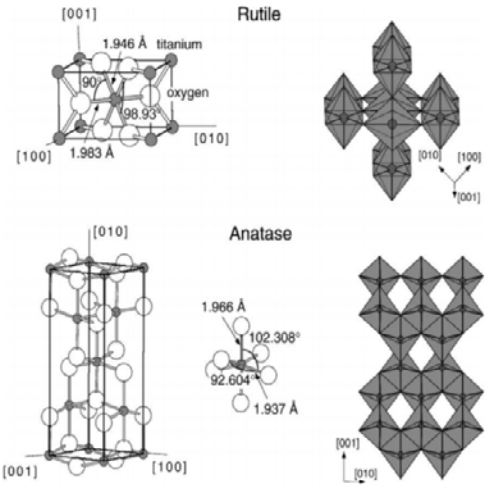

Figure 2.5. *Rutile and Anatase phase diagrams* (Diebold, 2003). *Reprinted with the permission of Elsevier*

TiO_2 acts as a photocatalyst and the sorption of Pu(V) and Pu(VI) on anatase surface differs in the presence and absence of light. Plutonium uptake efficiency at 24 hours contact duration was 10% and 70% with absence and presence of light, respectively, at pH 4.1. The Pu sorption to the anatase surface is confirmed using Fourier transform infrared spectroscopy (FTIR) (Romanchuk et al., 2016).

Studies have been done on titania microspheres prepared by the sol-gel process for application in inorganic ion-exchangers (Pius et al., 2004). Plutonium uptake

measurements were done using Pu(IV) stock solution in bicarbonate medium. Titania microsphere of size 1-2 μm and surface area of 148 m^2/g were used as the sorbent. These beads were synthesized using internal gelation process at 85 ºC. Slow exchange reaction for larger particles was noticed with distribution ratio (D) studies performed on the beads as shown in **Figure 2.6**. The value of D (mL/g) is the ratio of Pu per gram of sorbent to Pu per mL of aqueous solution. The kinetics was noted to be slow after initial fast sorption. It was also noticed that with an increase in pH from 8.6 to 11 there was an increase in distribution ratio from 570 mL/g to 1370 mL/g, respectively.

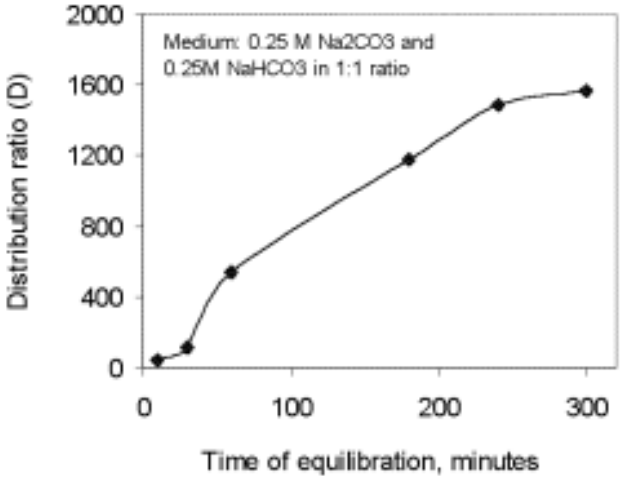

Figure 2.6*. Distribution ratio (mL/g) of Pu(IV) for titania microspheres.* (Pius et al., 2004). *Reprinted with the permission of Springer Nature*

Halloysites

Halloysites have a nanoscale tubular structure resulting in high adsorption capacity for certain substances. It is a dioctahedral kaoline clay mineral, with each layer separated by a monolayer of water molecules: $Al_2(OH)_4Si_2O_5 \cdot nH_2O$. The coaxial tubular structure of halloysites can be explained by the existence of the mismatched larger tetrahedral and comparatively smaller octahedral sheets at the atomic scale. The octahedral and tetrahedral sheets share oxygen of the tetrahedron and the Al-O bond in the octahedron constrains the shared oxygen that induces stress in the system causing the tubular coaxial structure as shown in **Figure 2.7** (Yuan et al., 2015). Studies have been conducted for uranium sorption

to halloysites; the highest K_D value reported was 200 mL/g at pH 3 (Kilislioglu & Bilgin, 2002).

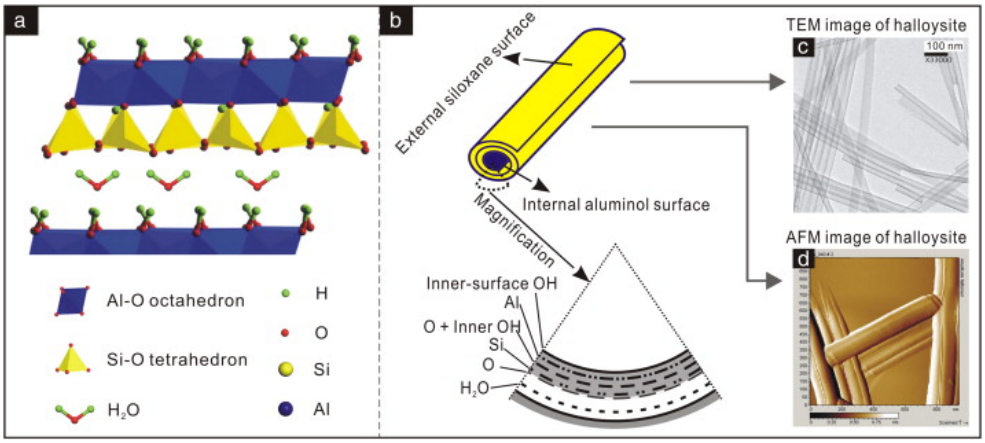

Figure 2.7. *Structure of halloysite* (Yuan et al., 2015) *Reprinted with the permission of* Elsevier

Plutonium uptake on various sorbents is shown in **Table 2.2**.

Table 2.2. *Uptake of plutonium by different sorbents*

Sorbent	**Uptake Pu concentration (M)**	**pH**	**K_D (mL/g)**	**Reference**
Manganese dioxide	Pu(IV) 5.9×10^{-5}	4	$\sim 10^4$	(Bhagyashree et al., 2013)
Bentonite	Pu(V) 1×10^{-10}	8	2.6×10^4	(Begg et al., 2014)
Hematite	Pu(VI) 3.63×10^{-9} Pu(IV) 9.51×10^{-10}	6.3 7.0	1.01×10^5 5.94×10^4	(Li & Kaplan, 2012)
Hematite	Pu(V) 1.5×10^{-8} Pu(V) 1.5×10^{-8}	3 8	3.6×10^1 1.17×10^5	(Powell et al., 2005)
Goethite	Pu(V) 1.5×10^{-8}	5 6.5 8	8.14×10^3 5.39×10^4 1.65×10^5	
Magnetite	Pu(V) 1.5×10^{-8}	3 5 8	5.25×10^2 2.95×10^4 2.54×10^5	(Powell et al., 2004)
Titanium dioxide	Pu(VI) 4×10^{-6}	7	1×10^5	(Olsson et al., 2003)

2.4 Polymeric resins

2.4.1 Extractive chromatographic resins

Extractive chromatographic resins have the attributes of liquid-liquid extraction methods and the handling ease of ion exchange resins making them very attractive to extract plutonium from aqueous solution. Some of the examples of extractive chromatographic resin are TEVA resin (Eichrom Technologies, Inc.) (Liu et al., 2015).

BenzoDODA encapsulated polymeric beads

BenzoDODA was produced by the condensation reaction of N,N-bis-(2-ethylhexyl)-2-chloroacetamide and 1,2-dihydroxybenzene. BenzoDODA was added to polyether sulfone solution and this resulting mixture was dropwise added to the aqueous bath to obtain BenzoDODA encapsulated porous PES beads (BEPBs) (Singh et al., 2015). Uptake studies were done using ^{239}Pu (>93%) in +4 oxidation state at different pH as shown in **Figure 2.8**. Pu sorption to BEPBs increases with the decrease in pH. Highest Pu sorption was observed at 6 M HNO_3.

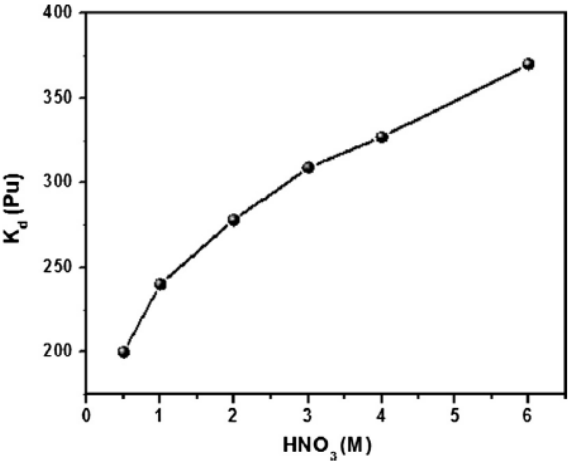

Figure 2.8. *Sorption of Pu(IV) on BEPBs at varying pH* (Singh et al., 2015)

Reprinted with the permission of Elsevier

The sorption trend of Pu to BEPBs with time is shown in **Figure 2.9**. The system reaches equilibrium with the contact duration of 100 minutes (mins). The quantity of Pu sorbed to BEPBs at equilibrium (q_e, µg/g) was calculated by **Equation 2.2**.

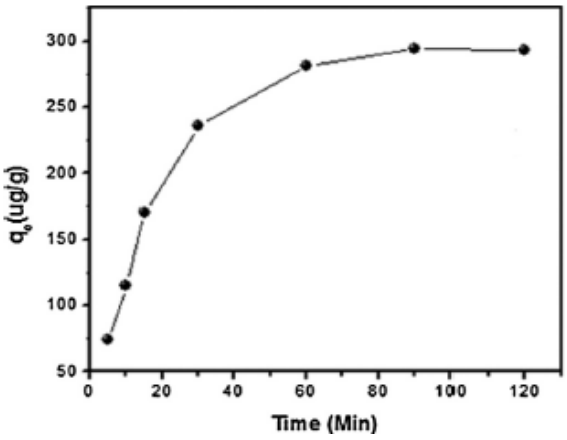

Figure 2.9. *Sorption of Pu(IV) to BEPBs with time* (Singh et al., 2015) *Reprinted with the permission of Elsevier*

$$q_e = \frac{V}{W} \times (C_o - C_e) \qquad \textit{Equation 2.2}$$

where V is the volume of the aqueous solution in mL, W is the weight of BEPBs in g, C_o and C_e are the initial and the equilibrium Pu concentration in solution, respectively, in µg/mL.

Pseudo first-order and pseudo second-order reactions were considered for fitting the experimental Pu sorption data. Lagergren's pseudo first-order model was used to fit the experimental sorption data using **Equation 2.3**.

$$\frac{dq}{dt} = k_1(q_e - q_t) \qquad \textit{Equation 2.3}$$

where q_t is the quantity of Pu sorbed to BEPBs (µg/g) at at time t and k_1 is the pseudo first-order rate constant, min^{-1}. Solving the above rate equation gives **Equation 2.4**. **Figure 2.10a** plots $\log(q_e\text{-}q_t)$ versus t.

$$\log(q_e - q_t) = log q_e - \frac{k_1}{2.303} t \qquad \textit{Equation 2.4}$$

Pseudo second-order model was given by **Equation 2.5**, where k_2 is pseudo second-order rate constant. The solution of **Equation 2.5** form is given by **Equation 2.6**. Plot of t/q_t versus t is given in **Figure 2.10b**.

$$\frac{dq}{dt} = k_2(q_e - q_t)^2 \qquad \textit{Equation 2.5}$$

$$\frac{t}{q_t} = \frac{1}{k_2 q_e^2} + \frac{1}{q_e} t \qquad \textit{Equation 2.6}$$

The kinetic study showed Pu sorption to these beads can be better explained by pesudo-second-order rate reaction as shown in **Figure 2.10** with correlation coefficient, R^2, of 0.9824 (Singh et al., 2015).

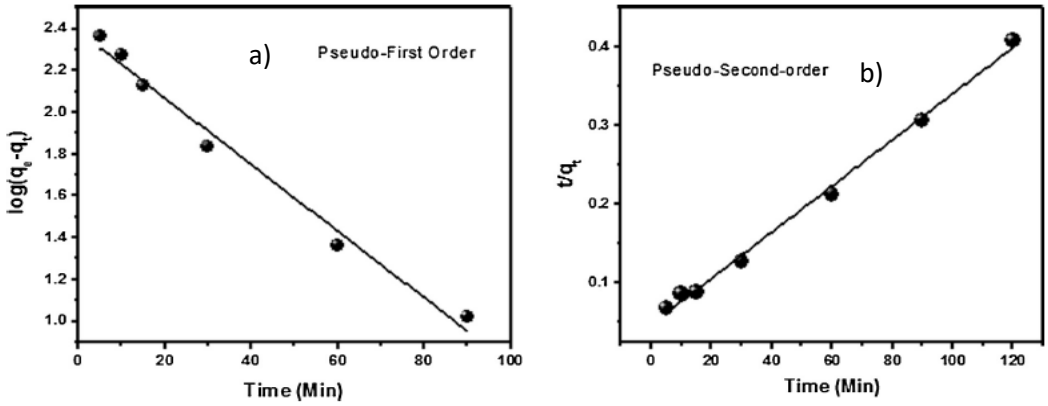

Figure 2.10. *a) Pseudo first-order plot with k_1 0.0366 (min^{-1}), b) pseudo second-order plot with k_2 1.78 (g μg^{-1} min^{-1}) for Pu sorption* (Singh et al., 2015)
Reprinted with the permission of Elsevier

TEVA resins

Liu et al. (2015) performed tetravalent plutonium uptake studies using vacuum box micro chromatography setup in acidic conditions. The box system consisted of 12 Eichrom TEVA resin columns. The columns were of 5 mm diameter and 70 mm in length which were filled with 0.70 g of TEVA extractive resin. The analysis involved conditioning the

column with 10 mL water and 10 mL of 9 M hydrochloric acid at 2 mL/min flow rate. The Pu(IV) solution in 9 M HCl media was transferred to the column at the rate of 1.5 mL/min. Plutonium yield varied from 70% to 98% depending on the sample specification (Liu et al., 2015). The resin displays high plutonium uptake in acidic conditions of 9 M hydrochloric acid for tetravalent plutonium.

2.4.2 Extractive scintillating resin

Polymeric resins have been synthesized using various approaches like suspension polymerization, emulsion polymerization, dispersion polymerization, multistage, precipitation reaction and microfluidic polymerization (Gokmen & Prez, 2012). The pressure of the system, liquid viscosity, immiscibility, temperature and stir speed are crucial factors that affect the formation of the porous polymer resins via the suspension polymerization method. The spherical shape of the resins is due to the interfacial tension with the least ratio of surface to volume.

Suspension polymerization used for the synthesis of these poly(4-methylstyrene), a.k.a. poly(vinyl toluene) resins consists of two immiscible phases: dispersion (oil) phase and continuous (water) phase. It is a heterogeneous polymerization reaction where the dispersion phase consists of a monomer, cross-linker, porogen, fluorophore and a polymeric initiator (Bliznyuk et al., 2015). A monomer is the building block of the polymeric matrix in which each monomer polymerizes together to form a polymer. Vinyl toluene is the monomer mostly used in styrene-based resin. The porous polymeric resins based on pore size can be classified into micro-, meso- and macroporous. Microporous resins have pores that are smaller than 2 nm, mesoporous resins have a range of pores

varying from 2 nm to 50 nm and macroporous resins have >50 nm sized pores (Gokmen and Prez, 2012). Porogen is added to control the surface area and porosity of the resin. Toluene, Span-80, and water are few of the porogens used for the synthesis of polymer resins. Initiators are mostly soluble in the monomer and are responsible for initiating the polymerization reaction with facilitating the growth of a polymeric chain. Crosslinkers are used to link the polymeric chains to one other. Crosslinking increases mechanical properties of the polymer and controls the extent of porosity. Divinylbenzene is one such crosslinker used with styrene-based monomers. Emulsifier or surfactants molecules consists of a hydrophobic and a hydrophilic end (Gokmen and Prez, 2012). Fluor is responsible for the scintillation. One of such fluor material used in the following study is 2-(1-naphthyl)-4-vinyl-5-phenyloxazole (vNPO) that is synthesized by 2-naphthalen-1-yl-5-phenyl-1,3-oxazole (αNPO) as shown in **Figure 2.11**. Recently the polymeric resins, such as poly(vinyl toluene) resin, have been used for detecting ionization radiation (Bliznyuk et al., 2015). The polymer beads with radionuclide selective ligands are referred as the resin in the current report.

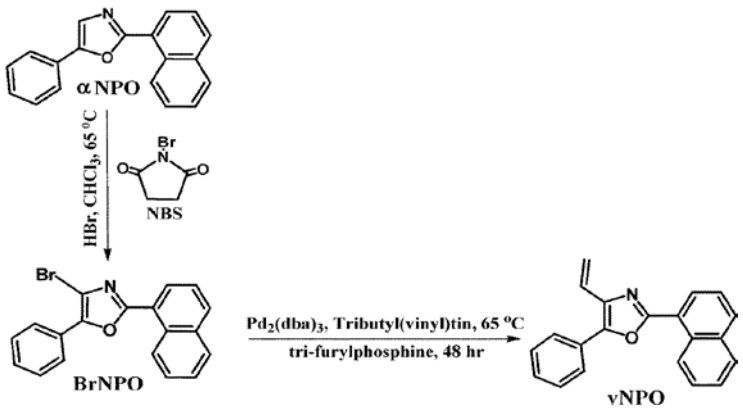

Figure 2.11. *Synthesis of 2-(1-naphthyl)-4-vinyl-5-phenyloxazole (vNPO)* (Seliman et al., 2015)

Reprinted with the permission of Royal Society of Chemistry

2.5 Plutonium radiation detection studies

2.5.1. Common techniques

Pu is an alpha emitter that can be detected using various techniques. One of the most basic techniques is using a zinc sulfide doped with silver scintillator coupled to a photomultiplier tube (PMT) system. It operates at a lower voltage compared to gas-flow proportional counters, which is an advantage (Cember, 2008). The disadvantage of a PMT is its fragile vacuum tube. Gas-flow proportional counters are also used for quantification of Pu. The alpha particles emitted result in gas ionization that is electrically amplified, and counts are measured. Gas handling can be one of the hindrances (Cember, 2008).

Liquid scintillation counting (LSC) is one of the more common methods to detect Pu. It measures the amount of radioactivity of the liquid sample by the rate of emitted photons and gives counting efficiency of nearly 100 %. Pu emits alpha particles of energy range 4 to 6 MeV and all this energy is transferred to the scintillation cocktail in a very short distance (Kessler, 1989). The monoenergetic alpha particles have a limitation of poor energy resolution that results in a broad pulse height spectrum. Pu ($^{239+240}$Pu) detection studies have been performed using TEVA resin columns in combination with LSC counter with α/β emission discriminate (Liu et al., 2015).

Pu detection is also done using alpha spectroscopy. A semiconductor detector used for alpha spectroscopy acts like a solid-state ionizing chamber. The advantages are their high energy resolution and relatively lower operating voltage when compared to other detectors (Kessler, 1989). The disadvantage of alpha spectroscopy is the time and effort to produce a good electroplated source.

2.5.3 Extractive scintillating resin integrated with flow cell detectors

Extractive scintillating resins are extractive chromatographic resins impregnated with a fluor resulting in a dual functionality media: concentration of radionuclides and radiation transducer. The organic polymer has a sorbent suspended throughout the matrix or coated on the surface. The sorbent can either be an organic ligand or inorganic material selective to the targeted radionuclides. The radionuclide accumulates on resins and its decay may result in deposition of energy in the matrix. This results in excitation of the matrix into a higher energy state that is transferred non-radiatively to fluor molecules present in the matrix. When these molecules de-excite they emit photons in the visible spectrum. This process is referred as scintillation. The emitted photons are counted using photomultiplier tube (Duval et al., 2016).

Flow cell detectors used in conjugation with extractive scintillating resins work on the principle of simultaneously concentrating and detecting the radionuclide. The setup consists of a small column filled with the resin placed in front of one or more PMTs as shown in **Figure 2.12**. The sensitivity of a PMT face decreases from the center to the edge causing fluctuations in the response of the detector are possible when using a small column. These detectors are used for real-time and on-line detection (Hughes & DeVol, 2006).

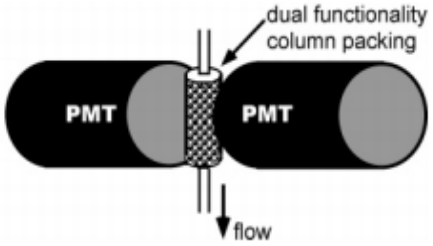

Figure 2.12. *Dual-functionality sensor for extraction and detection of radionuclide from aqueous solutions*

(Grate et al., 2008) *Reprinted with the permission of American Chemical Society*

CHAPTER 3

RESEARCH OBJECTIVE

Hypothesis**:** Hybrid extractive scintillating resin consisting of scintillating poly(vinyl toluene) (PVT) beads incorporated with inorganic compounds are suitable for extraction of plutonium from aqueous solution and detection using scintillation counting.

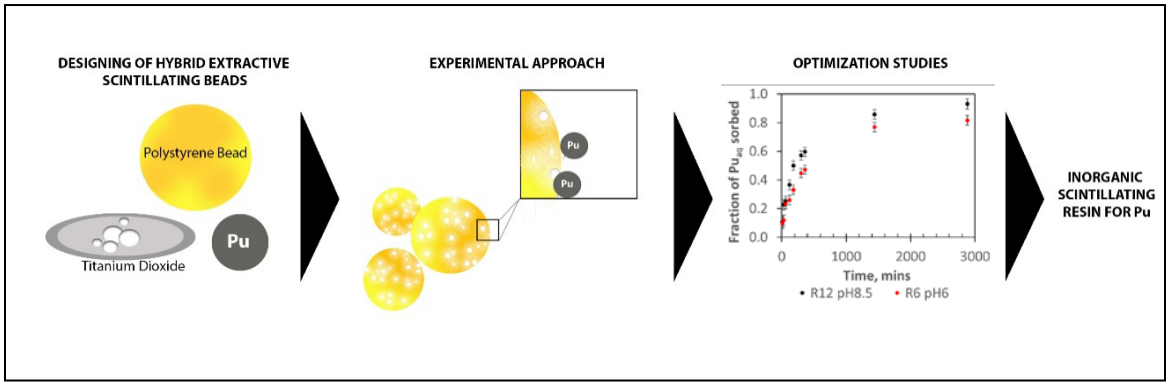

Figure 3.1. *Depiction of research objective*

Objectives: The following are the research objectives for quantification of aqueous plutonium using hybrid extractive scintillating resin.

1. **Synthesis of hybrid extractive scintillating resin (HESR)**

- Synthesis of poly(vinyl toluene) based resin using two techniques. The post-polymerization technique, HESR-I, consists of incorporating TiO_2 after the synthesis of beads using four methods: solvent aided adsorption (SAAd), heat aided adsorption (HAAd), and silane polymerization method (SiP). The pre-polymerization technique consists of incorporation of TiO_2 in monomer matrix and then synthesizing scintillating resin, HESR-II.

- Numerous factors were considered for the synthesis of HESR: the amount of TiO_2 in the resin matrix, choice of solvent and duration of the process.
- Physical characterization methods include use of thermogravimetric analysis (TGA) and transmission electron microscopy (TEM) to determine the incorporated inorganic material in the polymer matrix, scanning electron microscopy (SEM) imaging to determine surface morphology and energy-dispersive X-ray spectroscopy (EDX) to study the TiO_2 deposition on the surface.

2. Plutonium sorption and detection

- Pu sorption measurements using batch uptake experiments at different Pu concentrations.
- Pu detection efficiency determination using off-line measurement technique.

3. Optimization studies

- Perform pH studies to determine the trend in Pu(V) sorption with the change in pH and obtain optimum pH value for Pu(V) sorption to HESR.
- Perform kinetic studies to determine the rate of Pu(V) sorption to HESR.

CHAPTER 4

EXPERIMENTAL PLAN AND METHODOLOGY

4.1 Synthesis of hybrid extractive scintillating resin

Hybrid extractive scintillating resin comprises of two components: inorganic and organic. The inorganic component consists of a compound that is responsible for uptake of plutonium from the aqueous solution. The organic component constitutes the scintillating resin matrix in which the inorganic compound is embedded. Together these two compounds are responsible for plutonium extraction from the aqueous solution and its detection using scintillation technique.

4.1.1 Inorganic compound selection

Different grades and sizes of titanium dioxide was considered. Two phases of titanium dioxide (TiO_2); anatase (325 Mesh Powder, 45 Microns, Alfa Aesar) and rutile (1-3 nm size, PlasmaChem GmbH and 1.0-2.0 µm, Alfa Aesar).

4.1.2 Organic component synthesis: Suspension polymerization

The organic component of HESR constitutes the resin matrix with scintillating properties. The PVT beads were synthesized using the suspension polymerization process. The process involves two distinct immiscible phases: continuous phase (aqueous) and dispersion phase (organic).

Continuous phase was prepared by heating 300 mL distilled deionized (DDI) water up to 65°C. When the temperature stabilized, 0.3 g of poly(vinyl alcohol) (PVA, Sigma-Aldrich) was added and stirred at 400 rpm. PVA is polymer surfactant which aids monomer

droplets formulation during mixing. When PVA was completely dissolved, 0.3 g of hydroxypropyl methylcellulose (HPMC/methocel, Sigma-Aldrich) was added followed by 2.5 g sodium chloride (NaCl, Sigma-Aldrich). HPMC is a nucleating agent which acts as the core for the formulation of droplets. NaCl is used to control the ionic strength (Bliznyuk et al., 2015). The entire mixture was stirred at 400 rpm at 65°C until all the compounds completely dissolved. The mixture was cooled to room temperature.

Dispersion phase consists of the monomers, polymerization initiator, porogen and the crosslinker. Vinyl toluene (98% stabilized, Acros Organics), 4 mL, was used as the monomer. Azobisisobutyronitrile (AIBN, 98%, Sigma-Aldrich), 0.025 g, was added as the polymerization initiator followed by 0.11 g (3% by monomer weight) of αNPO or vNPO fluor. After this mixture was sonicated for 5 mins, 1.5 mL Span 80(VWR International) and 1 mL divinylbenzene (DVB, technical grade 8%, Sigma-Aldrich) were added. Span 80, the porogen, is non-ionic in nature and responsible for the formation of pores within the resin. DVB was used as the crosslinker. The mixture was again sonicated for 15 mins to form a homogenous solution.

The dispersed phase to continuous phase ratio used in the following experiments was to 1:10. Hence, the suspension used in the following experiments are considered as oil in water emulsion as the volume of the dispersed phase is greater than the volume of the continuous phase. **Figure 4.1** depicts the suspension polymerization process. From the bulk

of the continuous phase, 60 mL was transferred to three-necked round bottom flask. The flask was placed in the sand-bath to maintain a constant temperature. After the temperature reached a steady value of 60 °C, the homogenized dispersed phase, was added to the continuous phase using a pipette. The mixture was stirred at 380 rpm and the temperature was raised to 75 °C for 720 mins. A condensing column was attached to the three-necked flask and needles were placed through rubber stoppers to avoid pressure buildup. **Figure 4.2** shows the experimental apparatus setup for the synthesis of PVT beads.

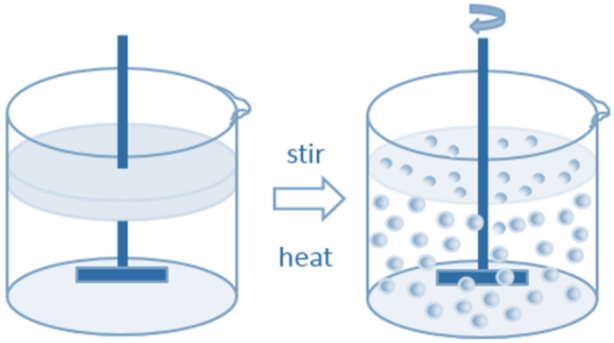

***Figure 4.1**. Suspension polymerization*

***Figure 4.2.** Suspension polymerization apparatus setup*

4.1.3 Hybrid extractive scintillating resin formulations

Two different approaches were taken to synthesize HESR. First, the inorganic compound was incorporated after suspension polymerization (post-polymerization type a.k.a HESR-I). Second, the inorganic compound was embedded in dispersed phase before suspension polymerization (pre-polymerization type a.k.a HESR-II).

4.1.3.a) Post-polymerization resin: HESR-I

HESR-I was synthesized using three different techniques:

i) Solvent aided adsorption (SAAd)

ii) Heat aided adsorption (HAAd)

iii) Silane polymerization method (SiP)

Solvent aided adsorption (SAAd)

Solvent aided adsorption method involves adsorption of TiO_2 particles on the already synthesized PVT beads in presence of a solvent as depicted in **Figure 4.3.** The PVT beads were synthesized using suspension polymerization process mentioned in **Section 4.1.2**. Synthesis of SAAd resins involved solvent selection based on its polarity. Poly(vinyl toluene) beads expand in the presence of medium to high polarity solvents like DMF. Three of the solvents used to swell the beads were: dimethylformamide (DMF) or chloroform. The TiO_2 dispersion stability in the solvent was crucial for uniform coating on PVT beads. Chloroform, DMF, and toluene were used to prepare TiO_2 suspension. DMF was the most suited solvent with high polarity and high TiO_2 dispersion stability. In a 20 mL glass vial, 0.25 g of PVT beads of size 106 µm- 212 µm was added followed by

5 mL of DMF and mixed for 1440 mins. A dispersion was prepared to consist 0.03 g TiO_2 (rutile, 1.0-2.0 µm, Alfa aesar) in 1.5 mL DMF mixture that was sonicated for 10 mins. This dispersion was then added to the vial containing the swollen PVT beads and sonicated for ~8 mins. The suspension of TiO_2 and PVT beads in DMF was then mixed using a rotary mixer for about 300 mins. The DMF was evaporated using rotary evaporator. Chloroform was added along with DMF in a rotary evaporator to form azeotropic solution mixture to reduce the boiling point. After the solvent was completely evaporated, the product was rinsed with distilled deionized (DDI) water and named SAAd(12) resin. The number in the parentheses, 12, represents weight percentage of TiO_2 on PVT beads. Similar nomenclature is used for other HESR-I configurations.

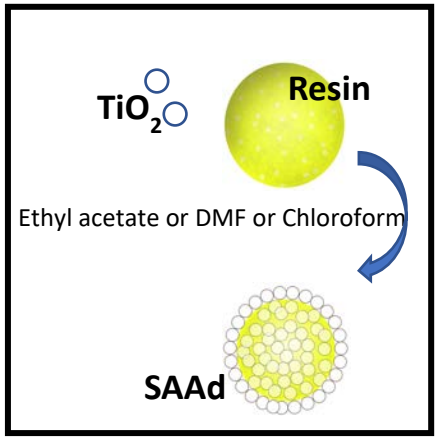

Figure 4.3. *SAAd mechanism*

The blank beads (or PVT beads), the beads with no TiO_2 coating, were subjected to different sonication time to study its effects on radioluminosity of the beads. The blank beads were subjected to all the steps of SAAd modification process except the addition of TiO_2. The sonication time varied from 0 mins to 15 mins.

Fluor coated SAAd(24) resins were synthesized by adding an extra amount of 0.008 g αNPO with 0.06 g TiO_2 to the already scintillating beads. All the remaining steps of SAAd modification process were the same. The additional fluor was added to overcome the possible interference with light output due to TiO_2 layers. It is not clear if the additional fluor just coats the beads or diffuses into the pores.

Heat aided adsorption (HAAd)

Heat aided adsorption method involves adsorption of TiO_2 particles on the already synthesized PVT beads in presence of heat. The PVT beads were synthesized using above mention suspension polymerization process as depicted in **Figure 4.4**. In a watch glass, 0.25 g of PVT beads of size 106 µm- 212 µm was added followed by 0.03 g TiO_2 (rutile, 1.0-2.0 µm, Alfa aesar) and mixed thoroughly. The glass transition temperature of PVT is between 93 °C and 118 °C depending on degree of crosslinking (Mark, 1999). The mixture was heated to 150 ºC for 120 mins. The mixture was then cooled a room temperature and rinsed with DDI water and named HAAd(12) resins. The procedure was followed for varying amount of TiO_2 similar to SAAd resins.

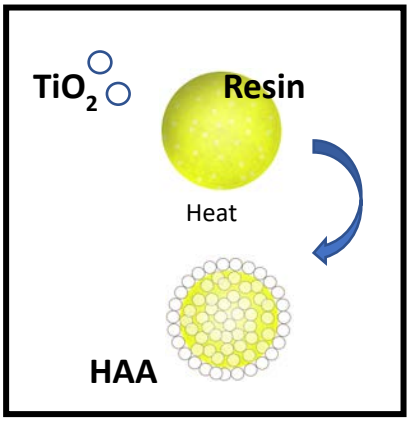

***Figure 4.4**. HAAd mechanism*

The blank beads were subjected to different temperatures to study its effects on radioluminosity of the beads. The blank beads were subjected to all the steps of HAAd modification process except the addition of TiO_2. The temperature varied from 50, 150 and 200 ºC.

Silane polymerization method (SiP)

SiP method involved the post-polymerization addition of silane function group, allylmethyldimethoxysilane, to attach TiO_2 particles to the scintillating resin surface as shown in **Figure 4.5**. TiO_2 particles (rutile, 1.0-2.0 µm, Alfa aesar) were functionalized with the silane functional group. About 0.4 g of TiO_2 was dispersed in a mixture of 5 mL

ethanol and 0.5 mL of DDI water in 20 mL scintillation vial. The vial was purged with nitrogen gas for 5 min and then transferred into the glovebox where 1 mL of allylmethyldimethoxysilane (97%, Sigma-Aldrich) was added. The mixture was stirred for 30 mins inside the glovebox at 36°C. Then the mixture was washed three times with ethanol.

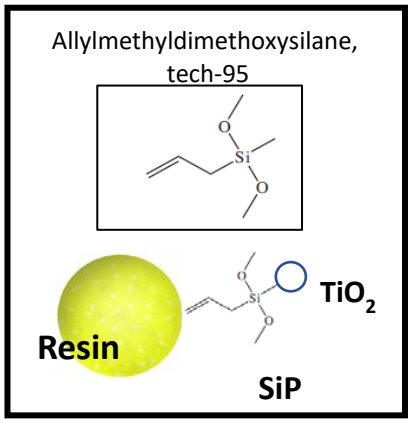

Figure 4.5. *SiP mechanism*

In a 20-mL glass vial, 0.25 g of PVT beads of size 106 µm- 212 µm was added followed by 5 mL of toluene. To this mixture, 0.06 g of the functionalized TiO_2 was added and stirred for 300 mins at room temperature. The product was then rinsed with DDI water.

4.1.3 b) Pre-polymerization resin: HESR-II

The pre-polymerized resins were synthesized using the procedure similar to that mentioned in **Section 4.1.2**. The additional step involved in the synthesis of HESR-II was the suspension of 0.15 g of TiO_2 (rutile, 1.0-2.0 µm, Alfa aesar) with vinyl toluene monomer. These TiO_2 particles were coated with 1.5 mL Span 80 porogen. This sample corresponded to HESR-II(4) where 4 stands for %TiO_2 by weight of monomer. A varying amount of TiO_2 from 4% to 57% by weight were synthesized. HESR-II was embedded with TiO_2 particles (1-2 µm) throughout the PVT matrix, unlike HESR-I which consisted of beads coated with TiO_2. After the resins were synthesized they were filtered through the Whatman™ 1454-110 Hardened Low Ash Grade 54 Quantitative Filter Paper (Diameter: 11cm, Pore Size: 22µm). The residual on the filter paper which was the final

polymerization product was rinsed using DDI water. The residue was dried at room temperature for two days.

HESR-II(73) was synthesized by reducing the amount of vinyl toluene monomer used in HESR-II(57) by half, from 4 mL to 2 mL and keeping all other reagents constant. This increased the cross-linking, amount of fluor and porosity twice by weight percent.

4.2 Characterization of hybrid extractive scintillating resin

HESR was characterized for quality control. The characterization studies were performed to understand: physical properties of the resins, Pu sorption, and detection.

Optical microscopy: Optical microscopy was performed using Celestron 44341 with the attached digital camera. The study was performed at 5x and 10x magnification. About 0.001 g of sample was loaded on the glass slides and placed under the lens. The particles were illuminated with UV light at 45º from the glass slide. The particles fluoresce in the presence of UV light due to embedded fluor particles in the resin matrix.

Scanning electron microscope: SEM was performed on HESR-I using Hitachi SU6600 to study surface morphology. A beam of electrons is used to generate detailed surface imaging. This technique was used to study the size distribution and the resin structure. The samples for SEM were prepared on a circular metal disc that was covered with adhesive tape. About 0.001 g of sample was evenly sprinkled on the adhesive surface and blow-dried to remove loosely attached particles. Focus ion beam (FIB) imaging studies were conducted using Hitachi NB5000 for SAAd resins.

X-ray dot mapping: This technique was used to study the distribution of elements in the sample. The SAAd resins were added in epoxy resin and after it was cured at 60 ºC in 2 hours, the resin surface was polished using 1000 mesh silicon carbide abrasives. X-ray dot mapping was performed by Hitachi 3400. The instrument collects the characteristic x-rays from the polished resin surface as a function of distance from the scanning probe. This was essentially used in understanding the overall composition of the resin at different cross-sections. Maps representing specific element are assigned a specific color.

Energy-dispersive X-ray spectroscopy: This spectroscopy method was used to determine the elemental analysis at a specific location in the sample. The sample surface was illuminated with a beam of high energy particles that excited the surface electrons from the sample. De-excitation of these electrons emits characteristics x rays that are used to determine the elemental composition of the sample. This technique was used in collaboration with other two characteristic techniques: Focus ion beam imaging and transmission electron microscopy.

Sieve analysis: The analysis was performed to determine the particle size distribution of HESR. Two different mesh size sieve plates were used to perform the distribution analysis: 212 and 106 µm. The sample was added to the 212-mesh size plate and sieved for 5 mins. The residual on plate constituted of particles that were bigger than 212 µm in diameter. The sieved product constituted of all the particles below 212 µm in diameter and these were sieved through 106-mesh size plate for 5 mins. The overall analysis generated three group size distribution of particles: particles greater than 212 µm in diameter, particles between 212 µm and 106 µm in diameter and particles below 106 µm in diameter.

4.3. Quantification of titanium dioxide

Titanium dioxide is responsible for plutonium uptake. The higher the amount of accessible TiO_2 in HESR, the greater the Pu uptake. To measure the amount of titanium dioxide in the HESR, TGA was performed using SDT Q-600 TA Instruments. The analysis was performed under nitrogen conditions with a gas flow rate of 10 mL/min. The temperature was ramped from room temperature to 850 °C at the rate of 30 °C/min. Isothermal was maintained for 5 min. The temperature is increased until the organic component of the resin decomposes leaving behind the inorganic TiO_2. As the decomposition point of TiO_2 is much higher than that of the PVT resin matrix it is a very precise method to determine the embedded TiO_2. Percent TiO_2 incorporated into the beads, by weight, was calculated using **Equation 4.1**. The total weight of the resin is given by the initial weight of the HESR loaded in alumina pan. The weight of titanium dioxide adsorbed/embedded on the resins is given by the weight of the residue in the alumina pan after the TGA analysis.

$$\%TiO_2\ imbedded = \frac{Weight\ of\ titanium\ dioxide\ in\ the\ \text{resins}}{Total\ weight\ of\ \text{resins}} \times 100 \qquad \textit{Equation 4.1}$$

4.4 Fraction plutonium sorbed

Vial selection studies were conducted to obtain least Pu wall sorption. Teflon, polycarbonate, polypropylene, and borosilicate glass vials were used in the study to account for wall sorption by conducting an activity balance on plutonium. After batch contact and final Pu activity measurement, the vials were emptied and gently rinsed with DDI water to remove any Pu solution droplets or resin particles. The vials were then filled with 5 mL of 1.5 M nitric acid solution to leach out the sorbed Pu(V) on the vial walls. The vials were washed with nitric acid for 24 hours using a rotary mixer. The activity of this washed solution was accounted as the Pu sorbed on the vial.

The resin utilized in the batch test was subsequently separated from the solution by centrifugation. The plutonium activity in the solution (~1 mL of aqueous Pu in 10 mL of scintillation cocktail: Ultimate Gold^{TM} AB) was counted in Perkin Elmer Quantulus 1220 LSC. The background count rate was subtracted from the gross count rate of the samples to obtain the net count rate. The overall mass balance is given by **Equation 4.2**,

$$Pu_{tot} = Pu_{aq} + Pu_{HESR} + Pu_{vial} \qquad \textit{Equation 4.2}$$

where Pu_{tot} is the amount of total Pu activity (Bq) used in a given experiment, Pu_{aq} is the Pu activity in aqueous solution at time t, Pu_{HESR} is the Pu adsorbed to the HESR (Bq) and Pu_{vial} is the Pu adsorbed on the vial walls (Bq). Fraction Pu adsorbed in case of Pu wall sorption is calculated by **Equation 4.3** and conditional distribution constant, conditional $K_{D,}$ is given by **Equation 4.4**,

$$Fraction\ Pu\ uptake = \frac{Pu_{tot} - (Pu_{aq} + Pu_{vial})}{Pu_{tot}} \qquad \textit{Equation 4.3}$$

$$K_D = \frac{Pu_{tot} - (Pu_{aq} + Pu_{vial})}{Pu_{aq}} \frac{V}{m} (\text{mL/g}) \qquad \textit{Equation 4.4}$$

where V is the total volume of solution used for uptake studies (mL), m is the mass of sorbent used for Pu uptake (g). The conditional K_D is calculated for the specific condition of 1440 minutes batch contact duration which is close to, but not at actual equilibrium. The error for the Pu sorption and detection were propagated from Pu counting statistics.

The quantity of Pu sorbed to the sorbent, q_t (mg/g), at a given time t, can be calculated by the **Equation 4.5**. It gives the measure of the amount of sorbate sorbed per unit mass of sorbent. $[Pu]_{tot}$ (mg/mL) is the initial concentration of Pu and $[Pu]_{aq}$ is its concentration at time t.

$$q_t = \frac{[Pu]_{tot} - [Pu]_{aq}}{m} \times V \qquad \textit{Equation 4.5}$$

4.5 Plutonium detection studies

4.5.1 Radioluminosity measurement using ^{241}Am point source

Radioluminosity spectrum provides a measure of light output from HESR. Experiments were performed using an Americium-241-point source with an activity of 37,000 Bq. About 0.04 g of sample was collected in a scintillation vial and was exposed to the ^{241}Am source from 0.5 cm from the sample as shown in **Figure 4.6**. The number of photons emitted is proportional to the amount of energy from the alpha particles deposited on HESR. Emitted photons are detected using Hidex Triathler liquid scintillation counter.

This is comparatively a faster method to check the scintillation properties of the resins by comparing the light output spectrum. But the measurements explained in **Section 4.5.2** is necessary to obtain actual Pu detection efficiency using HESR.

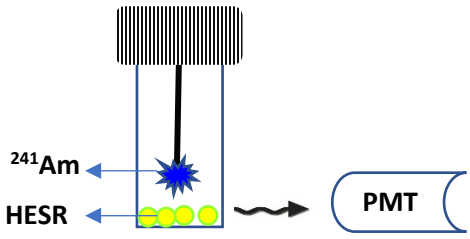

***Figure 4.6**. Radioluminosity measurement for HESR with ^{241}Am source*

4.5.2 Plutonium detection efficiency

The preliminary detection tests were performed using resins with αNPO and final tests with vNPO fluor. vNPO has a vinyl group attached to it which forms a chemical bond with the polymeric backbone of the resin reducing the probability of fluor leaching out of the resin as it is chemically bonded to it.

Plutonium detection efficiency of HESR was measured using column studies. Teflon column of 0.16 cm (1/16”) in diameter and 3 cm in length was used. The HESR, after the batch contact with aqueous Pu, was packed in the column. The batch contact gives the value of accumulated Pu on HESR (Bq) by activity balance calculations. The columns were dried at room temperature in dark to minimize photodegradation of the HESR. The plutonium accumulated in the column (cps) was measured using Perkin Elmer Quantulus 1220. The detection efficiency measurement procedure is depicted in **Figure 4.7** and is

explained in **Section 5.2.1** in detail. Hence, detection efficiency accounts for the sorbed Pu by measuring the light output from HESR given by **Equation 4.6**.

$$Detection\ efficiency = \frac{Net\ column\ count\ rate\ (cps)}{Accumulated\ Pu\ (Bq)} \times 100 \qquad Equation\ 4.6$$

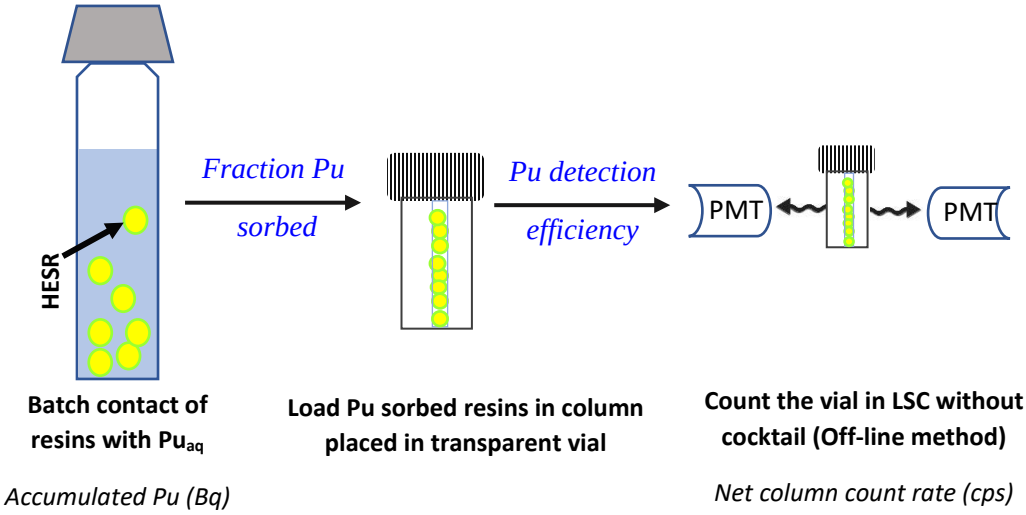

***Figure 4.7**. Detection efficiency measurement procedure for HESR with $^{238}Pu(V)$ source*

Minimum detectable concentration (MDC)

The minimum detectable concentration was calculated for batch cell setup using the **Equation 4.7** (Knoll, 2010).

$$MDC = \frac{2.71+4.65\sqrt{C_b t}}{tE_s E_d V}\ \text{Bq/mL} \qquad Equation\ 4.7$$

C_b is the background count rate, t is the count time, E_s is the sorption efficiency, E_d is the Pu detection efficiency, and V is the volume of the Pu solution.

4.6 Kinetic studies

After the preliminary experiments, kinetic studies were performed on HESR-II. Total of 12 different reactors were used: two different suspended solid concentration, three different Pu concentration of 45 mL volume were used at two different pH values. Kinetic studies were performed for each reactor at nine different time intervals. The summary is shown in **Table 4.1**. Polycarbonate vials, 120 mL, were used for the following study. Detection efficiency measurements were performed for all the 12 reactors at the end of 2880 mins. Isotherm was plotted for sorption data at 2880 mins. The sample label 1R(6-0.30) stands for the reactor 1 maintained at pH 6 and sorbate/sorbent ratio of 0.30. The remaining reactor labels also follow the same nomenclature format.

Table 4.1. *Kinetic study*

Reactors	pH	Calculated initial Pu Concentration (Bq/mL)	Suspended solids (mg)	Sorbate/sorbent Ratio (Bq/mg)
1R(6-0.30)	6	0.17	27	0.30
2R(6-0.04)	6	0.17	180	0.040
3R(6-1.00)	6	0.58	27	1.0
4R(6-0.15)	6	0.58	180	0.15
5R(6-3.20)	6	1.91	27	3.2
6R(6-0.50)	6	1.91	180	0.50
7R(8.5-0.30)	8.5	0.15	27	0.30
8R(8.5-0.04)	8.5	0.15	180	0.040
9R(8.5-1.00)	8.5	0.55	27	1.0
10R(8.5-0.15)	8.5	0.55	180	0.15
11R(8.5-3.20)	8.5	1.91	27	3.2
12R(8.5-0.50)	8.5	1.91	180	0.50

Two kinetic models were used to fit the experimental data:

1) Pseudo first-order model: The differential form of rate equation is given by **Equation 4.8** and its solution by **Equation 4.9**. k_1 is the pseudo first-order rate constant.

$$\frac{d[Pu]_{aq}}{dt} = -k_1[Pu]_{aq} \qquad \textit{Equation 4.8}$$

$$ln\frac{Pu_{aq}}{Pu_{tot}} = -k_1 t \qquad \textit{Equation 4.9}$$

2) Pseudo second-order-model: The differential form of rate equation is given by **Equation 4.10** and its solution by **Equation 4.11**. k_2 is the pseudo second-order rate constant.

$$\frac{d[Pu]_{aq}}{dt} = -k_2[Pu]_{aq}^2 \qquad \textit{Equation 4.10}$$

$$\frac{1}{Pu_{aq}} = k_2 t + \frac{1}{Pu_{tot}} \qquad \textit{Equation 4.11}$$

4.7 Adsorption isotherms

4.7.1 Langmuir isotherm

The Pu sorption data from the kinetic study was used for Langmuir isotherm studies. Langmuir isotherm was plotted for the Pu sorption data for contact duration of 2880 mins at pH 6 and 8.5.

The linear form of Langmuir isotherm is depicted by **Equation 4.12**. Here, C_e is the plutonium concentration at equillibrium. b(L/mg) is the Langmuir equilibrium constant which governs the active sites affinity. q_{max}(µg/g) is maximum sorption capacity.

$$\frac{C_e}{q_e} = \frac{1}{(b\ q_{max})} + \frac{C_e}{q_{max}} \qquad \textit{Equation 4.12}$$

The plot of C_e/q_e versus C_e gives sorption capacity is linearly proportional to the initial concentration. The slope of the line is inverse of $q_{max.}$ The plot of q_e versus C_e gives the sorption isotherm which depicts the trend in initial Pu concentration with sorption capacity.

4.7.2 Freundlich isotherm

Freundlich isotherm assumes non-ideal multilayered sorption to the heterogenous surface. The isotherm was plotted for the same data as mentioned in **Section 4.7.1**. **Equation 4.13** describes the linear form of Freundlich isotherm.

$$\log q_e = logK_f + \frac{1}{n}\log C_e \qquad \textit{Equation 4.13}$$

where K_f is Freundlich constant indicating sorption capacity and 1/n is a dimensionless parameter that varies between 0 and 1. The graph was plotted for $\log q_e$ versus $\log C_e$.

CHAPTER 5

RESULTS AND DISCUSSION

Titanium dioxide is the Pu sorbent incorporated in hybrid extractive scintillating resin for quantification of aqueous plutonium. Plutonium oxidation state selection and Pu sorption to TiO_2 is discussed in **Section 5.1**. TiO_2 was incorporated into PVT beads by various mechanisms: solvent (SAAd), heat (HAAd) and silane functional group (SiP) to obtain post-polymerized HESR-I. **Section 5.2** discusses the characterization of HESR-I followed by Pu sorption and detection efficiency. Pre-polymerized HESR-II was obtained by embedding TiO_2 in the dispersed phase before the initiation of suspension polymerization process. **Section 5.3** discusses the characterization of HESR-II followed by Pu sorption and detection efficiency. Kinetic data for HESR-II are discussed in **Section 5.4** and the data is fit to pseudo first-order and second-order models. Rate order has been determined for Pu sorption at pH 6 along with the isotherm plots.

5.1 Specifications of plutonium and titanium dioxide

5.1.1. Aqueous plutonium

The oxidation state analysis of the Pu stock solution was performed to analyze its composition using the solvent extraction and lanthanum fluoride coprecipitations method (Conroy et al., 2016). **Table 5.1** gives the oxidation state analysis results for the Pu stock solution used for the uptake experiments. The stock solution contains 93% of Pu(V), 5% of Pu(IV) and 2% Pu(VI). All the Pu sorption studies were performed using the same stock solution.

The Pu(V) solution which was used in batch uptake studies maintained its oxidation state as +5 throughout batch contact time. This deduction was made based on the Pu(V) control solution studies performed by Powell et al. where they showed the oxidation state of Pu(V) was unaltered above pH 4. Change in the oxidation state of aqueous Pu(V) was only observed at high pH after 60 days (Powell et al., 2008). Hence in the current research, the predominant oxidation state remains as Pu(V) in aqueous solution.

Table 5.1. *Oxidation state distribution of Pu in stock solution*

Oxidation state	**Solvent Extraction**	**LaF_3 Coprecipitation**
Pu(IV)	0.0232 ± 0.0038	0.0577 ± 0.0234
Pu(V)	0.9343 ± 0.0174	0.9423 ± 0.0234
Pu(VI)	0.0425 ± 0.0250	

Plutonium-238 in +5 oxidation state was used for uptake and detection studies as it has higher specific activity compared to other commonly occurring Pu isotopes. High

specific activity signifies Pu molar concentration of a given activity is low, hence reducing the potential for sorption to the vial walls at near neutral pH conditions. Pu(V) is dominant in flowing water compared to other oxidation states in the environment (Orlandini et al. 1986). Pu(V) is considered to move faster in groundwater compared to other oxidation states by an order of 2 to 3 causing great concern (Kaplan et al., 2004). In the near neutral environment, Pu(V) is the most stable of all. Hence, the experimental conditions were maintained close to natural conditions to assist the field application of this research.

Plutonium uptake studies on vial wall were performed using polypropylene, Teflon and polycarbonate vials. Pu wall sorption increases the uncertainty in the plutonium uptake measurements by HESR. Polypropylene, Teflon and polycarbonate vials displayed 51%, 37% and 23% plutonium sorption to the vial walls, at pH 7 and 1200 mins contact time, when no competing sorbent was present. Hence all the Pu uptake studies were performed using polycarbonate vials.

5.1.2 Plutonium sorption to titanium dioxide

Sorption of Pu to TiO_2 is pH dependent. Batch uptake experiments were performed to measure plutonium sorption for each of the two considered TiO_2 phases, rutile and anatase, at various pH conditions. The optimized pH was subsequently used for Pu uptake studies using HESR-I and HESR-II. Uptake was performed using 5 mL Pu solution of ~2.4 Bq/mL concentration and ~12 mg sorbent for 1440 mins contact duration. pH was adjusted using sodium hydroxide and hydrochloric solutions. **Equation 4.3** was used to calculate the fraction of Pu sorbed, but the Pu sorbed on vial walls was not accounted for

in this batch uptake study (Pu_{vial} = 0). Fraction Pu sorbed and conditional K_D values, hereafter, have been accounted for Pu sorbed on vial wall.

The increase in Pu uptake by TiO_2 with an increase in pH is shown in **Figure 5.1**, which agrees with Pu uptake studies performed by Olsson et al. (2003). Rutile has the maximum fraction Pu sorption of 0.97 with corresponding conditional K_D of 1.2×10^4 mL/g at pH 6.6. Anatase has the maximum fraction Pu sorption of 0.98 with corresponding conditional K_D of 2.9×10^4 mL/g at pH 5. The reported values of conditional K_D throughout this chapter are conservative because it is unknown if the measurement was made in the linear region of uptake. The detailed uptake tables are available in **Appendix A**.

Increase in Pu sorption with an increase in pH is speculated due to surface charge effect. TiO_2 particles inherit surface charge due to protonation and deprotonation resulting in surface positive and negative charge, respectively. Point of zero charge (PZC) is the pH value at which the net positive charge on the surface is equal to the net negative charge. The overall surface charge on a surface is positive below PZC and negative above PZC. The published PZC value for rutile ranges between pH 5.7-7 and for anatase between pH 4-5.5 (Kosmulski, 2011). Hence, the Pu sorption increases for anatase at a lower pH value compared to rutile. Pu(V) in aqueous solutions exists as cation species $PuO_{2(aq)}^{+}$. This influences the sorption of Pu on TiO_2 as Pu inherits positive charge and an overall negative charge on TiO_2 surface increases Pu sorption tendency at higher pH which is depicted in **Figure 5.1**. The higher the negative charge on the surface, the greater will be the Pu sorption. But other factors such as ionic strength, sorbent, etc. also govern the Pu sorption. For all further experiments, rutile was considered due to the availability of preferred size

of the particles and similar performance of both rutile and anatase at near neutral pH conditions.

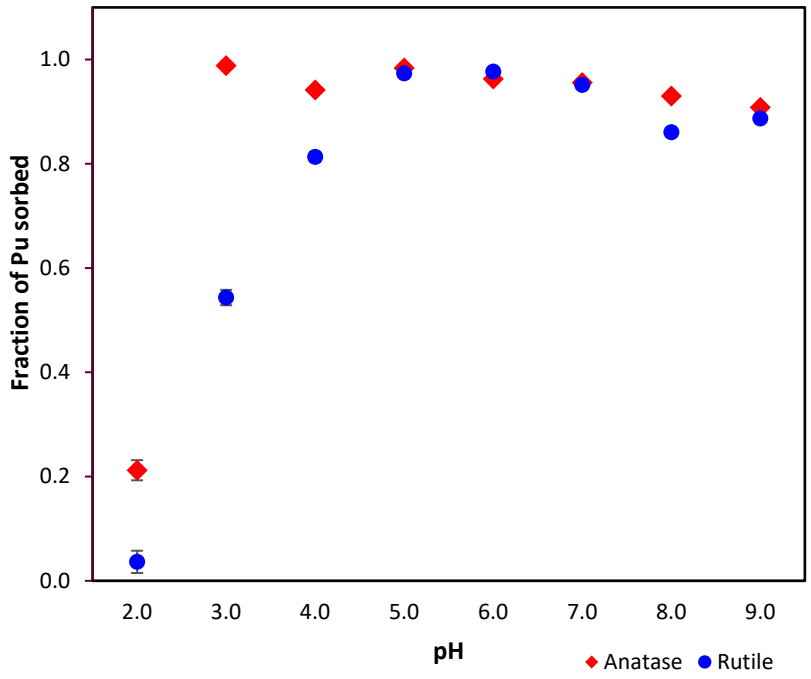

Figure 5.1. *Fraction Pu sorbed to rutile and anatase with change in pH.*

contact duration: 24 hours, initial Pu concentration: 2.4 Bq/mL, volume: 5 mL, sorbent: ~12mg

5.2 Post-polymerized hybrid extractive scintillating resin

Synthesis of HESR-I: solvent (SAAd), heat (HAAd) and silane functional group (SiP) for quantification of Pu is discussed in **Section 4.1.3**.

5.2.1 Mechanism of plutonium uptake and detection

The proposed mechanism of Pu sorption and detection using HESR-I is depicted in **Figure 5.2**. The concentration of sorbed Pu is high on the surface of the resin as TiO_2 is adsorbed to the surface. Batch uptake studies were performed to measure the fraction of Pu sorbed to the resins. The resins, after the batch uptake, were transferred to a Teflon tube to measure the Pu detection efficiency. Alpha decay from sorbed Pu deposits energy in the polymer matrix which results in the emission of scintillation light. The visible scintillation photons that are counted using a photomultiplier tube present in LSC.

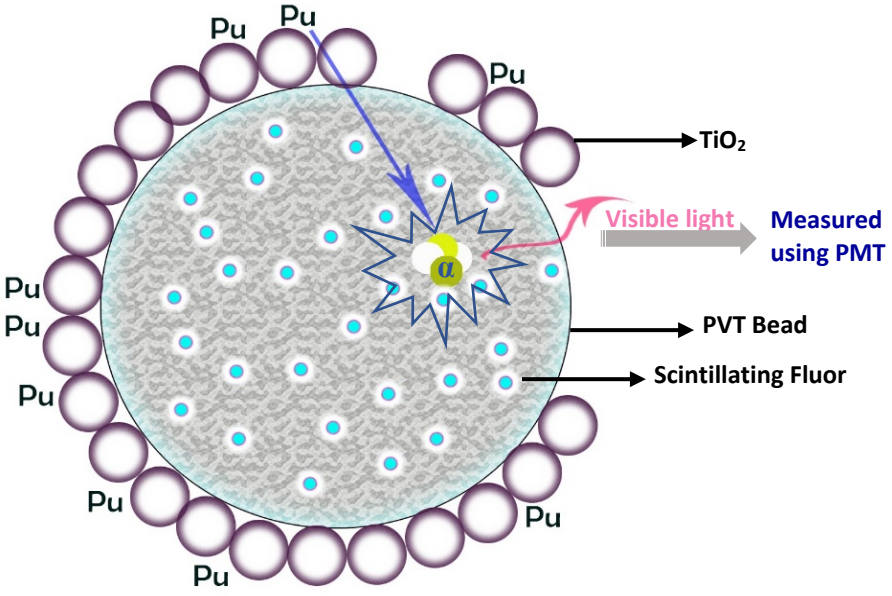

Figure 5.2. *HESR-I Pu sorption and detection mechanism*

5.2.2 Characterization results- Microscopy

Characterization studies were performed on HESR-I to understand and control resin properties. **Figure 5.3** shows microscopy images of HESR-I. **Figure 5.3a** shows SEM image of non-modified PVT beads. **Figure 5.3b** shows the SEM image of HAAd resins coated with TiO_2. **Figure 5.3c** and **5.3d** shows the FIB and optical microscopy image of SAAd resins, respectively.

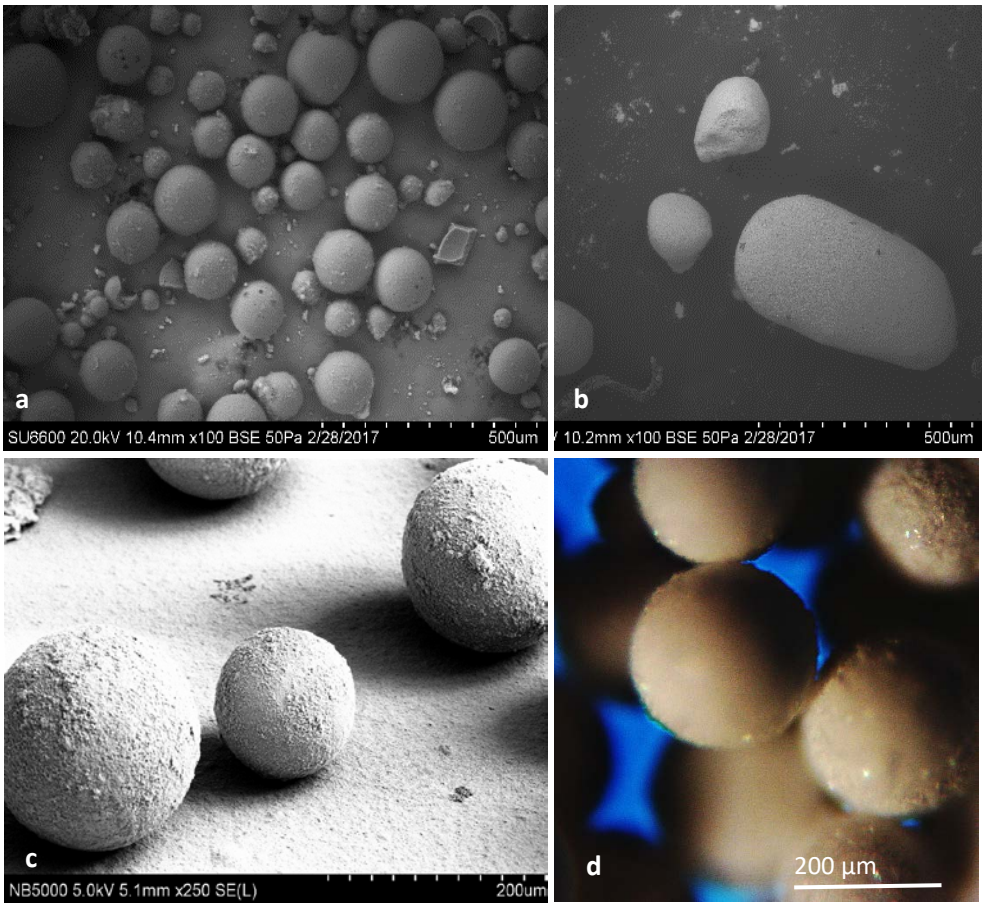

Figure 5.3. *a) Non-modified PVT beads (SEM using SU6600). b) HAAd resins modified at 170 °C (SEM). c) SAAd(12) resins with outer coating of TiO_2 (FIB using NB5000). d) Optical microscopy image of SAAd resins*

Focus ion beam imaging was performed on the SAAd resins to study the distribution of TiO_2 on the bead surface and estimate the layer thickness. The SAAd resin was initially coated with platinum and tungsten to form a protective coating for minimizing damage to the resin and increase the conductivity to get a smooth surface when cut using a gallium ion beam, respectively, as shown in **Figure 5.4 a), b)** and **c)**. EDX was performed on the inner sliced groove of the resin to estimate the resin composition which is depicted

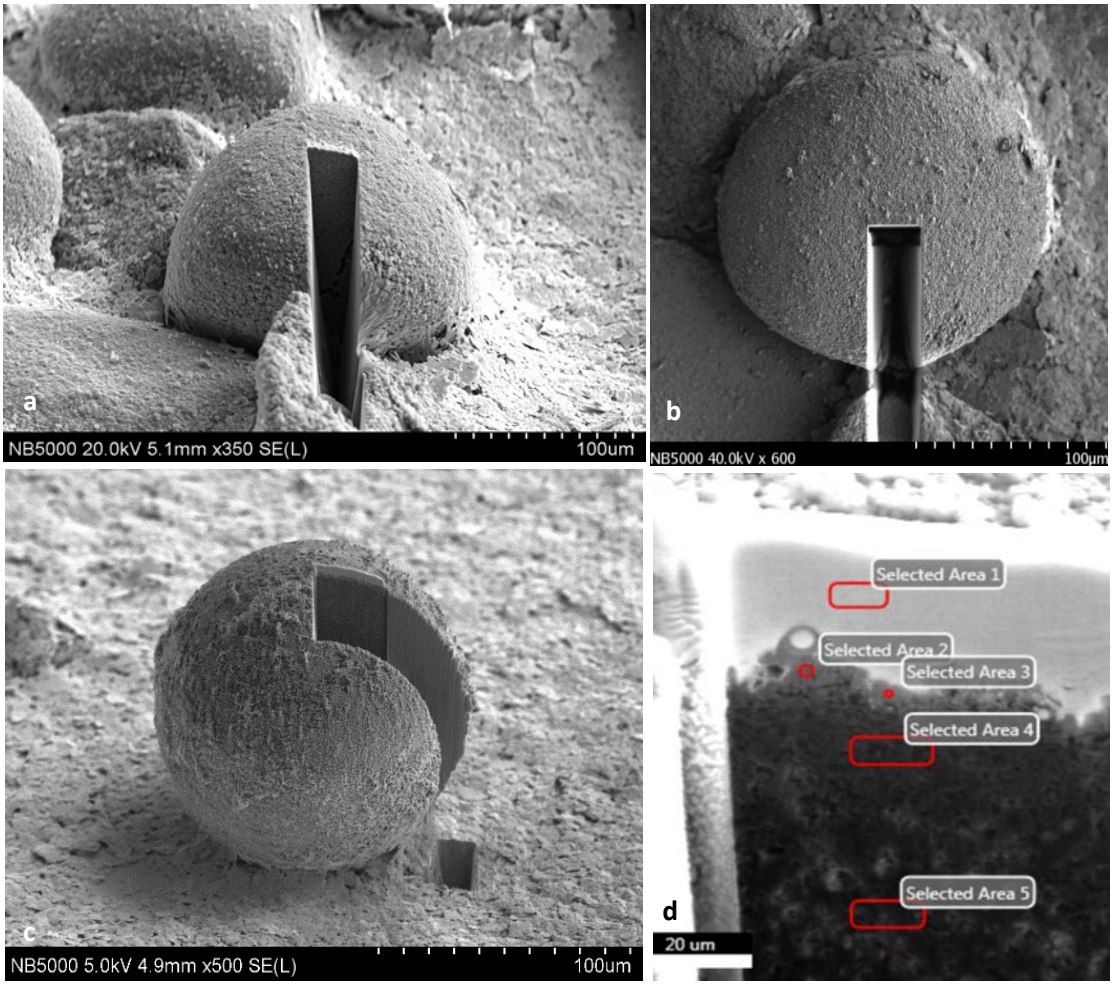

Figure 5.4*. Focus ion beam imaging on SAAd(12) resins.*
a) front view of the sliced resin, b) top view of sliced resin, c) side view of the sliced resin, d) EDX on inner groove of sliced resin with red boxes as the source for respective selected area.

in **Figure 5.4.d**. Area 1 is predominantly tungsten, 100% by weight. Area 2 is 32.7% carbon, 1.1% oxygen, 2.16% titanium and 64.1% platinum. Area 3 is 31.8% carbon, 1.5% oxygen, 1,4% titanium and 65.3% platinum. Area 4 and 5 are 100% carbon depicting PVT bead. Hence, the FIB imaging confirms SAAd resins were coated with TiO_2 on the surface and the PVT bead used for the coating was intact. Details are available in **Appendix B**.

5.2.3 Quantification of titanium dioxide in HESR-I

Quantification of TiO_2 particles is crucial for quantifying Pu sorption trend on HESR-I. Thermogravimetric analysis was performed on HESR-I to quantify coated TiO_2. The specifications are stated in **Section 4.3**. The polymer matrix was completely decomposed at 600 ºC leaving TiO_2 as the residue. Percent TiO_2 incorporated into the beads was calculated using **Equations 4.1**. **Figure 5.5** gives actual %TiO_2 in various formulations of HESR-I resin.

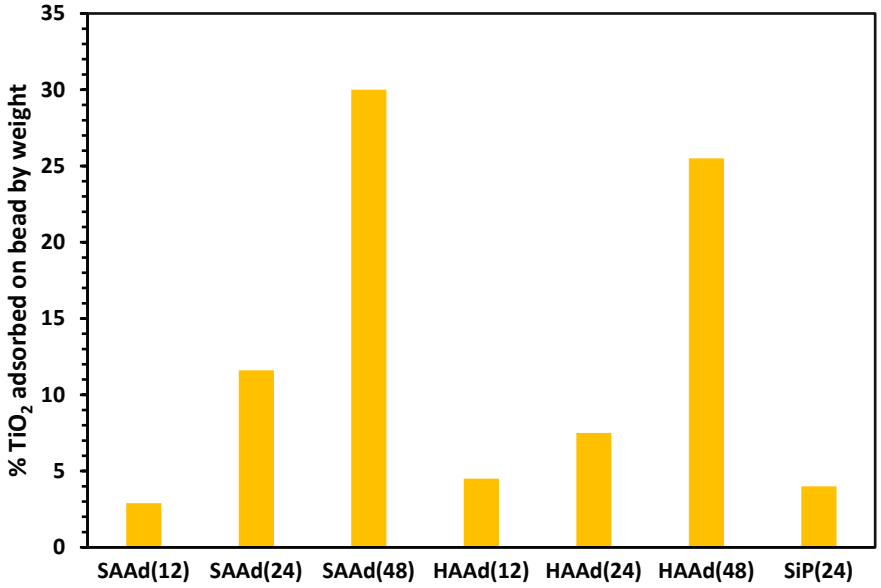

Figure 5.5. *Percentage of actual TiO_2 by weight incorporated as measured by TGA in various formulations of HESR-I*

The specific ratio of TiO_2 and PVT beads by weight was used for the formulation of HESR-I as described in **Section 4.1.3a**. The number in the parentheses represent the expected weight % of TiO_2 and the TGA results provide the actual weight % TiO_2 incorporated in the resin. SAAd(12) and HAAd(12) samples had 3-5% TiO_2 by weight in the beads. SAAd(24) and HAAd(24) samples had 8-12% TiO_2 by weight. SAAd(48) and HAAd(48) samples had 26-30% TiO_2 by weight. The TGA spectra is available in **Appendix C**.

5.2.4 Fraction Pu sorbed

Different HESR-I configurations: SAAd, HAAd, and SiP were studied for Pu sorption. The Pu(V) solution of concentration 0.3 Bq/mL of 10 mL volume and ~20 mg HESR-I was used for the batch uptake. The contact time was 1440 mins and pH at 6. The Pu sorbed on vial walls was rinsed using 1.5 M nitric acid and accounted using mass balance in fraction sorbed calculations. **Appendix A** has the detailed calculation table for fraction sorbed and conditional K_D values. **Figure 5.6** gives the comparison of all the post-polymerization HESR-I performance for plutonium uptake. Blank beads represent unmodified PVT beads with no TiO_2 and fraction Pu sorbed was 0.2.

SAAd resins displayed better Pu sorption compared to other formulations. Fraction Pu sorbed to SAAd(24) resins was 0.93 with corresponding conditional K_D of 6.5×10^3 mL/g. Fraction Pu sorbed to SAAd(12) and SAAd(48) resins were 0.86 (corresponding conditional K_D of 2.8×10^3 mL/g) and 0.47 (corresponding conditional K_D of 4.4×10^2 mL/g), respectively. An average of 1.8% of initial Pu activity was sorbed on

walls for SAAd(12) and SAAd(24) samples. SAAd(48) sample amounted to 8% of initial Pu activity of wall sorption and displayed an unexpected decrease in Pu sorption even with higher %TiO_2 by weight. The Pu batch test vial of SAAd(48) resins displayed cloudiness. Minute flakes of the resins were dispersed in solution and sorbed to the vial walls which was assumed to be TiO_2. Further studies on SAAd(48) resins are required to characterize their stability and robustness.

HAAd resins displayed reduced Pu sorption compared to SAAd resins. HAAd(12) TiO_2 coated beads had the least fraction Pu sorbed, 0.28, with corresponding conditional K_D of 1.9×10^2 mL/g. HAAd(24) and HAAd(48) showed similar Pu sorption trend with 0.4 fraction Pu sorbed corresponding to conditional K_D of 3.5×10^2 mL/g and 3.6×10^2 mL/g, respectively. An average of 3.5% initial Pu was sorbed on vial wall for HAAd(12) and HAAd(24) resins, and 7% for HAAd(48) resins. The overall reduced performance of HAAd resins compared to SAAd resins can be due to structural deformation of the resins at elevated temperature affecting the active sites. Cloudiness of vials during batch tests similar to SAAd(48) resins was noticed in HAAd(48) resins.

SiP resins displayed the least Pu sorption compared to other HESR-I resins. Fraction Pu sorbed was 0.2 with corresponding conditional K_D of 1.4×10^2 mL/g. Wall sorption was measured to be ~1% of initial Pu activity considered for batch uptake. The reduced Pu sorption can be explained by the silane branches on TiO_2 hindering the active sites on the surface.

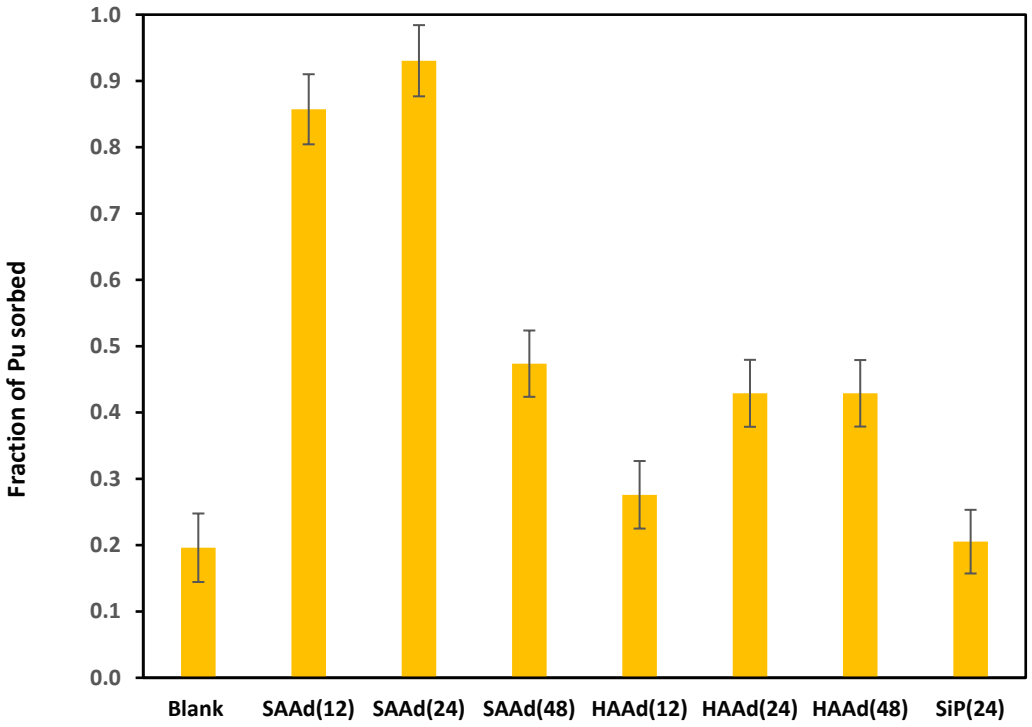

***Figure 5.6**. Fraction of Pu sorbed to HESR-I*

pH: 6, contact duration: 24 hours, initial Pu concentration: 0.3 Bq/mL, volume: 10 mL, sorbent: ~20 mg

5.2.5 Plutonium detection using HESR-I

5.2.5.a) Fluorescence using external UV illumination

The resins displayed fluorescence under external UV illumination as shown in **Figure 5.7**. As fluorescence is necessary but insufficient for scintillation, radioluminosity tests were conducted using ^{241}Am point source.

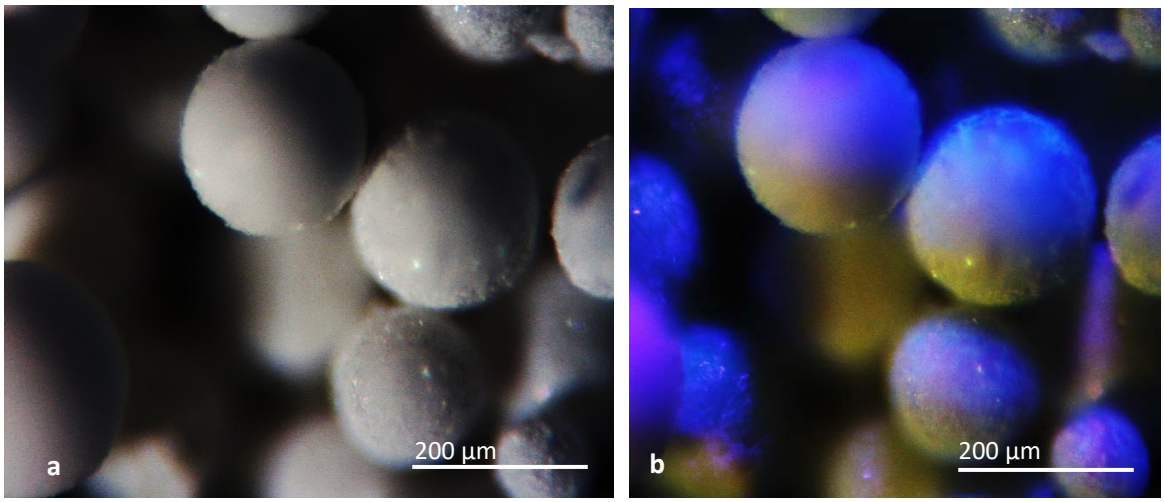

Figure 5.7. *Fluorescence of SAAd resins under a) incandescent lamp illumination b) UV illumination*

5.2.5.b) Radioluminosity measurement

Radioluminosity measurement using ^{241}Am as a point source is explained in **Section 4.5.1**. The number of photons emitted is proportional to the amount of energy from the alpha particles deposited on the resins. Hence the light output is one of the necessary measures of detection efficiency. Greater the peak height in the spectrum, better the scintillation property which is proportional to the plutonium detection efficiency. In all the radioluminosity graphs, the background peak at channel number ~90 corresponds to the thermal PMT noise or unwanted luminescence. The background peak facilitates the

distinction between the sample spectrum from the background. Blank beads, have fluor but no TiO_2, are used for relative comparison of radioluminosity spectrum with HESR-I.

SAAd

SAAd resins display reduced light output compared to the blank beads. **Figure 5.8** depicts the radioluminosity spectra of SAAd resin. Blank beads display the spectrum peak at channel number ~250 and the SAAd resins peak at channel number 100. The reduced light output of SAAd resins is evident from the shift in the spectrum peak at channel number ~250 to 100. The reason for the decrease in light output from SAAd resins with increasing TiO_2 on the surface needs additional investigation.

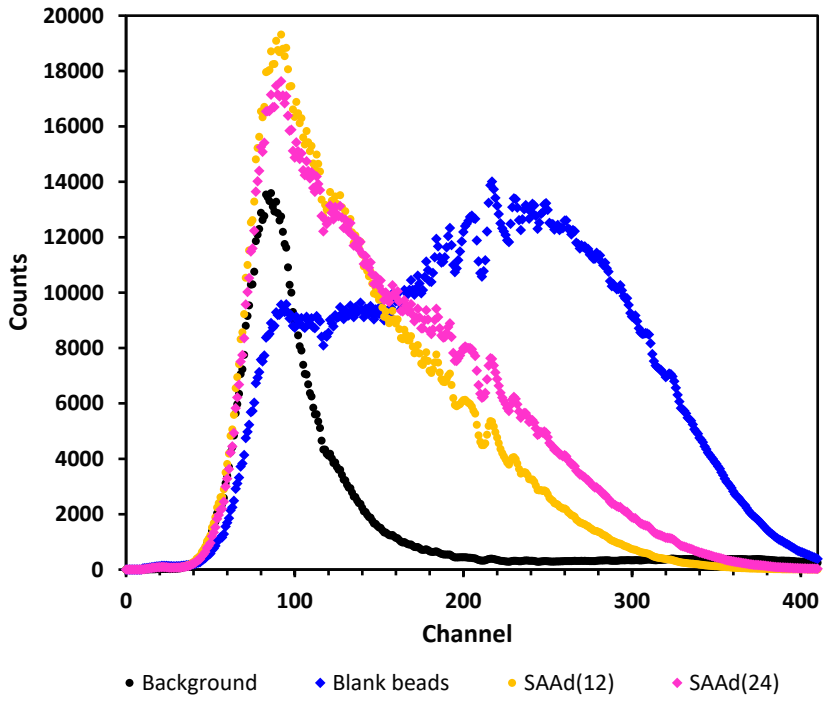

Figure 5.8. *Differential pulse height spectra from radioluminosity of SAAd resins of varying amount of adsorbed TiO_2 and count time of 10 mins*

The effect of sonication on blank beads was studied as the beads were dispersed in DMF using sonication during the process as mentioned in **Section 4.1.3a)**. **Figure 5.9** shows the peak shift to lower channel number, from 250 to 100, with sonication time. There was no significant peak shift in the blank beads which were subjected to suspension in DMF without sonication (0 min), which confirms that the beads were not damaged during rest of the process. Sonication generates acoustic cavitation in the solution. These cavitation sites induce high energy reactions of about ~5000ºC with pressures of about 1000 atm (Suslick & Price, 1999). As the rate of cooling is greater than 1010 K/s, the high energy developed dissipates in seconds (Suslick & Price, 1999). Such extreme conditions may degrade the optical properties of polymer matrix or the fluor itself, causing the peak shift towards lower channel in the radioluminosity spectra.

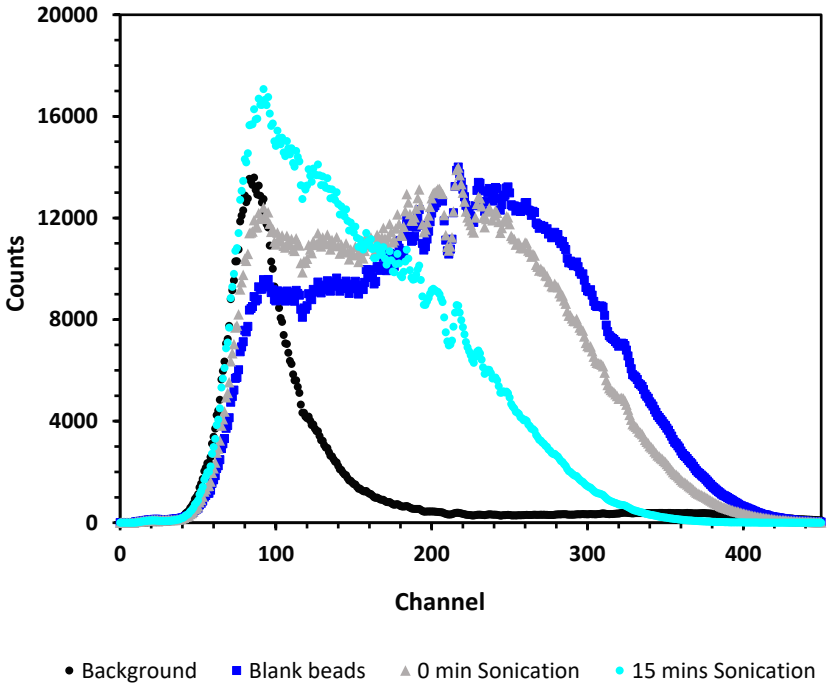

***Figure 5.9**. Differential pulse height spectra from radioluminosity of unmodified PVT beads (no TiO_2) processed under different sonication duration for count duration of 10 mins*

SAAd(24) resins were coated with an additional αNPO layer on the surface to investigate the light output as mention is **Section 4.1.3a)**. Using the SAAd method both TiO_2 and αNPO were incorporated on the PVT beads. As shown in the **Figure 5.10**, the fluor coated SAAd(24) resins showed a shift in peak to higher channel number compared to SAAd resins peak.

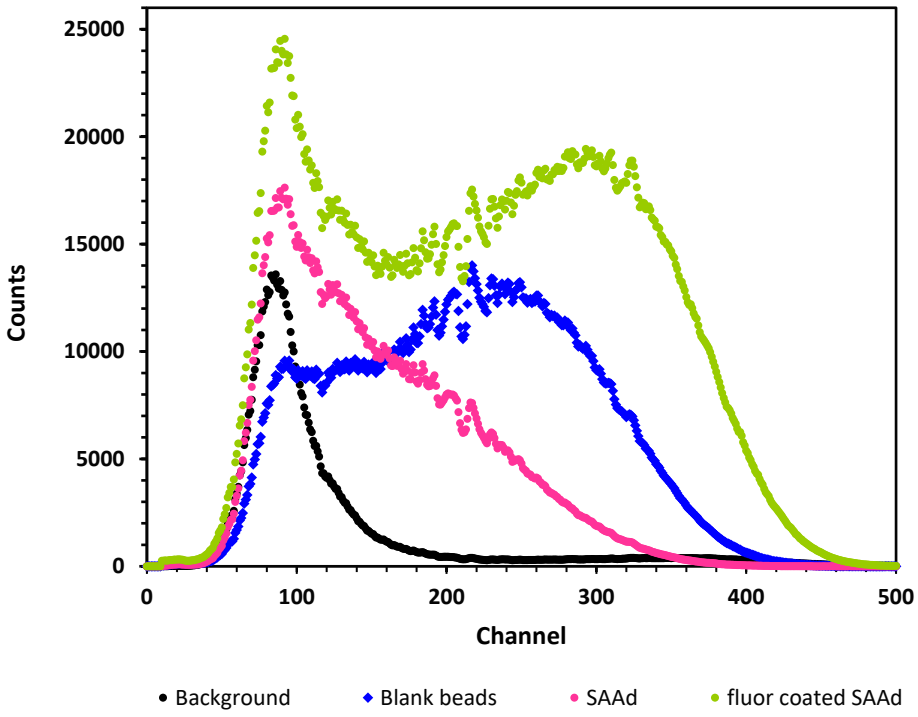

Figure 5.10. *Differential pulse height spectra from radioluminosity of fluor coated SAAd(24) resins versus SAAd(24) for count duration of 10 mins*

HAAd

HAAd resins displayed reduced light output compared to blank beads which was evident from the peak shift towards lower channel number, 250 to 100. This is shown in **Figure 5.11**. The light output from HAAd resins was reduced which might be due to damage caused to the beads due to elevated temperature.

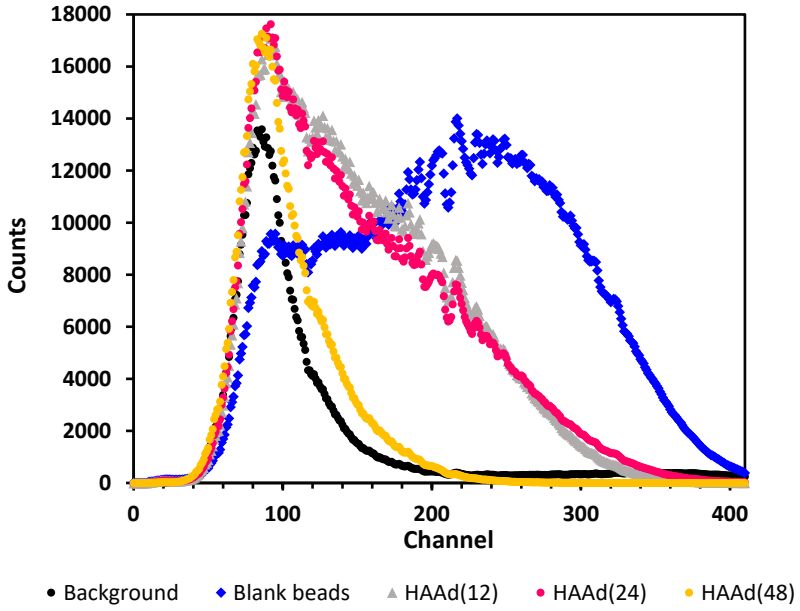

Figure 5.11. *Differential pulse height spectra from radioluminosity of HAAd resins for count duration of 10 mins*

Blank beads were subjected to elevated temperatures to study the corresponding peak shift as mentioned in **Section 4.1.3a)**. Temperature study was essential as HAAd resins were modified at 150 ºC during synthesis. **Figure 5.12** depicts the shift of spectra to lower channel with the increase in temperature. This shows the reduction of light output due to alteration of polymer matrix properties or fluor with an increase in temperature.

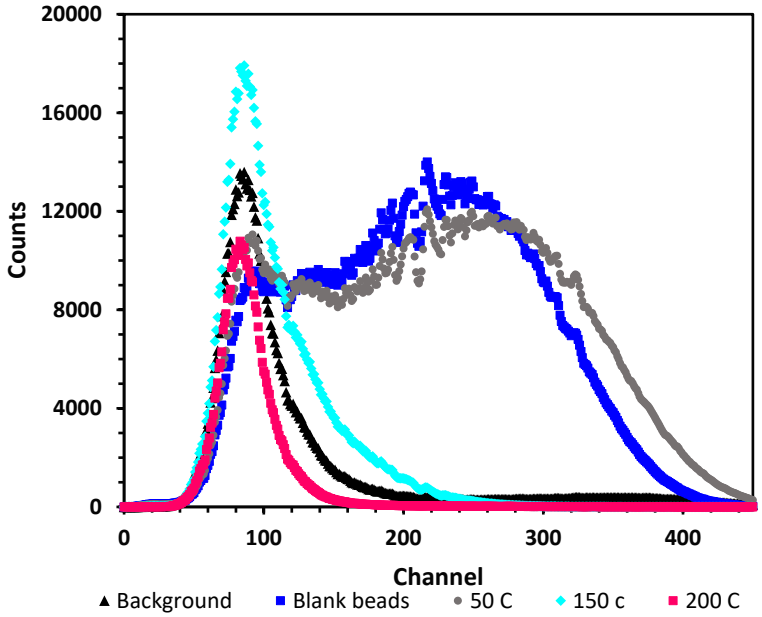

Figure 5.12. *Differential pulse height spectra from radioluminosity of unmodified PVT beads (no TiO_2) processed under different temperature for count duration of 10 mins*

SiP

SiP resins displayed reduced intensity of the peak at channel number ~200, **Figure 5.13**. The spectrum shift in SiP resins was not as prominent as SAAd or HAAd resins.

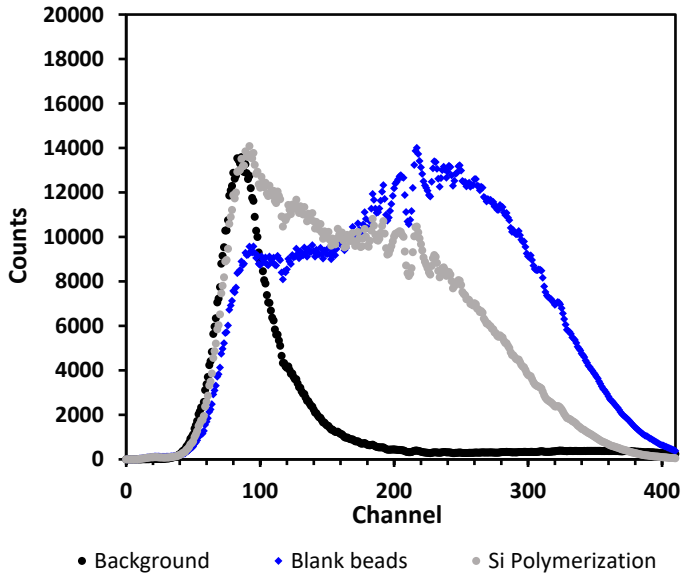

Figure 5.13. *Differential pulse height spectra from radioluminosity of SiP resins for count duration of 10 min*

5.2.5.c) Plutonium detection efficiency of HESR-I

Detection efficiency was measured for SAAd(24) resins and fluor coated SAAd(24) resins. Detection efficiency was not measured for other HESR-I due to unsatisfactory radioluminosity results implying low Pu detection. **Section 4.5.2** explains the detection method.

Fraction Pu sorbed to SAAd(24) resins was 0.75 with corresponding conditional K_D of 1.3×10^3 mL/g and 1.9% Pu detection efficiency. This signifies light output to detect the accumulated Pu using scintillation technique was not enough. The reduced light output may be due to obstruction of light due to the surface coated with TiO_2 and/or due to loss or degradation of fluor during sonication.

Fraction Pu sorbed to fluor coated SAAd(24) resins was 0.13 with corresponding conditional K_D of 6.7×10^1 mL/g and ~50% Pu detection efficiency. This signifies additional fluor coating on SAAd(24) resins increased Pu detection efficiency but decreases Pu uptake. The additional fluor coating is on the surface of the resin. The increased concentration of fluor on the surface may interfere with the accessibility of TiO_2 active sites for Pu sorption. **Table 5.2** summarizes the fraction Pu uptake and detection efficiency of the resins.

Table 5.2. *Performance of SAAd (bi layer) resins and fluor coated resins, 106-212 µm size*

Sample	Fraction Pu uptake	Pu detection efficiency (%)
SAAd(24)*	0.75 ± 0.10	1.9 ± 1.2
Fluor coated SAAd(24)	0.13 ± 0.05	49.8 ± 15.8

**Different SAAd(24) layer batch compared to one depicted in Figure 5.6*

5.2.6 Performance summary of HESR-I

SAAd resins had the highest fraction Pu sorption of 0.93 ± 0.05. HAAd resins comparatively had a smaller fraction Pu sorbed, 0.43 ± 0.05. This decrease in Pu sorption to HAAd resin is attributed to the bead degradation at the high temperature, 150 ºC, utilized in making the beads. SiP resins displayed poor Pu uptake with 0.2 fraction of sorbed Pu. Radioluminosity measurements displayed poor light output indicating poor detection efficiency of the systems. SAAd resins showed detection efficiency of 1.9 ± 1.2 % for 0.75 ± 0.10 fraction Pu sorbed to the resins as shown in **Table 5.3**. Overall, HESR-I did not display satisfactory Pu sorption coupled with Pu detection efficiency results.

Table 5.3. *Summary of HESR-I (106-212 µm) performance*

Type	Fraction Pu sorbed	Radioluminosity	Pu detection efficiency (%)
SAAd(12)	0.86 ± 0.05	Peak shift from	
SAAd(24)	0.93 ± 0.05	~250 to 100	1.9%
SAAd(48)	0.47 ± 0.05	channel number	
Fluor coated SAAd(24)	0.13 ± 0.05	No peak shift	49.8%
HAAd(12)	0.28 ± 0.05	Peak shift from	-
HAAd(24)	0.43 ± 0.05	~250 to 100	
HAAd(48)	0.43 ± 0.05	channel number	
SiP(24)	0.21 ± 0.04	Reduced peak intensity and shift to ~200 channel number	-

5.3 Hybrid extractive scintillating resin using pre-polymerization process

The HESR-II was synthesized using the method explained in **Section 4.1.3b)**. Different batches were synthesized by varying the TiO_2 loading as shown in **Table 5.4**. The number in parentheses denotes weight percent of expected TiO_2 incorporated in the dispersed phase. HESR-II(4) stands for hybrid extractive scintillating resin containing 4% titanium dioxide in dispersed phase by weight. It is essential to understand that the expected $\%TiO_2$ incorporation in the dispersed phase is different from actual $\%TiO_2$ embedded in the polymerized HESR-II. The expected amount of TiO_2 which is incorporated in the organic matrix does not entirely get embedded in the resins. Some of the TiO_2 is lost in the continuous phase during the polymerization as TiO_2 has a higher affinity towards water and gets washed away during the last step which is the filtration process.

Table 5.4. *Distribution of expected TiO_2 by weight in HESR-II*

Sample	Expected $\%TiO_2$ in HESR-II (by weight)
HESR-II(4)	4
HESR-II(8)	8
HESR-II(14)	14
HESR-II(25)	25
HESR-II(40)	40
HESR-II(57)	57
HESR-II(73)	73

5.3.1 Mechanism of plutonium uptake and detection

Figure 5.14 depicts the proposed mechanism of Pu uptake and detection by HESR-II. Embedded TiO_2 is dispersed throughout the resin. The pores and the connecting channels in HESR-II facilitate uptake of Pu by TiO_2 particles situated inside the resin. Pu sorption to TiO_2 is facilitated through the pore channel system for the movement of Pu within the resin. Pu then accumulates on the embedded TiO_2 particles. The process of excitation of the matrix and energy transferred is same as HESR-I explained in **Section 5.2.1**.

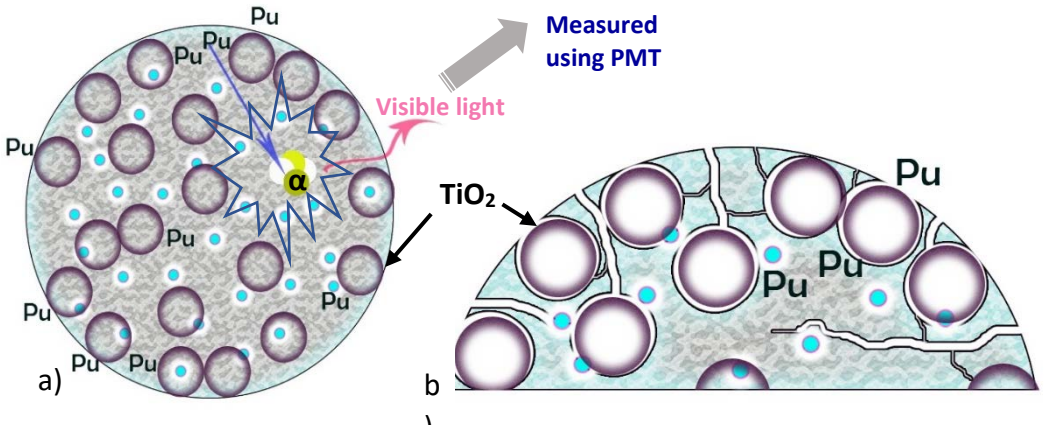

Figure 5.14. *a) Proposed mechanism of Pu uptake and detection, b) enlarged image of embedded TiO_2 and associated pore roots in HESR-II*

5.3.2. Characterization studies

Characterization studies were performed on HESR-II to study resin properties. **Figure 5.15** and **5.16** shows SEM and FIB imaging of HESR-II(57). Gallium ion beam was used to dissect the bead to investigate TiO_2 distribution within the bead.

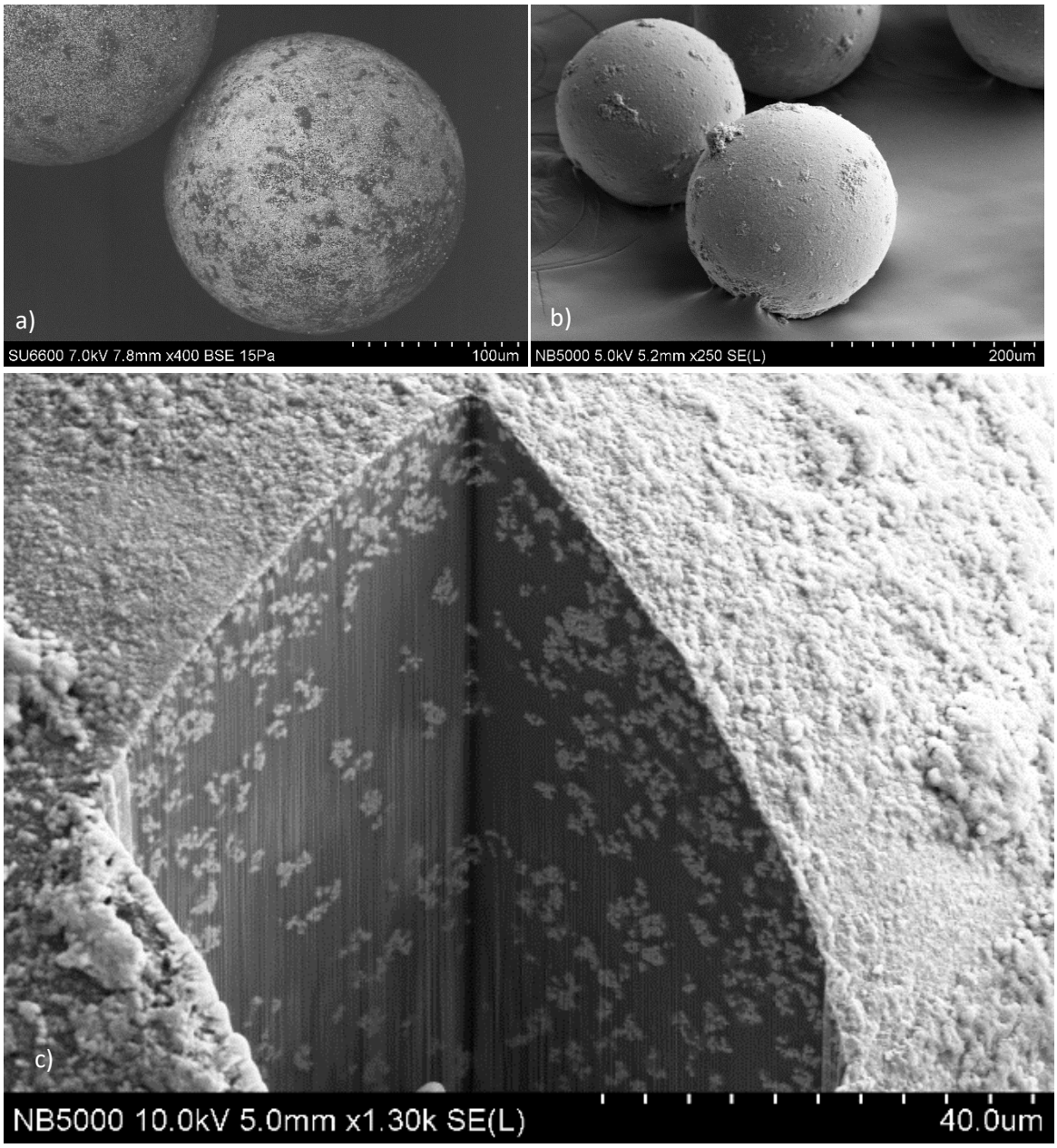

Figure 5.15. *a) SEM, b) FIB displaying HESR-II(57). c) Gallium ion beam dissect displaying TiO_2 distribution within HESR-II(57).*

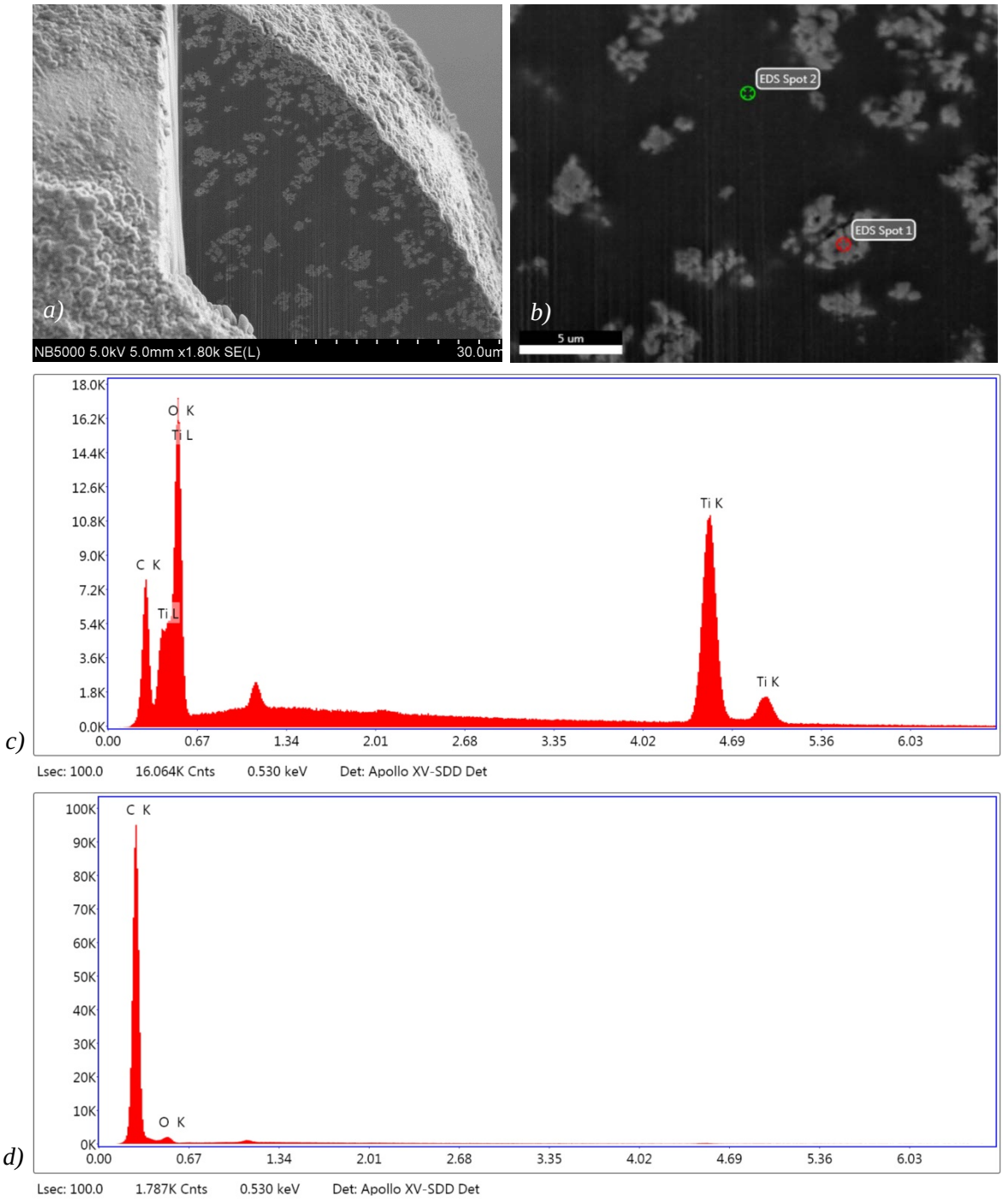

Figure 5.16. *a) FIB secondary electron image of HESR-II(57). b) Selected region 1 and 2 for EDX. c) EDX displaying 93% of TiO_2 by weight present in selected region 1 (lighter region). d) EDX displaying 0% TiO_2 by weight in selected region 2 (darker region).*

The pre-polymerization process resulted in the resins which range from ~300 µm to less than 106 µm in diameter. **Section 4.1.3b)** discusses the synthesis of HESR-II(4) to HESR-II(73). **Figure 5.17** summarizes the sieve analysis of HESR-II. The sieve analysis was performed with the sieves of apertures 212 µm and 106 µm. HESR-II(4) sample had a nearly equal yield of <106 µm and 106-212 µm sized particles. There was an overall decrease in <106 µm sized particles yield from HESR-II(4) to HESR-II(57). The yield of <106 µm particle size increased in HESR-II(73) compared to HESR-II(57).

The polarity of the solvent is one of the factors which determines the resin size. As the overall solvent polarity increases, the particle size of the resins decreases (Lok & Ober, 1985). There exist a trend of decreased particles size as the amount of monomer decreases for the same amount of continuous phase (Balakrishnan & Ford, 1982). The amount of monomer used in the synthesis of HESR-II(73) was half of HESR-II(57) keeping all the other reagents constant as discussed in **Section 4.1.3b)**. The monomer, vinyl toluene, is non-polar in nature and the continuous phase is highly polar. Reducing the monomer amount increased the overall polarity of mixture increasing the yield of smaller particles in HESR-II(73).

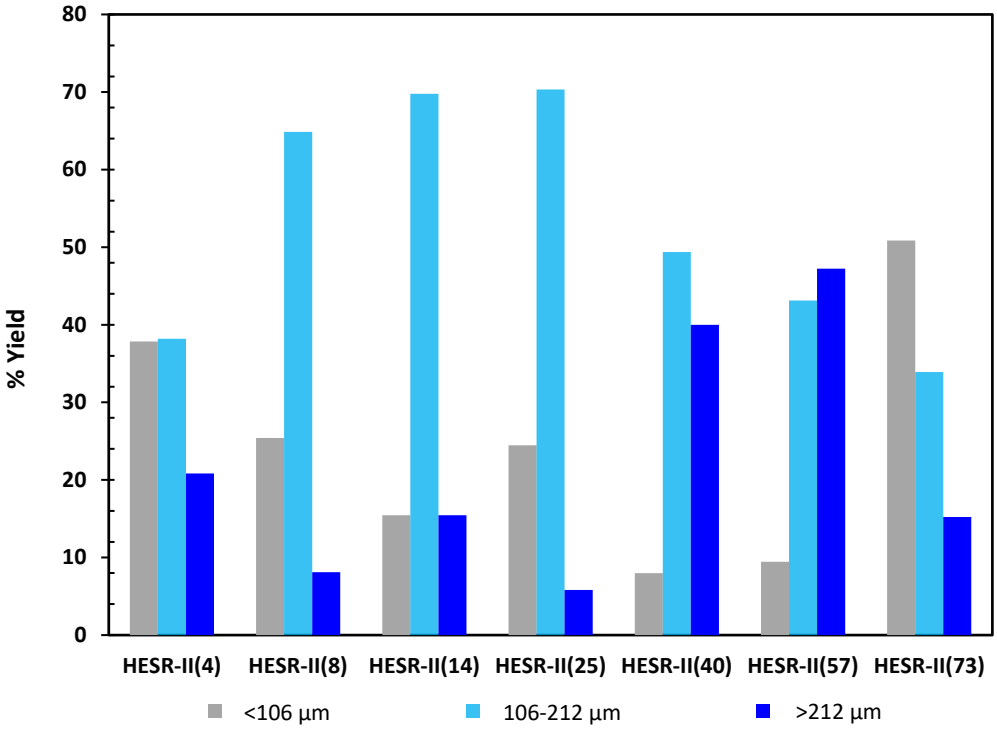

Figure 5.17. *Sieve analysis of HESR-II*

5.3.3 Quantification of titanium dioxide

Thermogravimetry analysis (TGA) was used to determine the amount of TiO_2 present in HESR-II. The specifications are same as described in **Section 4.3**.

Figure 5.18 depicts % TiO_2 by weight in HESR-II calculated using **Equation 4.1**. During the polymerization process, some amount of initial TiO_2 from dispersed phase gets in the continuous phase which is lost during filtering of the final product. As evident from the **Figure 5.18**, the resins size of <106 µm had the highest amount of embedded TiO_2 in all the cases. TGA measurements only provide the value of total amount of TiO_2 present in the resin. Its limitation is in the uncertainty associated with accessible and non-accessible

TiO_2 within the resin for Pu sorption. The TGA spectra as well as the mass balance of TiO_2 in the system are available in **Appendix C**.

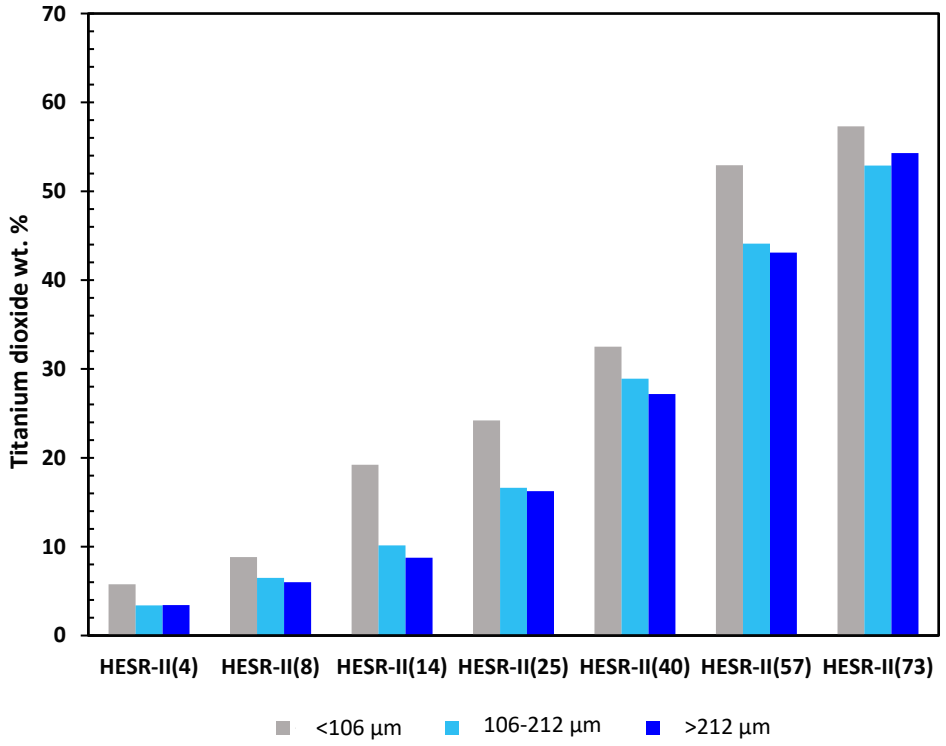

Figure 5.18. *Weight % of TiO_2 in HESR-II measured by TGA*

5.3.4 Plutonium uptake studies

A Pu(V) solution of volume 10 mL with concentration 0.3 Bq/mL and ~20 mg HESR-II resins were used for the batch uptake experiment. The contact time was set for 1440 mins. pH of the system was set at 6. The details are mentioned in **Section 5.2.4**.

Figure 5.19 depicts the fraction of Pu sorbed to HESR-II. HESR-II(57) displayed on an average of 0.74 fraction Pu sorbed with corresponding conditional K_D of 1.3×10^3

mL/g. HESR-II(73) showed on an average 0.8 fraction Pu sorbed with corresponding conditional K_D of 2×10^3 mL/g. It was noticed that fraction of Pu sorbed was proportional to the amount of TiO_2 present in the resins.

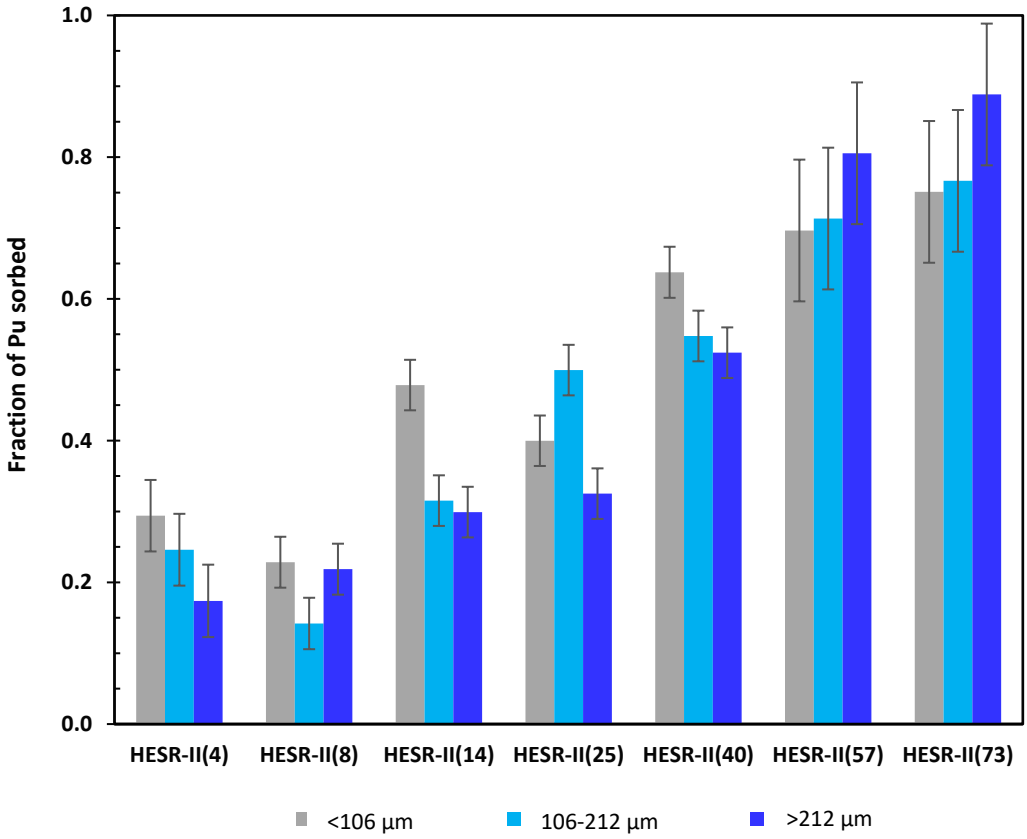

Figure 5.19. *Fraction of Pu sorbed to HESR-II*

pH: 6, contact duration: 24 hours, initial Pu concentration: 0.3 Bq/mL, volume: 10 mL, sorbent: 20 mg

5.3.5 Plutonium detection studies

5.3.5.a) Fluorescence using external UV illumination

HESR-II fluoresces under UV illumination as shown in **Figure 5.20**. As fluorescence is a necessary but not sufficient for scintillation, radioluminosity measurements were performed.

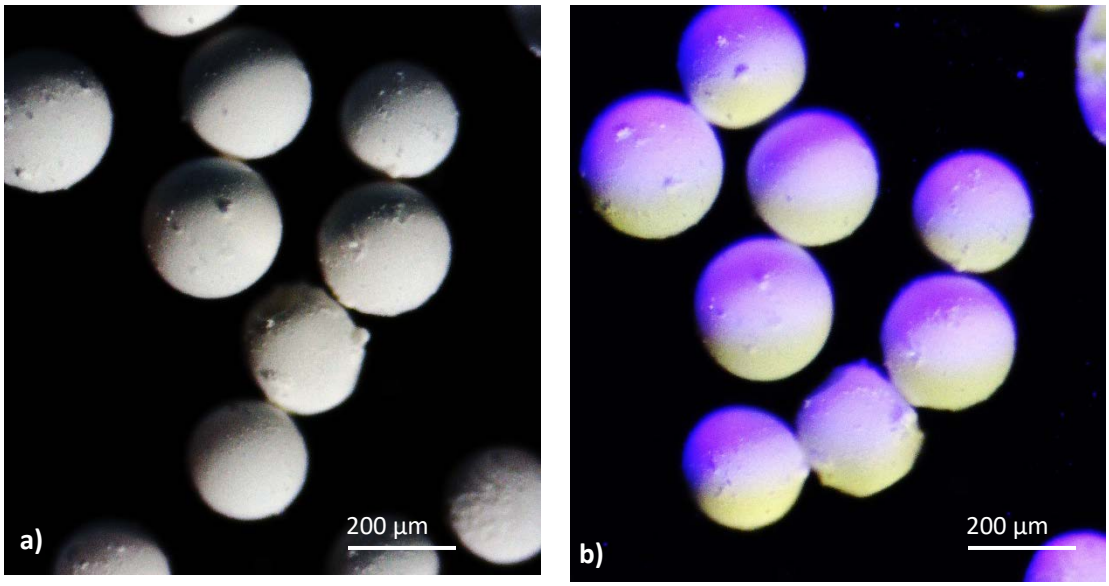

Figure 5.20.. *Fluorescence of HESR-II under a) incandescent lamp and b) external UV illumination*

5.3.5.b) Radioluminosity measurement

Figure 5.21 depicts the radioluminosity spectra using ^{241}Am a point source for HESR-II, 106-212 µm. There was no significant peak shift to lower channel number with increase in weight % of TiO_2 in HESR-II. TiO_2 in HESR-II is distributed throughout the resin matrix, unlike HESR-I where TiO_2 is concentrated only on the surface of the resin. HESR-II displayed potential for moderate to high Pu detection efficiency.

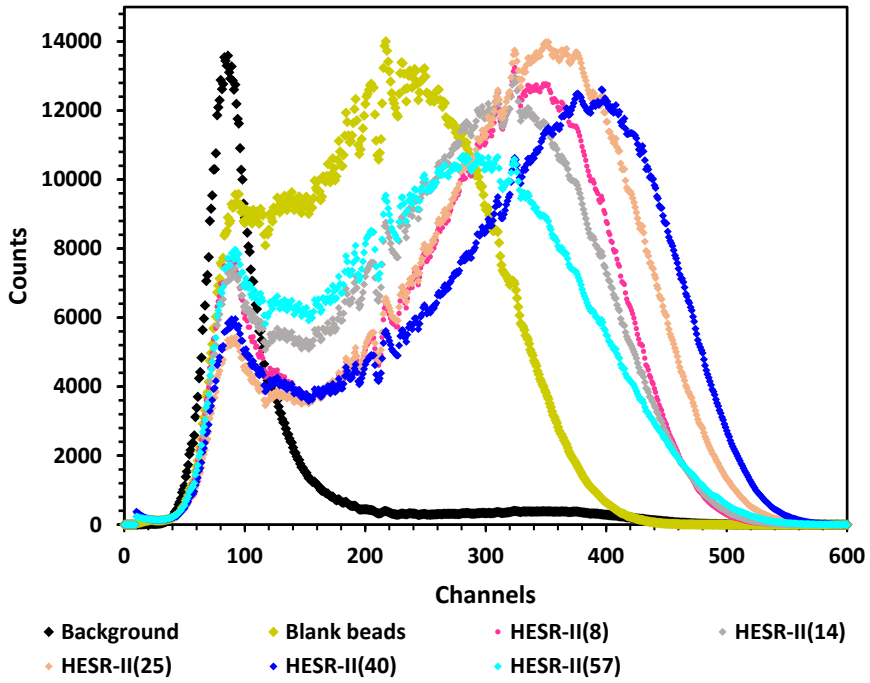

Figure 5.21. *Differential pulse height spectra from radioluminosity of HESR-II, 106-212 µm for count duration of 10 mins*

5.3.5.c) Plutonium detection efficiency

HESR-II displayed overall high Pu detection efficiency compared to HESR-I. **Figure 5.22** depicts fraction Pu sorbed and Pu detection efficiency for the resin size <106 µm. The Pu detection efficiencies vary between 20%- 30% for all the resin types.

Pu detection efficiency varied greatly with resin size as shown in **Figure 5.23**. Pu detection efficiency for HESR-II(57), particle size of <106 µm, was 36%. HESR-II(57) of particle size 106-212 µm displayed highest detection efficiency of 96%. The reason for the decrease in detection efficiency for <106 µm sized resin needs investigation.

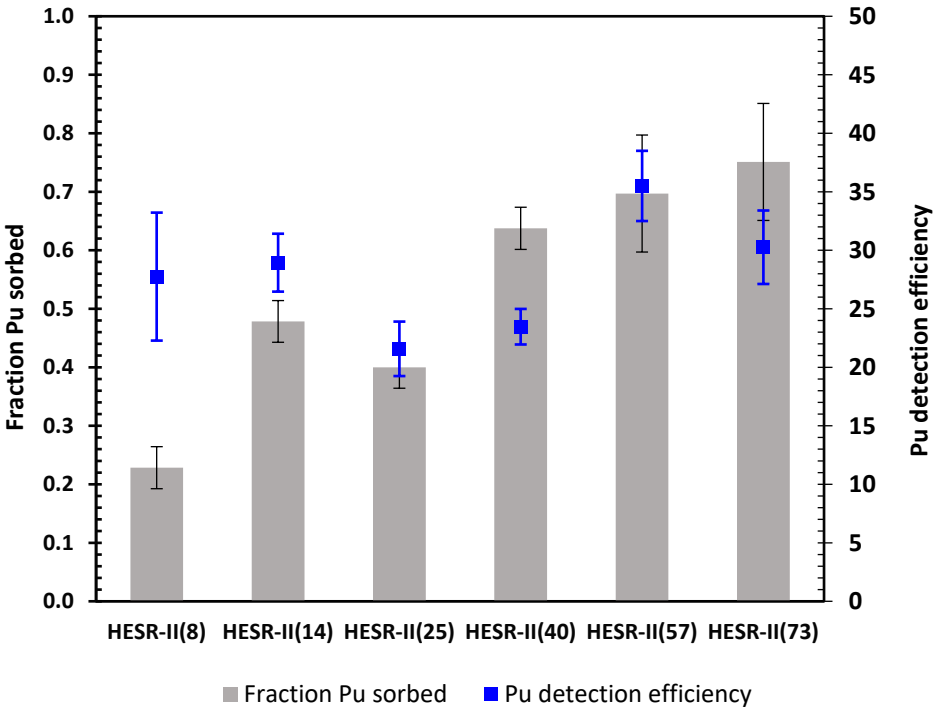

Figure 5.22. *Fraction of Pu sorbed and detected by HESR-II (<106 µm) for initial loading of 0.3 Bq/mL* ^{238}*Pu(V)*

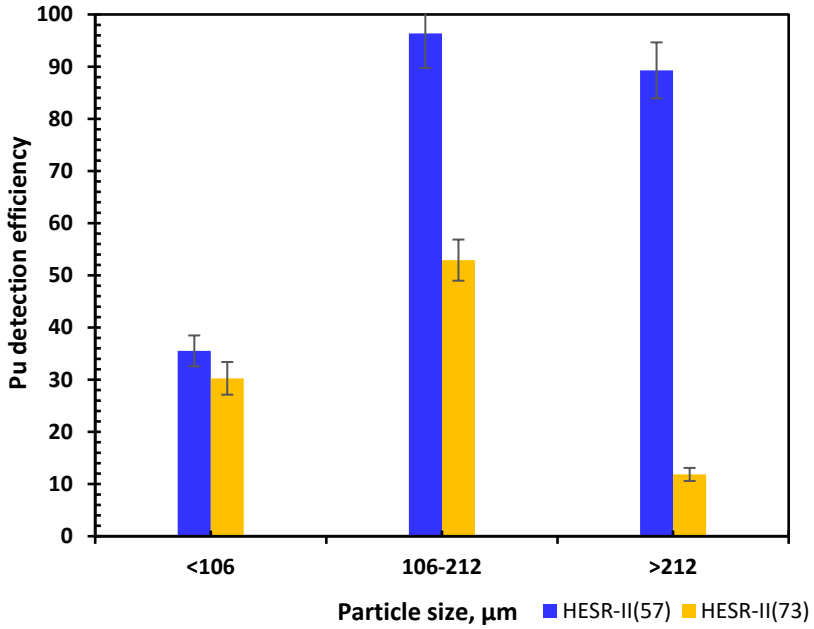

Figure 5.23. *Pu detection efficiency as a function of resin size for HESR-II(57) and (73) initial loading= 0.2 Bq/mL of Pu(V), batch contact time=24 hours, pH=6*

Highest detection efficiency for HESR-II(73) was 52% with the particle size 106-212 µm. The lower Pu detection efficiency of HESR-II(73) compared to HESR-II(57) can be explained by the difference in their composition as mentioned in **Section 4.1.3b)** and higher TiO_2 % in the matrix as shown in **Section 5.3.3**. HESR-II(73) has twice the crosslinking and amount of porogen compared to HESR-II(57) which may cause obstruction of energy deposition from alpha particles to the polymer matrix.

Figure 5.24 shows the pulse height spectra for HESR-II(57) of different size resin with sorbed ^{238}Pu as the source. Pulse peaks around channel number 350 for resin size >212 µm and 106-212 µm. The pulse for <106 µm peaks at channel 260.

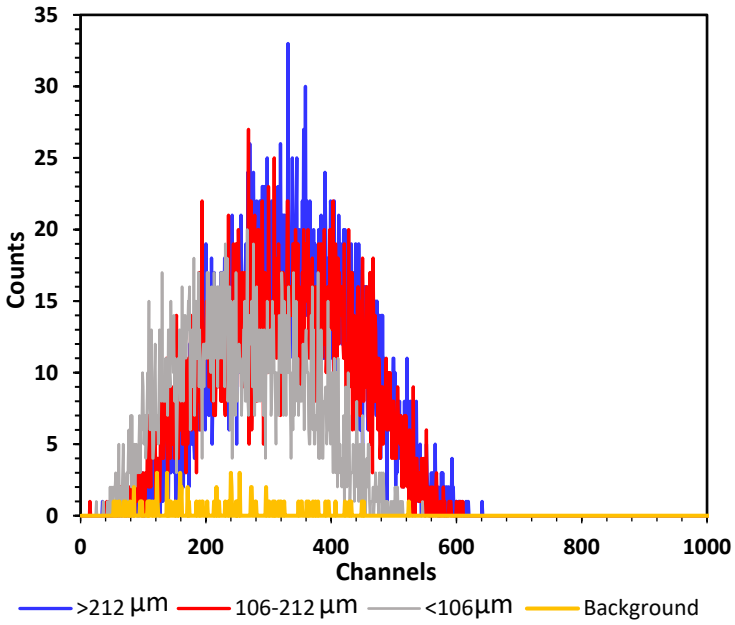

Figure 5.24. *Differential pulse height spectra as function of HESR-II(57) size with ^{238}Pu(V) as source*

5.3.6 Performance summary of HESR-II

HESR-II(57) with 57% of TiO_2 by weight displayed the highest average fraction Pu sorption of 0.74 ± 0.10 for 24 hours contact duration. There was a difference in Pu detection efficiency with the resin size. HESR-II(57) size of <106 μm had 35.5 ± 3.0 % Pu detection, 106-212 μm with 96.4 ± 6.6 % and >212 μm with 89.3 ± 5.4%. Lower detection efficiency of smaller resin size is attributed to obstruction of alpha energy deposition to the polymer matrix or hindrance to the light output by TiO_2 particles, but a targeted investigation is needed. HESR-II performed overall better than HESR-I. **Table 5.5** summarizes the various systems used for Pu uptake and detection.

Table 5.5. *Summary of HESR-II (106-212 μm) performance*

Type	Fraction Pu sorbed	Pu detection efficiency (%)
HESR-II(4)	0.25 ± 0.05	
HESR-II(8)	0.14 ± 0.04	
HESR-II(14)	0.32 ± 0.04	
HESR-II(25)	0.50 ± 0.04	
HESR-II(57)	0.71 ± 0.10	96%
HESR-II(73)	0.77 ± 0.10	50%

Note: Radioluminosity spectra peak shift to lower channel number relative to blank beads was not noted for HESR-II.

5.3.5 Resin degradation

The Pu sorption to HESR-II decreased as the resins aged. A kinetic study was performed for resin 1 and resin 2, which are two batches of same HESR-II(57) formulation of size 106-212 µm. Aged resin 1 denotes a batch of resin that was intermittently exposured to fluorescent light at room temperature for 3 months versus fresh resin 1 which was not exposed to the light. Resin 2 denotes a freshly prepared batch of resin. The Pu(V) solution of volume 10 mL with concentration 0.3 Bq/mL and 25 mg of resins were used for the batch uptake experiment at pH 6 for aged resin 1 and resin 2. The total contact time for aged resin 1 and resin 2 was 14100 mins and 28800 mins, respectively, as shown in **Figure 5.25**. The initial Pu concentration for fresh resin 1 was 0.2 Bq/mL for ~20 mg sorbent.

The fraction Pu sorbed for fresh resin 1 was 0.8 at 1440 mins contact duration with corresponding conditional K_D of 1.9×10^3 mL/g. The aged resin 1 showed reduced Pu sorption, 0.3, at contact duration of 1440 mins. The fraction Pu sorbed at contact duration of 1440 mins for fresh resin 2 was 0.8.

The fraction Pu sorbed for resin 1 at batch contact duration of 1440 mins decreased significantly from 0.8 to 0.3 after uncontrolled exposure to fluorescent light at room temperature for 3 months. Kinetic studies performed on a new batch of HESR-II(57), resin 2, shows fresh resin has faster kinetics and higher Pu sorption. This depicts degradation of resins with time. TiO_2 is photocatalytic in nature. Polymer degradation using TiO_2 has been studied by Shang et al. (2003). They demonstrated the formation of reactive oxygen species during photodegradation of polystyrene plastic by TiO_2 (Shang et al., 2003). The decrease in the performance of the aged resin is speculated due to the formation of degradation

byproducts with Pu(V) reducing its affinity for sorption on resin or hindering the reduction of sorbed Pu(V) to Pu(IV). Fresh resin has been used for all the experiments in this research except where stated otherwise.

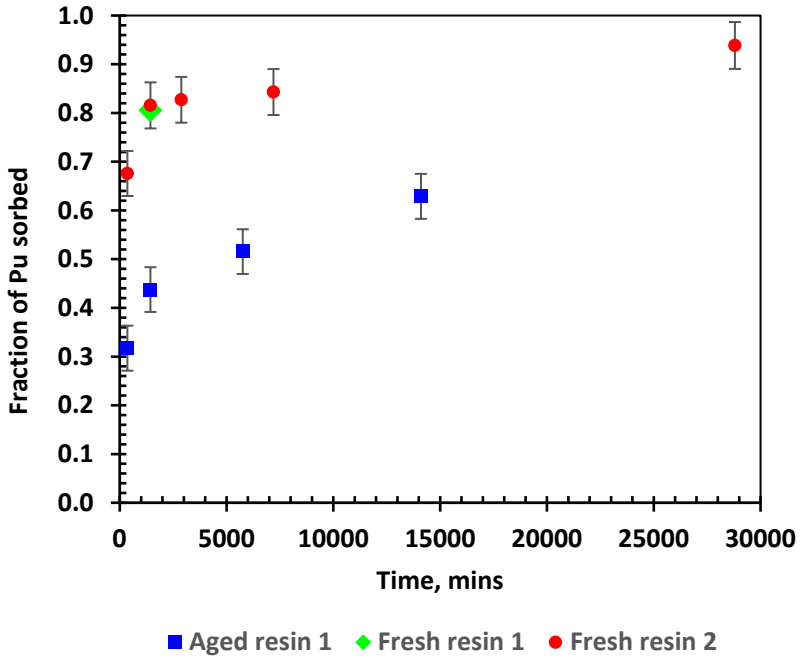

Figure 5.25. *Fraction of Pu sorbed. Aged resin: intermittently exposure to the fluorescent light at room temperature for 3 months. Fresh resin: not exposed to light.*

Aged resin 1, fresh resin 2: pH=6, sorbent=25 mg, initial Pu concentration=0.3 Bq/mL, volume=10 mL. Fresh resin 1: initial Pu concentration=0.2 Bq/mL, sorbent= ~20 mg, volume=10 mL, pH=6, contact = 1440 mins.

Microscopy imaging revealed the surface morphology and the structural deformity associated with the resin aging as shown in **Figure 5.26**. Further studies need to be conducted to understand the photodegradation of the resin.

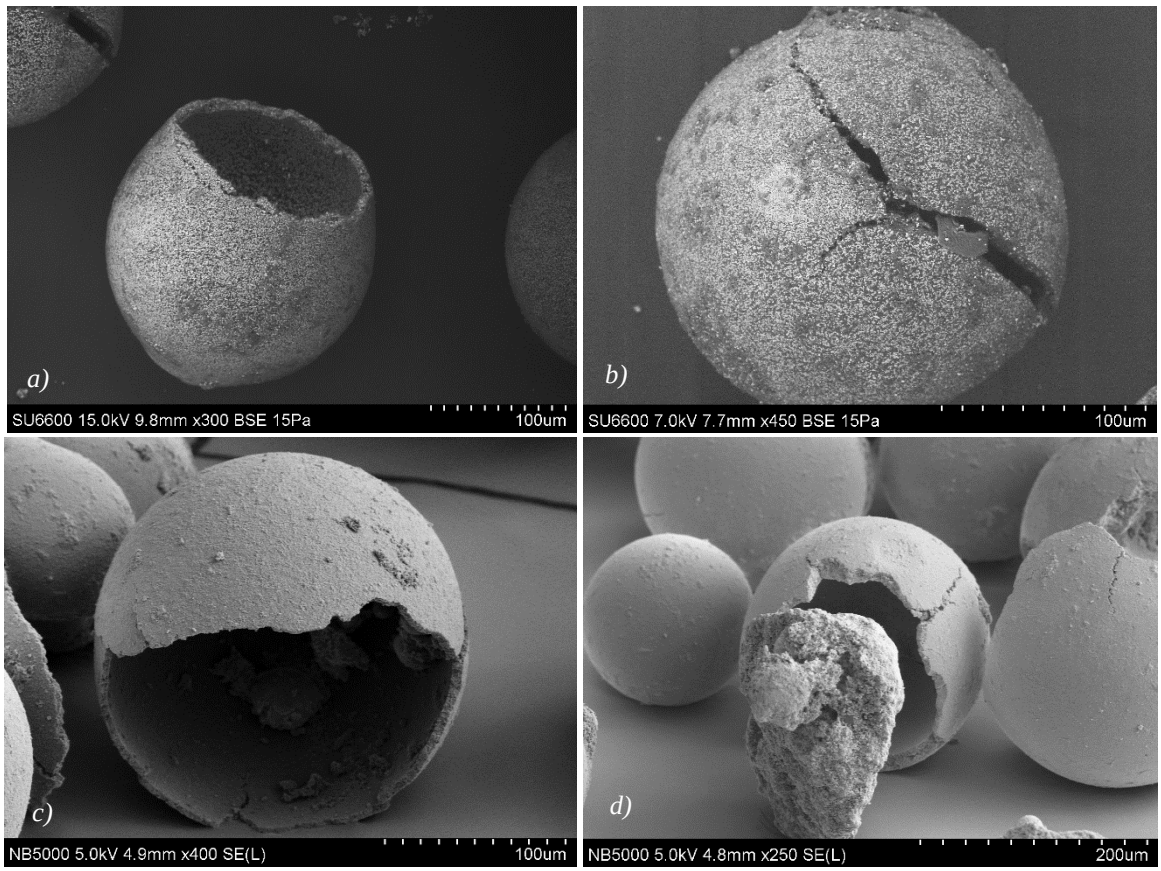

Figure 5.26. *a) b) SEM, c) d) FIB of aged HESR-II(57) intermittently exposure to the fluorescent light at room temperature for 3 months.*

5.4 Kinetic studies

HESR-II(57) was selected for kinetic studies because of the superior Pu uptake property and good Pu detection efficiency. The fraction of Pu sorbed versus contact time was plotted for each reactor to see the trend in Pu sorption. As evident from the **Figure 5.27**, Pu sorption to HESR-II(57) is slow. The overall kinetics of Pu(V) is considered to be slow with respect to other oxidation states of Pu based on studies performed by Begg et al. (2013) on montmorillonite. This is because of the two-step process involved in the sorption of Pu(V) where first it gets sorbed to the solid surface and further gets reduced to Pu(IV). The slower uptake trend of Pu(V) was explained by the slower reduction rate of these species to Pu(IV) on the resin surface.

The rate of Pu sorption to HESR-II(57) is proportional to the number of active sites available for Pu binding. The kinetics of Pu sorption to resins for the reactors with lower sorbate/sorbent ratios at given Pu concentration was slower due to limited availability of active sites for Pu binding. About 15% of plutonium was sorbed in first 10 mins for reactor 1R(6-0.30) and 3R(6-1.00) corresponding to the q_t value of 6.6×10^{-8} mg/g (mg of Pu sorbed per g of sorbent) and 2.4×10^{-7} mg/g, respectively. There was no significant increase in Pu sorption until 120 mins. Pu uptake studies performed by Begg et al. (2013) noted 10-15% Pu sorption within 60 mins of batch contact. Kinetics was observed to be comparatively faster for reactors with lower sorbate/sorbent ratios at given Pu concentration because of a higher number of Pu binding sites available on the resins. For higher sorbent amount reactors, 2R(6-0.04) and 4R(6-0.15), there was about 25% Pu sorption in first 10 mins and 50% sorption during initial 120 mins of batch contact. Dzombak et al. (1986) concluded

that with sorption kinetics of the sorbate slows as the ratio of sorbate/sorbent increases which agrees with the present research results in this report.

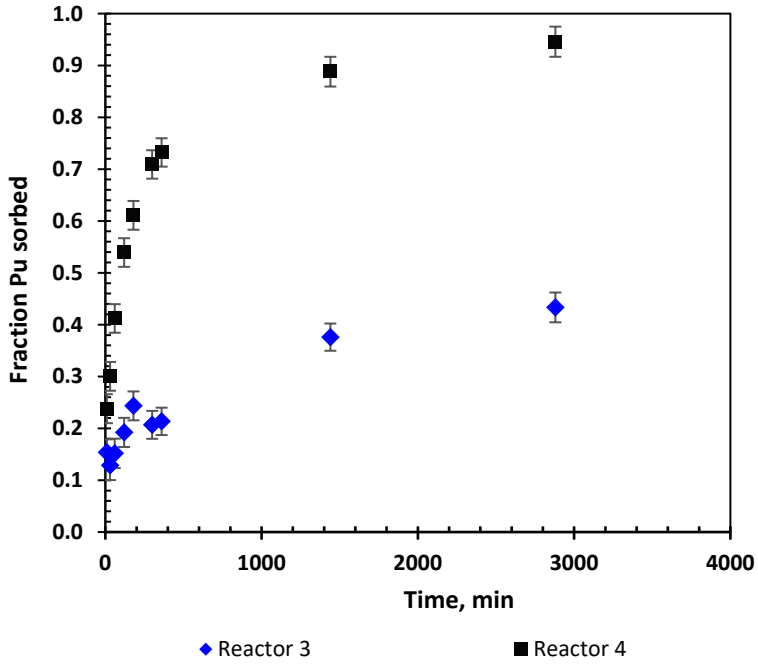

Figure 5.27. *Sorption kinetics of HESR-II(57) in reactors 3 and 4, 106-212 µm sized particles. volume= 45 mL. Reactor 3= 3R(6-1.00), Reactor 4= 4R(6-0.15)*

Based on the kinetic data it was noticed that Pu sorption to HESR-II(57) increases with an increase in pH that can be explained by the point of zero charge for TiO_2 (rutile) which occurs between pH 5.7-7 (Kosmulski, 2011). Pu(V) exists as a hydrated cation in aqueous solution with a higher affinity towards net negative surfaces which explains the sorption trend in **Figure 5.28.** This influences the sorption of Pu(V) on TiO_2 as it exists in hydrated cation inheriting overall positive charge, an overall negative charge on TiO_2 surface increases Pu sorption. Hence, there is an increase in Pu uptake as the pH increases.

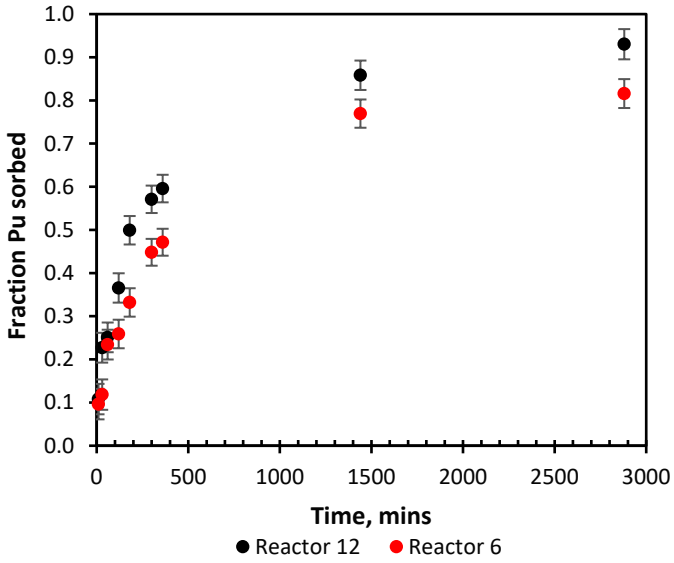

Figure 5.28. *Sorption kinetics of HESR-II(57) in reactors 6 and 12, 106-212 µm sized particles. volume=45 mL.*
Reactor 12=12R(8.5-0.50), Reactor 6=6R(6-0.50)

Pu uptake studies performed by Olsson et al. (2003) showed an increase of Pu sorption to TiO_2 with an increase in pH (pH 2-10). The K_D reported by Singh et al. (2015) for Pu uptake with BEPBs for 120 mins contact duration was 370 mL/g. The conditional K_D for Pu sorption to HESR-II(57) for 1440 mins contact time was 1081 mL/g and 4736 mL/g at pH 6 and 8.5, respectively. This indicates the kinetics of the HESR-II(57) is slow but has high Pu sorption properties.

5.4.1. Pseudo first-order model

Pseudo first-order rate equation was used to model the rate of disappearance of $[Pu(V)]_{aq}$ from the solution. **Equation 5.1** gives the overall reaction. $\equiv TiO_2$ represents the solid TiO_2-HESR surface on which Pu is sorbed. Hence a plot of $\ln([Pu]_{aq,t}/[Pu]_{aq,i})$ versus

time generates required rate constant, k_1 (min^{-1}) as slope which is the rate of disappearance of $Pu(V)_{aq}$ for given rate **Equation 4.9**.

$$\equiv TiO_2 + Pu(V)_{aq} \overset{k1}{\leftrightarrow} \equiv TiO_2Pu(V) \qquad \textit{Equation 5.1}$$

Pseudo first-order model considers the aqueous Pu concentrations for obtaining the rate constant. The model fits the best for reactors 7R(8.5-0.30) followed by 1R(6-0.30) with correlation coefficient, R^2, of 0.99 and 0.97. Both these reactors had low sorbent quantity and the lowest initial plutonium concentration. **Figure 5.29** and **Figure 5.30** depicts the pseudo first-order model at pH 6.

For the reactor 8R(8.5-0.04) with high sorbent quantity and the lowest initial Pu concentration, the correlation coefficient was 0.429. Ho et al. (1999) in their kinetic studies concluded that if the sorption is a multiple pseudo first-order stepped reaction the plot will be a combination of multiple linear sections representing each reaction step. Pu(V) sorption to a surface involves two steps. The first is the sorption of Pu(V) to the resin surface and the second the reduction of sorbed Pu(V) to Pu(IV). The multiple linear sections are more prominent in reactors with higher sorbent mass as shown in **Figure 5.30**. The graphs at pH 8.5 are listed in **Appendix E**. The pseudo first-order model fit at pH 8.5 was similar to pH 6. **Table 5.6** summarizes the rate constants and the correlation coefficients, R^2, which were obtained from the plotted graphs.

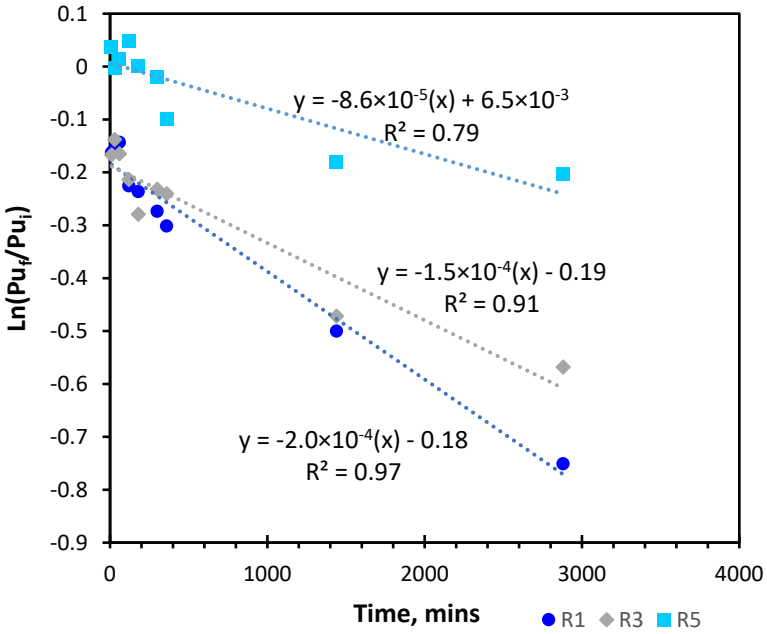

Figure 5.29. *Pseudo first-order model, R1=1R(6-0.30), R3=3R(6-1.00), R5=5R(6-3.20)*

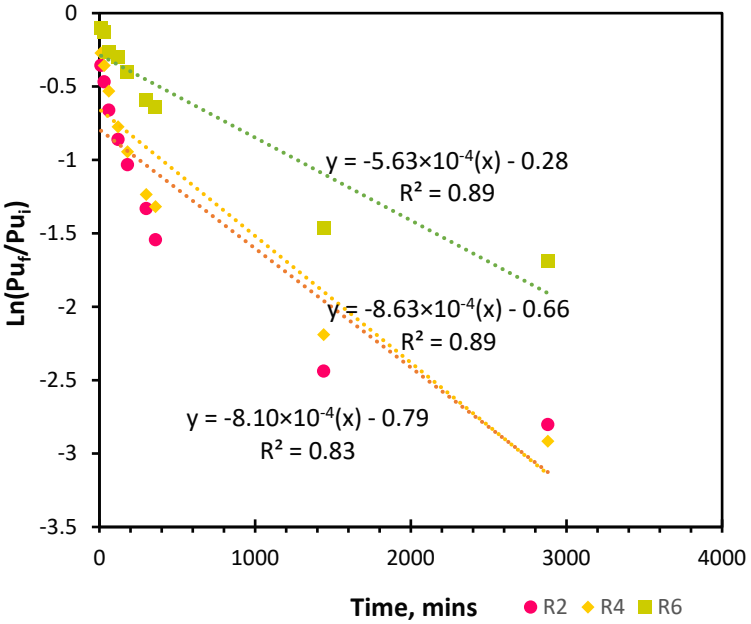

Figure 5.30. *Pseudo first-order model, R2=2R(6-0.04), R4=4R(6-0.15), R6=6R(6-0.50)*

Table 5.6. *Pseudo first-order rate constants*

Reactor	Rate constant, min^{-1}	R^2
1R(6-0.30)	2.04×10^{-4}	0.97
2R(6-0.04)	8.10×10^{-4}	0.83
3R(6-1.00)	1.46×10^{-4}	0.91
4R(6-0.15)	8.63×10^{-4}	0.89
5R(6-3.20)	8.59×10^{-5}	0.79
6R(6-0.50)	5.63×10^{-4}	0.89
7R(8.5-0.30)	6.58×10^{-4}	0.99
8R(8.5-0.04)	4.47×10^{-4}	0.43
9R(8.5-1.00)	6.86×10^{-5}	0.77
10R(8.5-0.15)	8.73×10^{-4}	0.88
11R(8.5-3.20)	1.02×10^{-4}	0.90
12R(8.5-0.50)	8.59×10^{-4}	0.94

5.4.2. Pseudo second order rate model

Pseudo second-order rate equation was used to model the rate of disappearance of $[Pu(V)]_{aq}$ from the solution. **Equation 5.2** gives the overall reaction considered for the second-order kinetic model. Hence a plot of $1/[Pu]_{aq,t}$ versus time generates required rate constant, k_2 (Bq^{-1} min^{-1}) as slope which is rate of disappearance of $Pu(V)_{aq}$ from the solution for the rate **Equation 4.11**.

$$\equiv TiO_2 + Pu(V)_{aq} \overset{k2}{\leftrightarrow} \equiv TiO_2Pu(V) \qquad \textit{Equation 5.2}$$

Pseudo second-order model considers the aqueous Pu concentrations for obtaining the rate constant as depicted in **Figure 5.31** and **5.32**. Pseudo second-order model fits better for almost all the reactors compared to pseudo first-order model for Pu sorption to HESR-II(57). Pseudo second-order model fits the best for 10R(8.5-0.15) and 12R(8.5-0.50) with the correlation coefficient of 0.999 and 0.997, respectively. Both these systems had high sorbent quantity with high and intermediate initial Pu concentration.

Singh et al. (2015) performed a kinetic study of Pu(IV) on BEPBs. They used pseudo first-order model and pseudo second-order model. Comparing the correlation coefficient for both the models it was concluded that pseudo second-order model fits better. Pseudo first order model fit well for the initial step of the reaction but not for the entire sorption duration. It was concluded that the rate-limiting step for sorption of Pu on BEPBs might be due to chemical sorption or the mass transport.

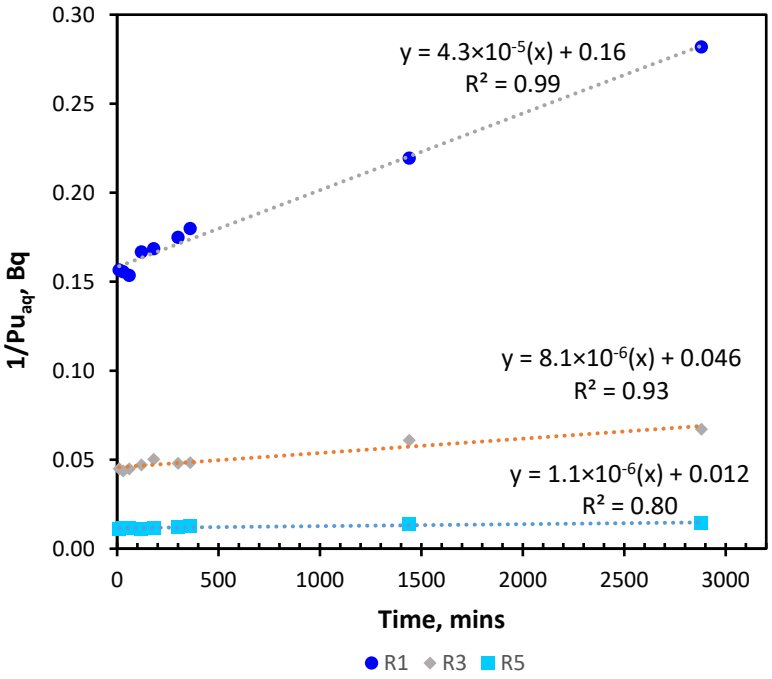

Figure 5.31. *Pseudo second-order model*

R1=1R(6-0.30), R3=3R(6-1.00), R5=5R(6-3.20)

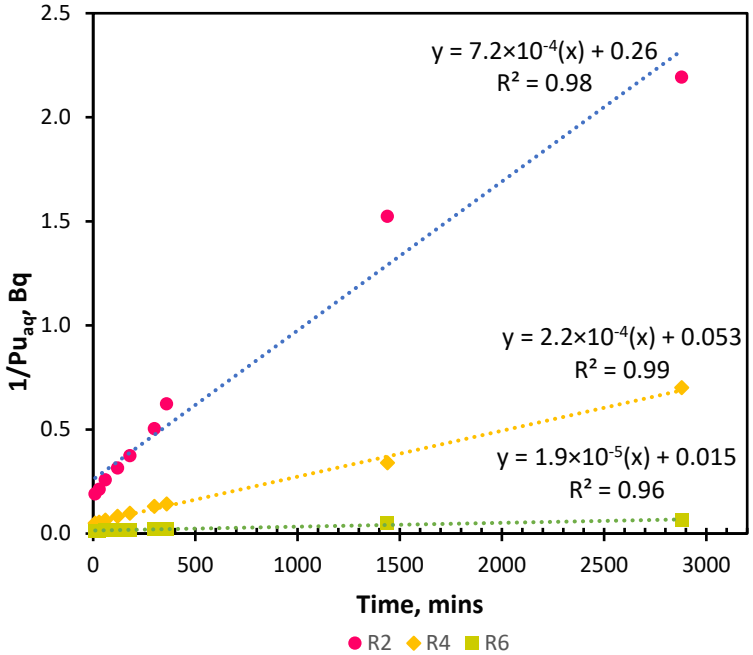

Figure 5.32. *Pseudo second-order model*

R2=2R(6-0.04), R4=4R(6-0.15), R6=6R(6-0.50)

Hence, it was concluded that the sorption of Pu(V) on the surface of HESR-II(57) was explained better with pseudo second-order model which agrees with the literature survey. Comparatively faster initial Pu(V) sorption for all the reactors followed by a slower rate is due to the availability of fresh active sites on the resins and hence the driving force for sorption is much higher. As time passes and Pu(V) accumulates, the equilibrium is shifted backward reducing the sorption rate. Further slow reduction of sorbed Pu(V) to Pu(IV) shifts the equilibrium forward increase the sorption of $Pu(V)_{aq}$ to the resin. Pseudo second-order model fits better compared to pseudo first-order for both pH 6 and 8.5. Graphs for reactors at pH 8.5 are listed in **Appendix E**. **Table 5.7** summarizes the rate constants and the correlation coefficients, R^2, which were obtained from the plotted graphs.

Table 5.7. *Summary of pseudo second-order rate constants, HESR-II(57)*

Reactor	Rate constant, $Bq^{-1}\ min^{-1}$	R^2
1R(6-0.30)	4.31×10^{-5}	0.99
2R(6-0.04)	7.16×10^{-4}	0.98
3R(6-1.00)	8.06×10^{-6}	0.93
4R(6-0.15)	2.21×10^{-4}	0.99
5R(6-3.20)	1.10×10^{-6}	0.80
6R(6-0.50)	1.85×10^{-5}	0.96
7R(8.5-0.30)	3.72×10^{-4}	0.98
8R(8.5-0.04)	4.94×10^{-4}	0.64
9R(8.5-1.00)	3.22×10^{-6}	0.79
10R(8.5-0.15)	1.96×10^{-4}	0.99
11R(8.5-3.20)	1.36×10^{-6}	0.92
12R(8.5-0.50)	5.28×10^{-5}	0.99

5.4.2 Reaction order

Rate equation of the Pu sorption to HESR-II(57) is given by **Equation 5.3**. 'R' denotes the rate of reaction, 'k' is the overall rate constant, 'x' is the rate order in terms of TiO_2 and 'y' in terms of Pu. 'k'' ($Bq^{-1}min^{-1}$) is pseudo second-order rate constant of Pu sorption to resins for given amount of TiO_2 which was obtained from the **Table 5.7**. **Figure 5.33** shows the plot of log k' versus log[Pu]. Rate order, y, is 1.5 obtained from the slope of the plot. Fractional rate order denotes multiple step sorption process which indicates an intermediate Pu reduction step as mentioned in the literature. Overall rate constant of the reaction, k, obtained from the intercept of **Equation 5.5**, is 2.4×10^{9} $mol^{-1}s^{-1}$.

$$R = k[TiO_2]^x[Pu]^y \qquad \textit{Equation 5.3}$$

$$k' = k[Pu]^y \qquad \textit{Equation 5.4}$$

$$log\ k' = log\ k + y\ log[Pu] \qquad \textit{Equation 5.5}$$

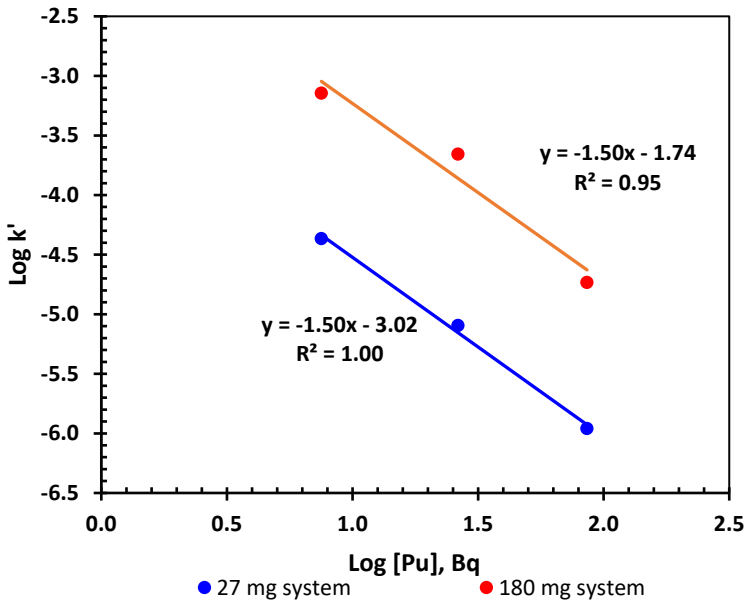

Figure 5.33. *Reaction order plot for pseudo second-order model*

5.4.3 Plutonium detection efficiency

Plutonium detection studies were performed using batch uptake followed by off-line detection as explained in **Section 4.5.2**. Batch uptake test was considered more favorable because of the slow Pu(V) sorption kinetics on HESR-II, as explained in **Section 5.4,** and the less resident time of sorbate (plutonium) at sorbate-sorbent interface system in a flow cell.

Table 5.8 summarizes the detection efficiency for the resin from each reactor at the end of 2880 mins. The Pu sorbed resins, after the batch contact, were transferred to a column and allowed to dry at room temperature for two weeks. Theoretically, all the reactors should have the same Pu detection efficiency.

Table 5.8. *Summary of detection efficiency*

Reactor	Pu Detection efficiency (%)	Detection error (%)
1R(6-0.30)	74.5	9.7
2R(6-0.04)	86.2	6.2
3R(6-1.00)	84.2	5.3
4R(6-0.15)	92.7	2.1
5R(6-3.20)	115.2	17.6
6R(6-0.50)	101.9	3.3
7R(8.5-0.30)	93.5	7.1
8R(8.5-0.04)	96.7	7.0
9R(8.5-1.00)	78.5	13.4
10R(8.5-0.15)	99.4	2.4
11R(8.5-3.20)	98.2	10.7
12R(8.5-0.50)	96.9	2.7
	Average: 93.2 **SD: 11.1**	

The detection response of HESR-II(57), 106-212 µm, using the data from these twelve reactors was plotted in **Figure 5.34**. The x-axis is the sorbed activity which is the measure of accumulated Pu after batch uptake and the y-axis is the net count rate which is the count rate obtained by column experiments with Pu concentrated resins. The net column count rate (cps) as given by the **Equation 4.6**. The Pu detection efficiency, 99.9%, is obtained from the slope of the trendline which has a correlation coefficient of 0.997.

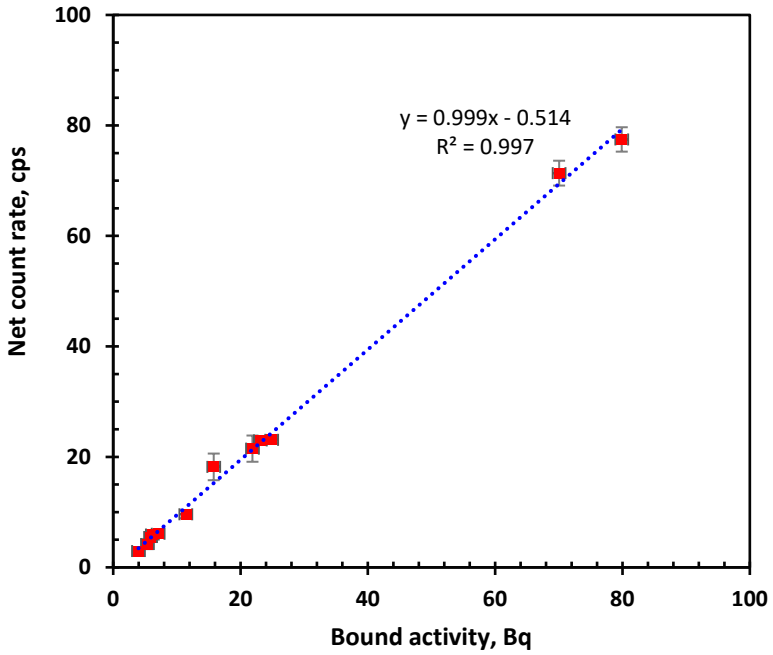

Figure 5.34. *Linear detection response of the HESR-II(57), 106-212µm*

Figure 5.35 is the pulse height spectrum for 12R(8.5-0.50) at the end of 2880 mins batch contact duration and the count time of 120 mins. The spectrum is relative to the background which was measured keeping all the conditions same as 12R(8.5-0.50) setup.

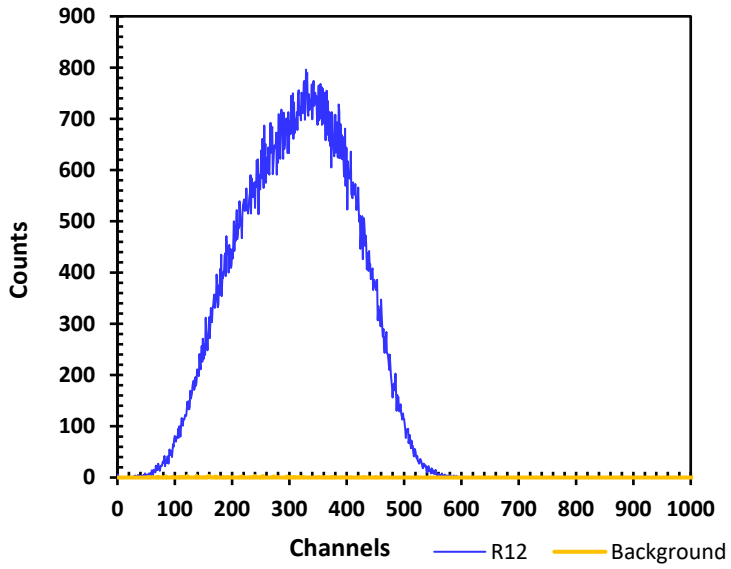

Figure 5.35. *Pulse height spectra for R12 after 2880 mins batch contact duration with sorbed* ^{238}*Pu as the source and count time of 120 mins.* $R12 = 12R(8.5\text{-}0.50)$

Minimum detectable concentration

Pu detection limit of HESR-II(57) was calculated for batch cell setup. A Pu(V) solution of volume 45 mL and concentration 1.9 Bq/mL was transferred to 120 mL polycarbonate vial containing 180 mg HESR-II(57). The contact duration in the batch cell was 24 hours at pH 8.5. MDC calculated using the **Equation 4.7**. C_b was 3.9 CPM, volume was 45 mL, calculated E_s was 73.7%, calculated average E_d was 93.2%, and the count time was 180 mins. The calculated MDC of aqueous Pu for batch cell setup was 0.38 Bq/L which is below the MCL with respect to gross alpha-emitting radionuclides of 0.56 Bq/L set by the United States Environmental Protection Agency for drinking water (EPA, 2000).

5.4.4 Langmuir Isotherm

Plutonium sorption to HESR-II(57) is explained by Langmuir isotherm. The linear form of Langmuir isotherm is depicted by **Equation 4.12**. From the **Figure 5.36**, slope of the line is inverse of $q_{max.}$ The obtained maximum sorption capacity for the current study is 1.04×10^{-3} µg/g. After 360 mins there was an increase in sorption is due to shift in equilibrium because of the assumed reduction of sorbed Pu(V) to Pu(IV) facilitating further uptake of $Pu(V)_{aq}$. Hence, q_{max} is anticipated to be higher than the currently measured if the system reaches actual equilibrium. The specific activity of the isotope also governs the value of q_{max}. The specific activity of ^{238}Pu is 6.34×10^{11} Bq/g and 1.45×10^{8} Bq/g for ^{242}Pu. Hence, the mass of ^{238}Pu will be less than that of ^{242}Pu by three orders of magnitude for the given activity. The Langmuir model assumes the sorbate forms only monolayer on sorbent with no diffusing between the planes of sorption.

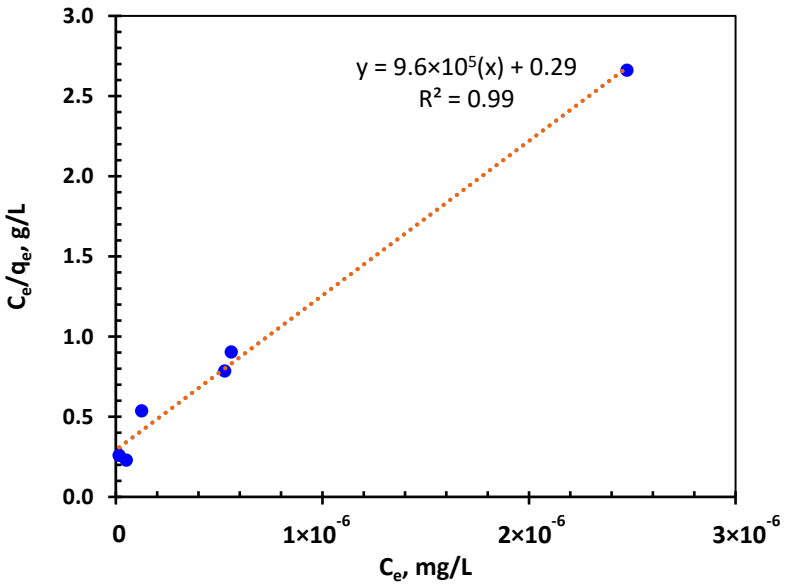

***Figure 5.36**. Linear Langmuir isotherm to obtain value of q_{max}*

Increasing the initial Pu concentration results in an increase in sorbed Pu as depicted from the sorption isotherm in **Figure 5.37**. The sorption limiting factor in case of lower initial Pu concentration is the number of Pu(V) aqueous ions transferred from bulk to the resin active sites. In case of higher initial Pu concentration, there is an observed proportional increase which means the insufficient active sites on the resins acts as the limiting factor for Pu sorption. This agrees with the isotherm studies performed by Singh et al. (2015) for Pu sorption using BEPBs.

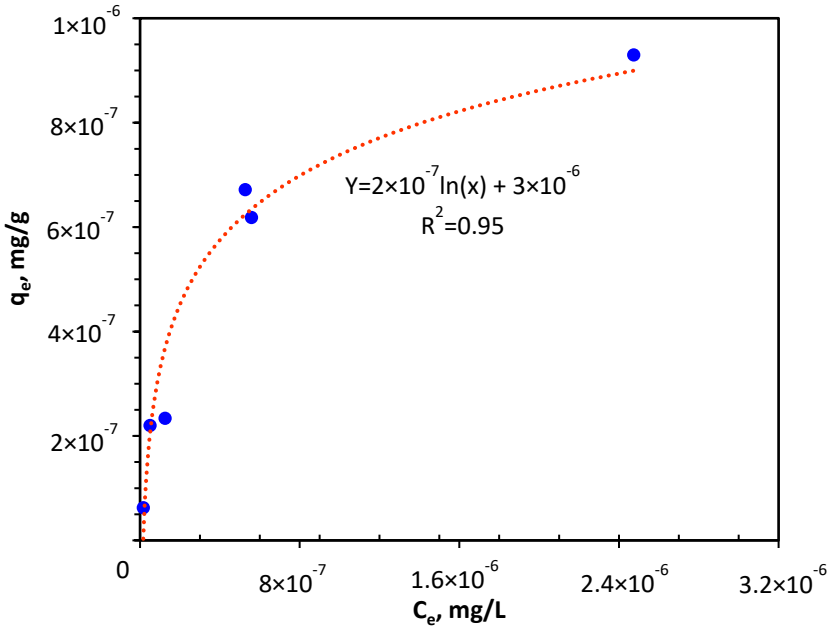

Figure 5.37. *Langmuir sorption isotherm*

CHAPTER 6

CONCLUSION

Plutonium sensors for groundwater and surface water can be very beneficial for monitoring contaminated sites. This research has hence aimed at the development of hybrid extractive scintillating resin capable of uptake and detection of Pu under near-neutral pH conditions. HESR-II(57) displays an average of 93% Pu detection efficiency at pH 6-8.5 for ^{238}Pu(V). HESR-II(57) displays linear Pu detection response and minimum detectable concentration of Pu(V) is 0.38 Bq/L. It is below the MCL with respect to gross alpha-emitting radionuclides of 0.56 Bq/L set by the United States Environmental Protection Agency for drinking water. HESR detection system can be used with minimal alteration in pH for natural water samples.

HESR-I displayed reasonable Pu uptake but poor radioluminosity and Pu detection. SAAd resins had the highest fraction Pu sorption of 0.93 ± 0.05. HAAd resins comparatively had a smaller fraction Pu sorbed, 0.43 ± 0.05. SiP resins displayed poor Pu uptake with fraction Pu sorption of 0.2 ± 0.04. Radioluminosity measurements of all the three formulations show poor light output indicating poor detection efficiency of the systems. SAAd resins displayed detection efficiency of 1.9 ± 1.2%. Due to low Pu detection efficiency of HESR-I, these resins are not suitable for off-line or on-line detection system.

HESR-II displayed promising Pu uptake and Pu detection values at near neutral pH. Highest performance was showed by HESR-II(57) with 57% of TiO_2 by weight and average fraction Pu sorption of 0.74 ± 0.10 (conditional K_D of 1.3×10^3 mL/g) at 1440 mins

contact duration. There was a difference in Pu detection efficiency with the resin size. HESR-II(57) size of <106 µm had 35.5 ± 3.0 % Pu detection, 106-212 µm with 96.4 ± 6.6 % and >212 µm with 89.3 ± 5.4%. HESR-II performed overall better than HESR-I. In the studies performed by Singh et al. (2015), extractive resin BEPBs used for ^{239}Pu sorption in +4 oxidation state displayed highest Pu sorption at 6 M HNO_3 with K_D of ~375 mL/g. Commercially available Pu extractive chromatographic resin, TEVA, displays 70-98% Pu(IV) uptake in acidic conditions of 9 M hydrochloric acid. Hence, HESR-II performs better than the currently available Pu extractive resin with an underlying advantage of high performance at near neutral pH.

Pseudo second-order model was a better fit for Pu(V) sorption to HESR-II(57) in comparison to pseudo first-order model which supports the published results by Singh et al. Sorption of Pu(V) is initially faster because of higher driving force due to the availability of active sites. As time passes, Pu(V) accumulates and the equilibrium is shifted backwards reducing the sorption rate. The sorbed Pu(V) further reduces to Pu(IV) shifting the equilibrium forward which increases the sorption of $Pu(V)_{aq}$ to HESR-II(57). Overall rate constant of the reaction is 2.4×10^{9} $mol^{-1}s^{-1}$. Plutonium sorption to HESR-II(57) is explained by Langmuir isotherm and the maximum Pu sorption capacity on HESR-II(57) is 1×10^{-3} µg/g.

Future work

The sorption of Pu to HESR is a function of the amount of TiO_2 present in the resin. But SAAd(48) and HAAd(48) resin displayed a reduced Pu sorption relative to SAAd(24) and HAAd(24) resin. Further experiments to investigate the reason for reduced Pu sorption can help understand (48) TiO_2 weight % resin behavior.

The fluor is responsible for scintillation properties in the resin. Fluor coated SAAd(24) resin showed an increase in Pu detection efficiency, but Pu sorption decreased with the additional fluor coating on the surface of the resin. The fluor particles may have affected the PZC value of TiO_2 resulting a change in Pu sorption behavior. Experiments to investigate how the presence of additional fluor on the surface affects Pu sorption can help explain the unusual behavior.

The Pu detection efficiency of HESR-II(73) decreased relative to HESR-II(57). The two samples varied in % TiO_2 embedded, amount of porogen and cross-linking. Performing experiments to study the Pu detection efficiency as a function of porosity and cross-linking will help elucidate properties of HESR-II(73).

APPENDICES

APPENDIX A

Fraction Uptake and Detection Efficiencies

Table A.1. *Anatase and Rutile Pu uptake*

pH value	Rutile	Anatase	Fraction of Pu sorbed				Conditional K_D	
			Rutile	error	Anatase	error	Rutile	Anatase
	mg						mL/g	
2.1	11.8	10.7	0.036	0.021	0.212	0.019	16	126
3.4	12.3	12.2	0.543	0.015	0.988	0.003	484	34400
4.3	10.9	10.8	0.813	0.010	0.942	0.006	2000	7460
5.2	15.5	10.2	0.974	0.004	0.984	0.003	11900	29200
6.6	19.2	11.8	0.977	0.004	0.963	0.005	11000	11000
7.2	12.1	10.8	0.951	0.005	0.956	0.005	8100	9990
8.9	11.2	11.3	0.861	0.008	0.930	0.006	2750	5860
9.3	12.4	12.9	0.887	0.008	0.908	0.007	3160	3830

Initial Pu concentration 2.4 Bq/mL, batch volume 5 mL and 24 hours contact time.

Table A.2. *Performance of HESR-I for Pu sorption*

Sample	Weight mg	Fraction of Pu sorbed	error	Conditional K_D mL /g
Blank	21.1	0.196	0.052	116
SAAd(12)	21.3	0.857	0.053	2820
SAAd(24)	20.7	0.931	0.054	6470
SAAd(48)	20.4	0.474	0.050	441
HAAd(12)	19.9	0.276	0.051	192
HAAd(24)	21.7	0.429	0.051	346
HAAd(48)	20.9	0.429	0.050	359

Initial Pu concentration 0.3 Bq/mL, batch volume 10 mL and 24 hours contact time.

Table A.3. *Performance of HESR-II for Pu sorption*

Sample	Particle size µm	Weight mg	Fraction of Pu sorbed	error	Conditional K_D mL /g
	<106	21.4	0.294	0.050	195
HESR-II(4)	**212-106**	24.3	0.246	0.051	134
	>212	21.0	0.174	0.051	100
	<106	21.7	0.228	0.036	136
HESR-II(8)	**212-106**	22.0	0.142	0.036	75.2
	>212	20.3	0.219	0.036	138
	<106	19.5	0.478	0.036	470
HESR-II(14)	**212-106**	23.2	0.315	0.036	199
	>212	20.0	0.299	0.036	213
	<106	21.8	0.400	0.036	306
HESR-II (25)	**212-106**	23.3	0.500	0.036	428
	>212	20.5	0.325	0.036	235
	<106	19.2	0.638	0.036	916
HESR-II (40)	**212-106**	23.9	0.548	0.036	507
	>212	24.9	0.524	0.036	442
	<106	23.9	0.755	0.037	1290
HESR-II (57)	**212-106**	22.1	0.655	0.036	860
	>212	21.4	0.568	0.036	614
	<106	22.2	0.751	0.096	1360
HESR-II (73)	**212-106**	22.8	0.767	0.097	1440
	>212	24.5	0.888	0.099	3250

Initial Pu concentration 0.3 Bq/mL, volume 10 mL and 24 hours contact time.

Table A.4. *Performance of HESR-II for Pu detection*

Sample	Fraction sorbed Pu sorbed	Fraction Pu sorbed error	Pu detected %	Detection error %
HESR-II (57)	0.755	0.037	19.30	1.30
HESR-II (40)	0.638	0.036	23.50	1.50
HESR-II (25)	0.400	0.036	21.60	2.30
HESR-II (14)	0.478	0.036	28.90	2.50
HESR-II (8)	0.228	0.036	27.80	5.50

Initial loading of 0.3 Bq/mL ^{238}Pu(V) on <106 µm HESR-II

Table A.5. *Performance of HESR-II(57) for Pu detection (kinetic studies)*

Reactor	Net column count rate (CR), CPS	Net CR error CPS	Activity accumulated (Batch uptake) Bq	Batch error Bq	Detection %	Detection error %
1R(6-0.30)	2.93	0.01	3.97	0.52	73.95	9.61
2R(6-0.04)	6.10	0.02	7.06	0.51	86.43	6.20
3R(6-1.00)	9.50	0.02	11.41	0.72	83.31	5.26
4R(6-0.15)	22.83	0.06	24.90	0.57	91.72	2.11
5R(6-3.20)	18.33	0.05	15.79	2.41	116.04	17.72
6R(6-0.50)	71.52	0.17	70.04	2.25	102.12	3.29
7R(8.5-0.30)	5.49	0.02	5.87	0.45	93.53	7.11
8R(8.5-0.04)	5.94	0.02	6.15	0.44	96.70	7.01
9R(8.5-1.00)	4.21	0.01	5.38	0.92	78.23	13.39
10R(8.5-0.15)	23.01	0.04	23.11	0.55	99.55	2.39
11R(8.5-3.20)	21.49	0.06	21.88	2.38	98.23	10.67
12R(8.5-0.50)	77.90	0.18	79.88	2.21	97.51	2.70

Table A.6. *HESR-II(57) degradation*

Time (hrs)	Weight (mg)	Initial Activity (Bq)	error	Final Activity (Bq)	error	Fraction Pu sorbed	error
Resin 1 -Aged							
6	25.1	3.230	0.112	2.210	0.093	0.317	0.046
24	25.2	3.230	0.112	1.820	0.085	0.438	0.046
96	25.3	3.230	0.112	1.570	0.079	0.515	0.046
235	25.4	3.230	0.112	1.200	0.070	0.629	0.046
Resin 2- Fresh							
6	19.1	3.24	0.112	1.05	0.0657	0.676	0.0462
24	25.8	3.23	0.112	0.596	0.0517	0.816	0.0473
48	25.5	3.26	0.112	0.563	0.0497	0.827	0.047
120	25.6	3.26	0.112	0.511	0.0477	0.843	0.0471
480	25	3.26	0.112	0.2	0.0335	0.939	0.0481

Specifications mentioned in Figure 5.23.

APPENDIX B

EDX Results

The parameter R stands for spatial resolution in μm. Terms Z, F and A are EDX matrix correction parameters for elemental analysis study. K_{ratio} gives the measure of the relative intensity of spectral lines and describes the effect of the atomic number which governs the backscatter effect and stopping power, absorption, and fluorescence. K-, L-, and M-series are the associated x-rays. **Table B.1-B.5** correspond to selected regions in **Figure 5.4 b)**.

Table B.1. *Selected Area 1 of Figure B.4 sample*

Element x-ray	Weight %	Atomic %	Net Int.	Error %	K_{ratio}	Z	R μm	A	F
W L	100.00	100.00	1577.7	4.61	0.4364	0.4216	0.4222	1.0364	1

Table B.2. *Selected Area 2 of Figure B.4 sample*

Element x-ray	Weight %	Atomic %	Net Int.	Error %	K_{ratio}	Z	R μm	A	F
C K	32.68	86.01	1412.7	3.69	0.1757	0.4527	0.2608	1.1875	1.0
O K	1.11	2.19	41.71	15.48	0.0023	0.3253	0.2006	0.6334	1.0
Ti K	2.16	1.43	39.67	27.07	0.0029	0.1291	0.1141	0.9787	1.0
Pt L	64.05	10.38	450.58	7.30	0.2794	0.3770	0.5577	1.0357	1.1

Table B.3. *Selected Area 3 of Figure B.4 sample*

Element x-ray	Weight %	Atomic %	Net Int.	Error %	K_{ratio}	Z	R µm	A	F
C K	31.83	85.26	1595.0	3.55	0.1713	0.4566	0.2607	1.1792	1.0
O K	1.51	3.05	67.19	11.16	0.0032	0.3279	0.2003	0.6395	1.0
Ti K	1.39	0.93	29.63	37.75	0.0019	0.1298	0.1137	0.9777	1.1
Pt L	65.27	10.77	535.22	7.39	0.2867	0.3800	0.5574	1.0348	1.1

Table B.4. *Selected Area 4 of Figure B.4 sample*

Element x-ray	Weight %	Atomic %	Net Int.	Error %	K_{ratio}	Z	R µm	A	F
C K	100.00	100.00	2124.72	12.47	0.5956	0.2853	0.2853	2.0874	1.00

Table B.5. *Selected Area 5 of Figure B.4 sample*

Element x-ray	Weight %	Atomic %	Net Int.	Error %	K_{ratio}	Z	R µm	A	F
C K	100.00	100.00	4256.10	12.24	0.5956	0.2853	0.2853	2.0874	1.00

Microscopy image displayed structural deformity of aged resin as shown in **Figure B.1** and **B.2**.

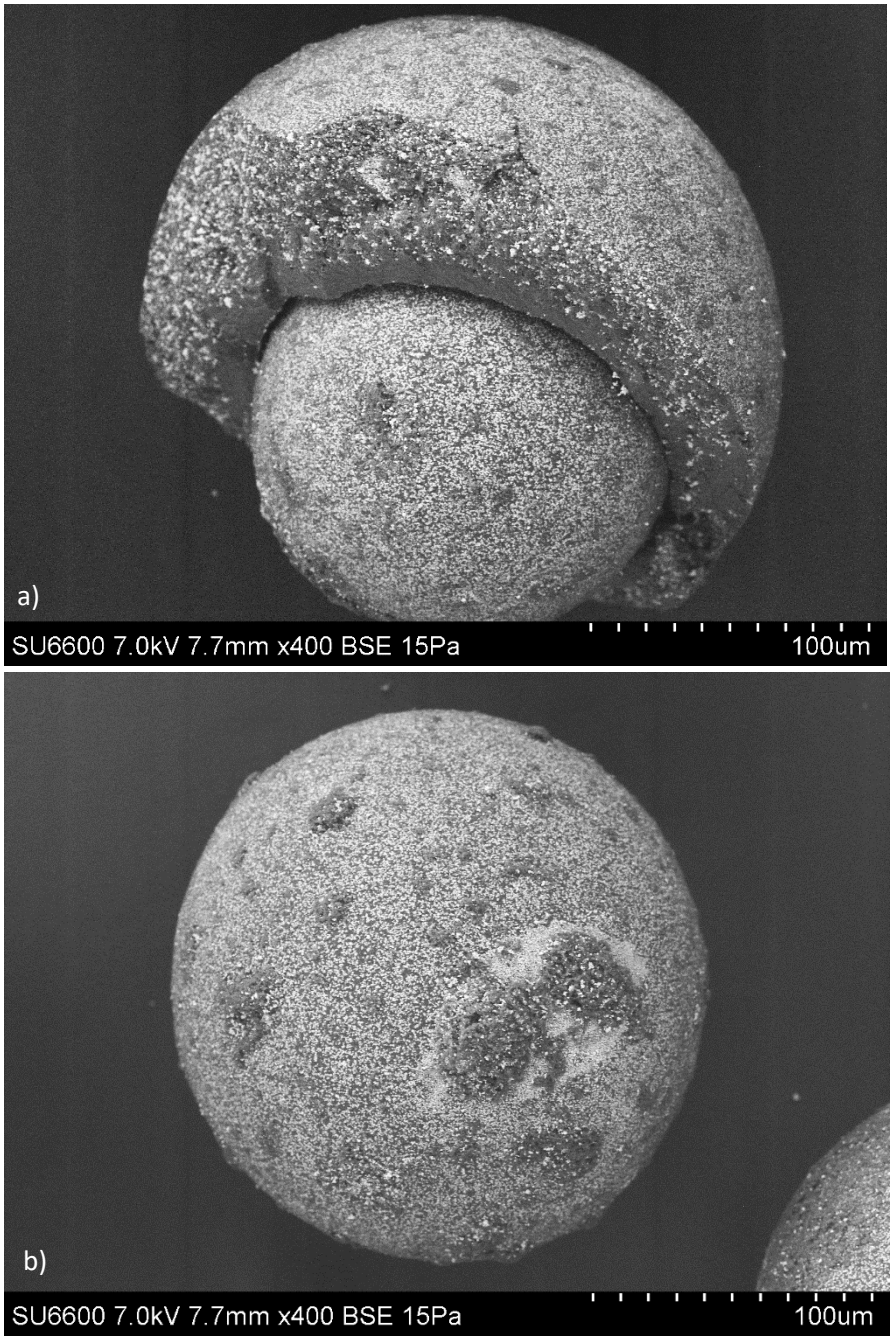

Figure B.1. *a) b) SEM image of aged resin HESR-II(57).*

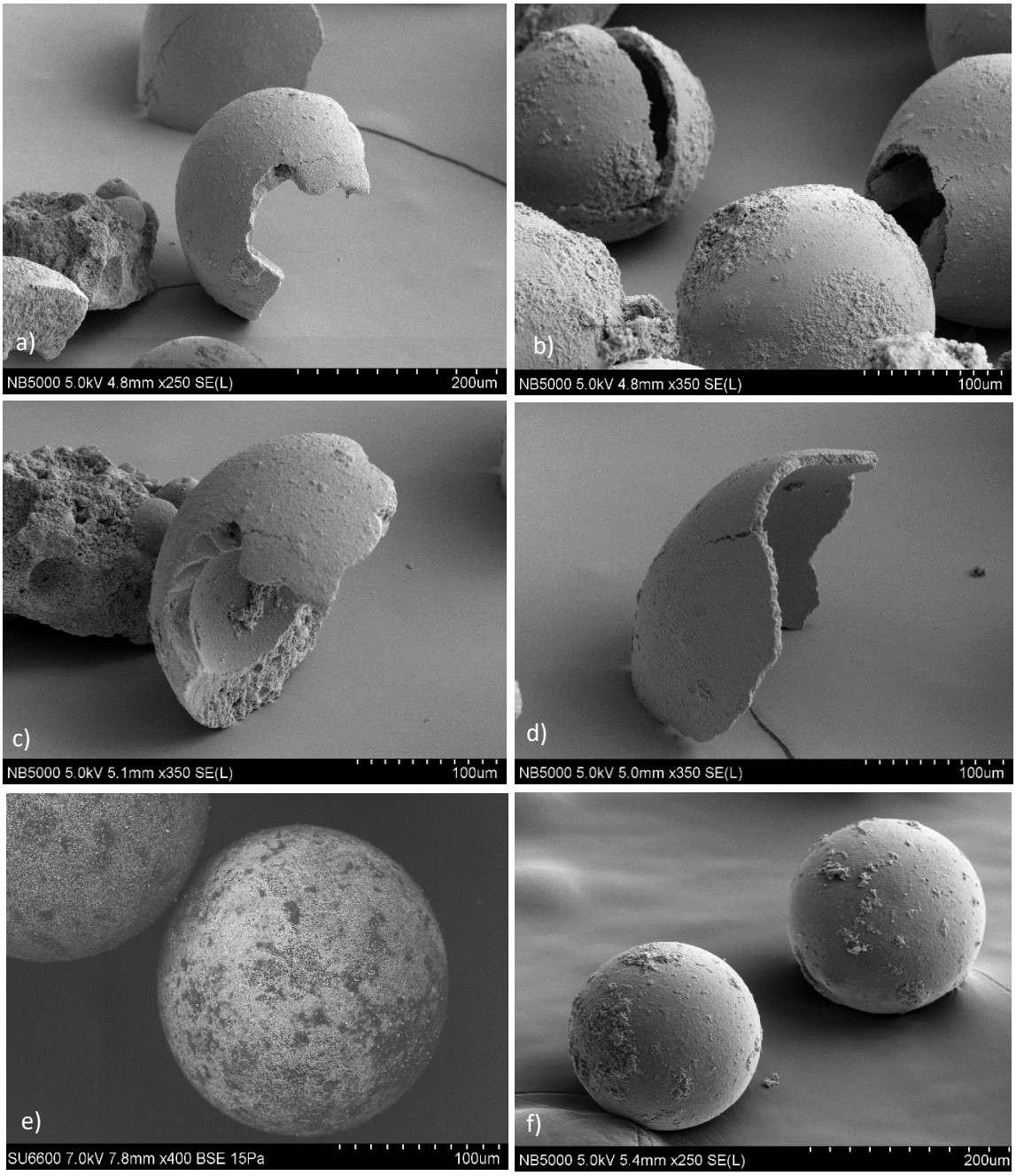

Figure B.2. *FIB image of a) b) c) d) aged HESR-II(57), e) f) fresh HESR-II(57)*

APPENDIX C

Thermogravimetric Analysis

The spectrum for both HESR-I and HESR-II samples follow the similar trend as shown in **Figure C.1** and **C.2**.

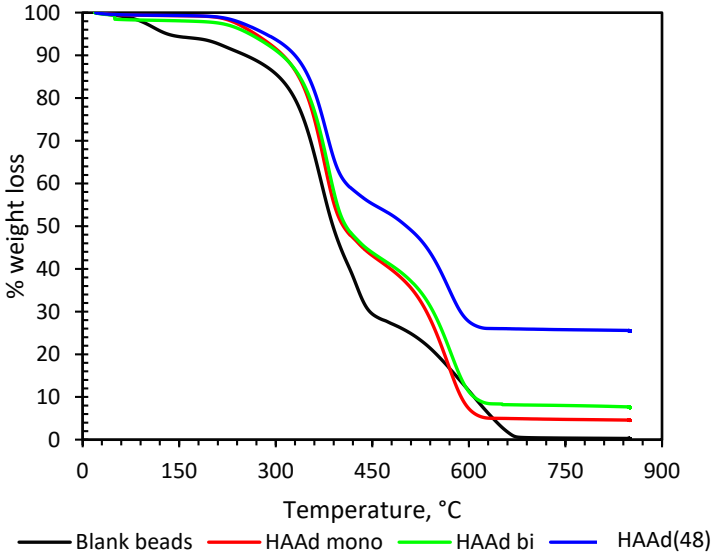

Figure C.1. TGA for HAAd resin, blank beads size was106-212µm

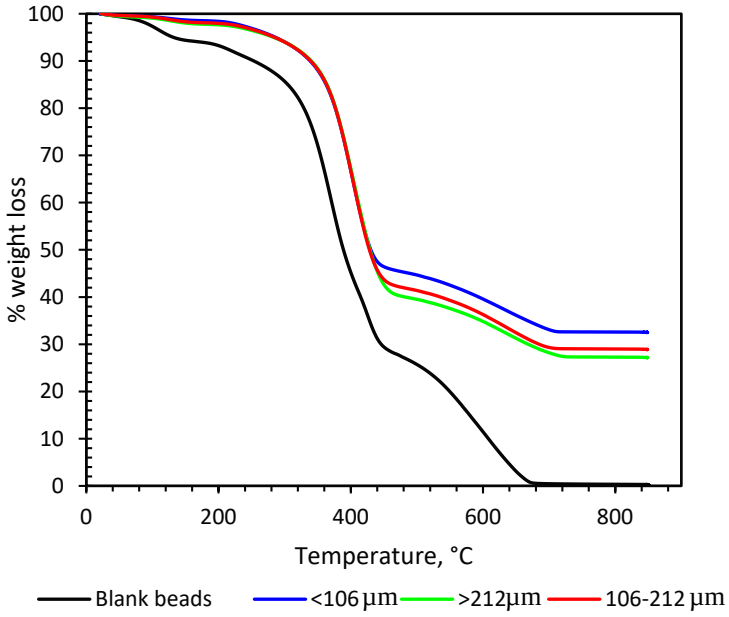

Figure C.2. TGA for HESR-II(40), blank beads size was106-212µm

Table C.1. *Mass balance of TiO_2 in HESR-II*

Sample	Expected TiO_2 g	Actual TiO_2 g	incorporated %
HESR-II(4)	0.15	0.12	80.5
HESR-II(8)	0.30	0.26	85.5
HESR-II(14)	0.60	0.50	83.6
HESR-II(25)	1.20	1.21	101.1
HESR-II(40)	2.40	2.19	91.3
HESR-II(57)	4.80	4.32	90.0

APPENDIX D

Halloysite

Halloysite-TiO_2 method

Halloysite incorporated with TiO_2 consists of the modified outer surface of halloysite using the silane functional group making it hydrophobic. About 0.5 g of halloysite particles (Sigma-Aldrich) were dispersed in a mixture of 5 mL ethanol and 0.5 mL of DDI water in 20 mL scintillation vial. The vial was purged with nitrogen gas for 5 min and then transferred into the glovebox where 1 mL of alkoxysilanes was added. The mixture was stirred for 0.5-2.0 h inside the glovebox at 36°C and then removed and washed three times with ethanol.

About 0.25 g TiO_2 (rutile, 1-3 nm size, PlasmaChem GmbH) was suspended in DMF in 20 mL scintillation vial and sonicated for 15 mins to form an even suspension. Silane functionalized halloysites, 0.1 g, was added to the TiO_2 suspension and sonicated for 15 mins. TiO_2 being hydrophilic is driven into the center of the hollow halloysite matrix. **Figure D.1** depicts the mechanism for incorporating TiO_2 nanoparticles in the inner hollow spacing of halloysite using surface modification using allylmethyldimethoxysilane (silane) functional group.

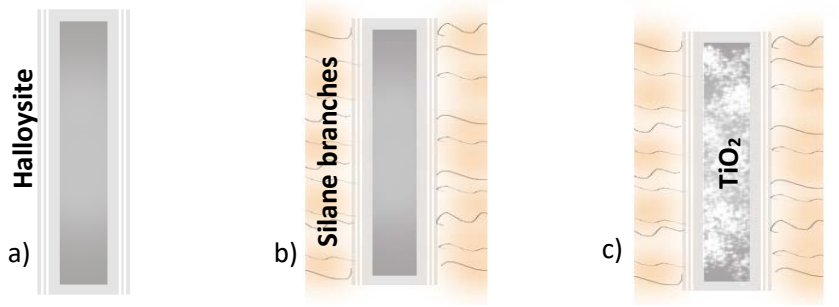

Figure D.1.*. a) Halloysite, b) Surface modification of halloysite by silane functional group, c) Incorporation of TiO_2 in the hallow region of halloysite*

Microscopy was performed using Hitachi H-9500 and H-7600. TEM was used to determine the presence of TiO_2 in the halloysite tubes. As TiO_2 has higher density compared to aluminosilicate halloysites, TEM images displayed TiO_2 darker compared to halloysite. It was further confirmed using EDX.

Halloysites were modified with the silane functional group on the outer surface. This contributed to making the outer surface hydrophobic and aiding the incorporation of TiO_2 nanoparticles in the halloysite. The method has been explained in **Section 4.1.3a.** **Figure D.2a** depicts the TEM imaging of the modified halloysite samples incorporated with TiO_2 in the inner cylinder. **Figure D.2b** depicts the EDX result of the TiO_2 incorporated halloysite confirming the presence of TiO_2 particles in the selected sample region.

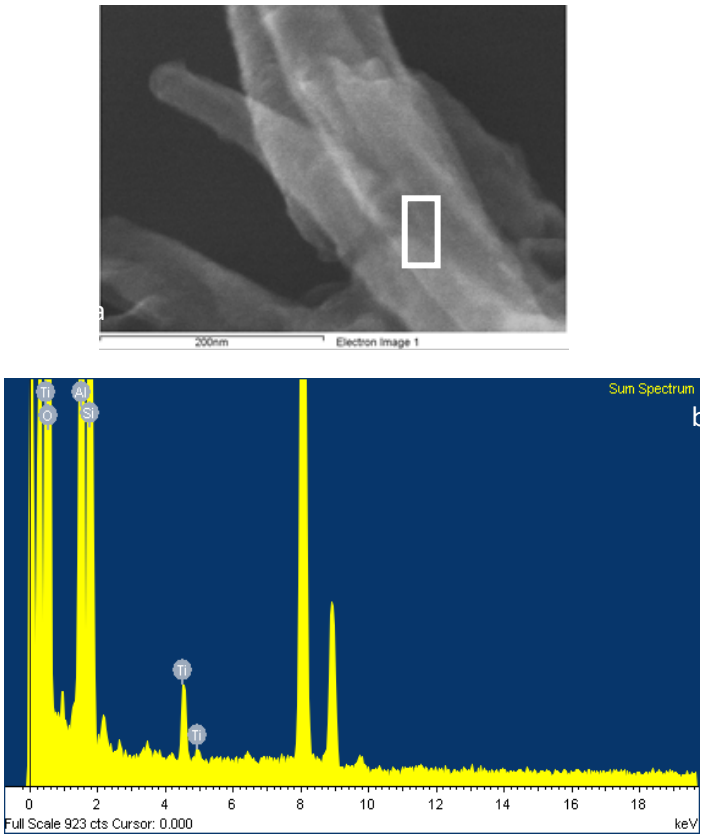

Figure D.2 a) Halloysite-TiO_2 sample b) corresponding EDX analysis of selected area in white box

Figure D.3a shows the cross-linked modified halloysites. Allylmethyldimethoxysilane (silane) brushes present on the halloysite surface polymerized forming a bulky lump. **Figure D.3 b, c, d,** and **e** depict TEM imaging of the halloysite incorporated with TiO_2. As TiO_2 has more density than halloysite particles, it appears darker in TEM image. The TEM and EDX results did not confirm whether the TiO_2 particles were incorporated within the halloysite particles or were trapped in the cross linked silane functional group bulk.

TGA could not be used to quantify the TiO_2 incorporated in halloysites as both halloysites and TiO_2 have a very high boiling point. Further Pu uptake and detection studies were terminated because of the inability to confirm whether the TiO_2 particles were

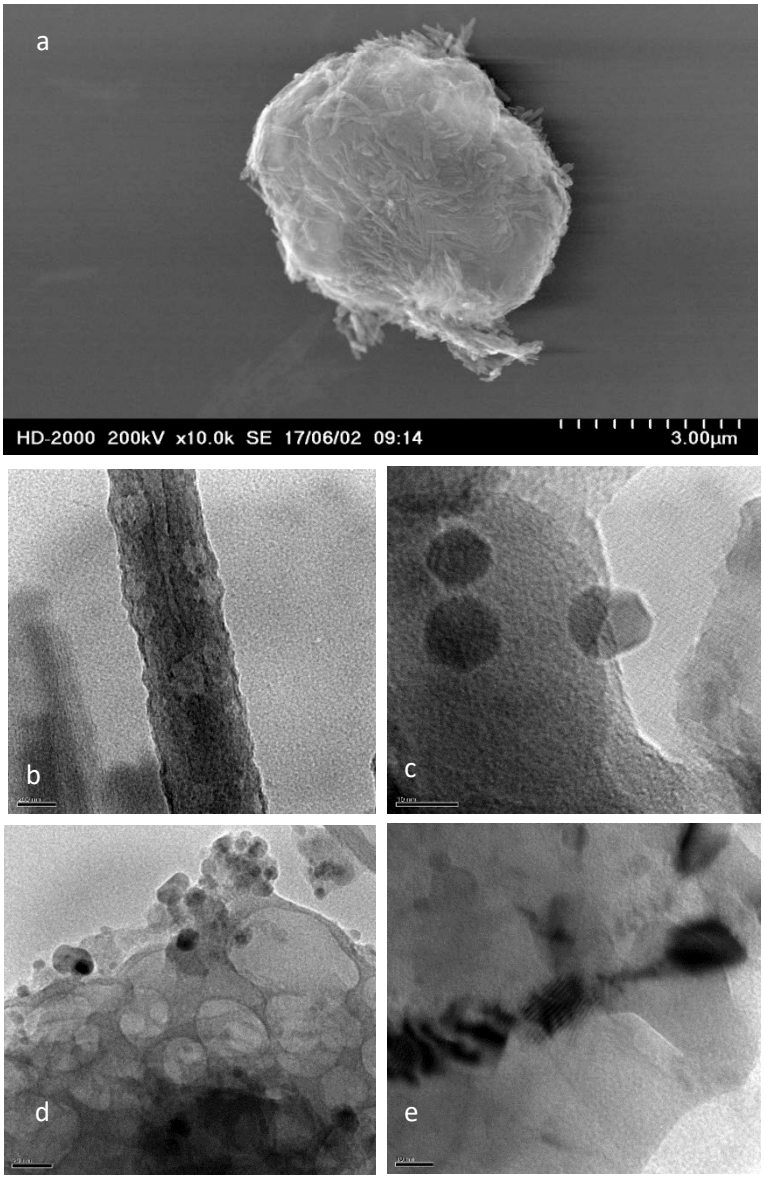

Figure D.3. *a) SEM image of modified halloysite sample b,c,d,e) TEM, results showing of presence TiO_2 in modified halloysite sample*

incorporated within the halloysite particles or were trapped in the cross-linked silane functional group bulk. The TiO_2 particles used to incorporate in halloysite were 1 nm in diameter, extremely small to separate from the aqueous solution in the centrifuge after batch contact. This was assuming TiO_2 particle may detach from the modified halloysites into the aqueous solution during mixing in batch uptake studies based on what was noticed with other formulations in this study.

As the performance of SAAd, HAAd and SiP resins was satisfactory, further Pu uptake and detection studies were only performed on these three formulations and halloysite formulation studies were terminated.

APPENDIX E

Kinetic Studies

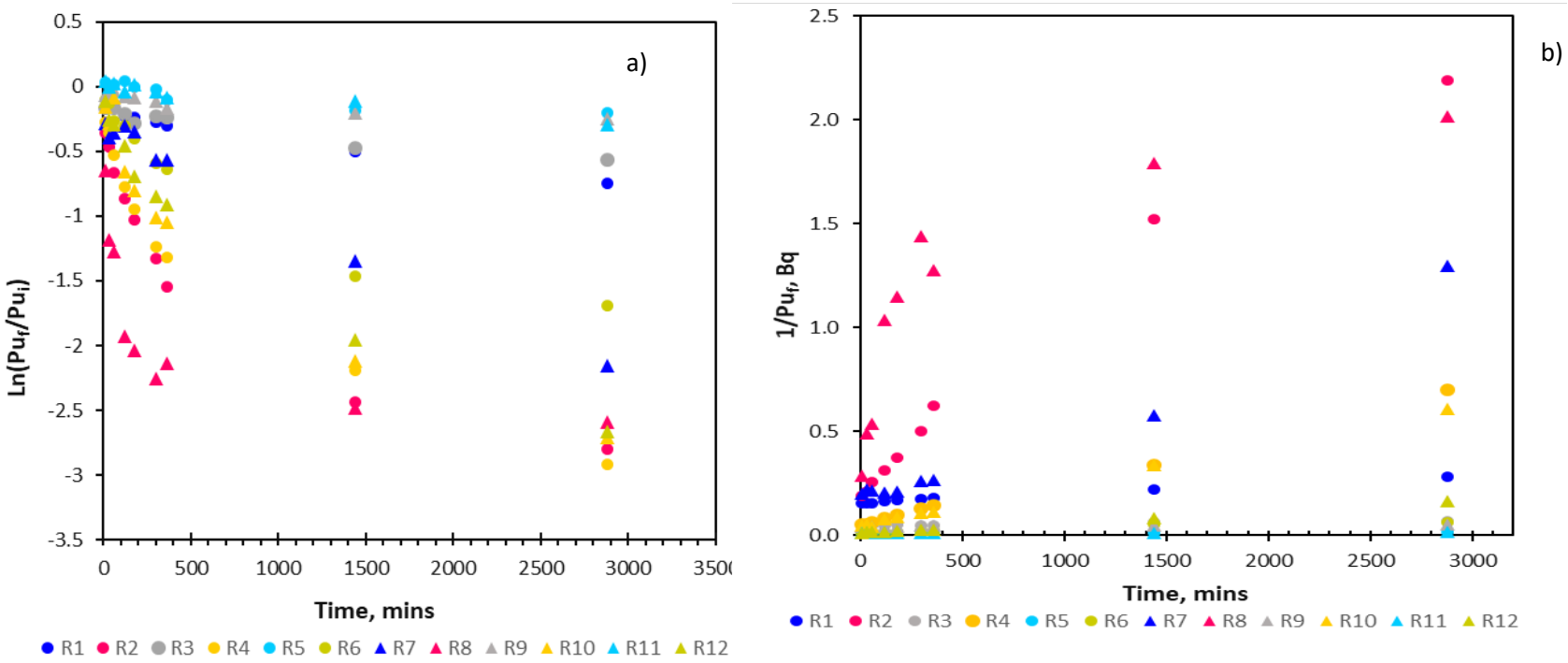

Figure E.1. a) Pseudo first-order, b) Pseudo second-order data for HESR-II(57), 106-212 µm, corresponding to the details mentioned in Table 4.1.

Ho's second-order model: Ho's second-order model is referred as pseudo second-order model in few studies (Wu et al., 2009) (Qiu et al., 2009). To distinguish between pseudo second-order kinetics equation that is based on aqueous plutonium concentration as explained in the previous model from the kinetic equation in terms of sorbed Pu, this model was referred as Ho's second-order-model in present research report (Qiu et al., 2009). The experimental data were fit into the **Equation E.2**. t/q_t versus t was plotted (Ho, 2006). Value of the rate constant, $'k_2$, was obtained from the intercept of the plot.

$$\frac{dq_t}{dt} = {}'k_2(q_e - q_t)^2 \qquad \textit{Equation E.1}$$

$$\frac{t}{q_t} = \frac{1}{{}'k_2 q_e^2} + \frac{1}{q_e}t \qquad \textit{Equation E.2}$$

$$\equiv \mathrm{TiO_2} + \mathrm{Pu(V)} \overset{'\mathrm{k2}}{\longleftrightarrow} \equiv \mathrm{TiO_2(Pu(V)_s + Pu(IV)_s)} \qquad \textit{Equation E.3}$$

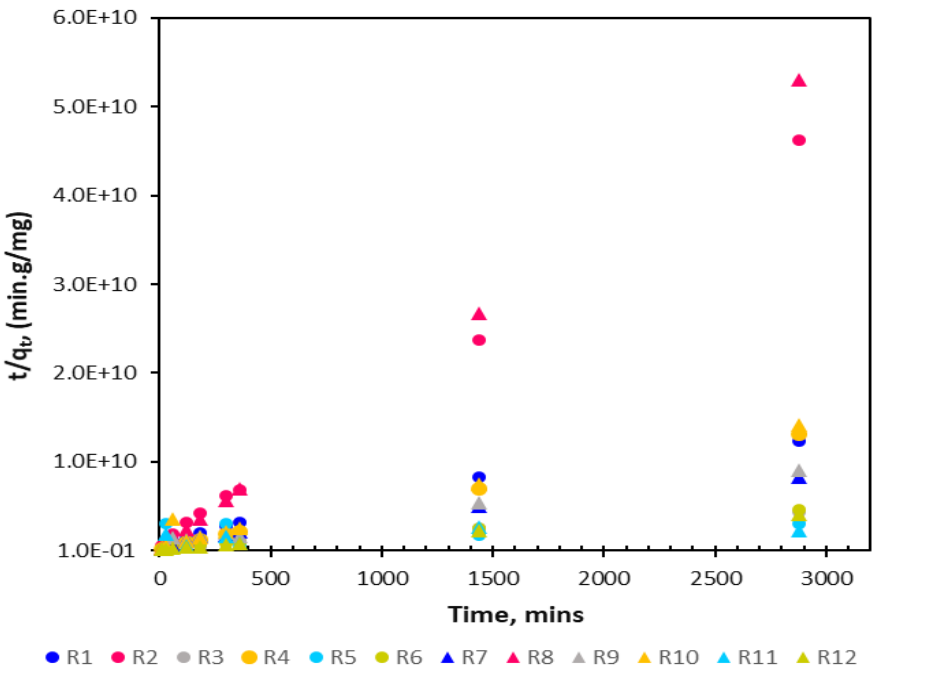

Figure E.2 Ho's kinetic model

Table E.1. *Rate constants for second-order models*

Reactors	pH	Sorbate/sorbent ratio Bq/mg	Pseudo second-order			Ho's second-order	
			$Bq^{-1}min^{-1}$	$(Bq/mL)^{-1}$ min^{-1}	R^2	$(Bq/g)^{-1}$ min^{-1}	R^2
1R(6-0.30)	6	0.33	4.31E-05	1.94E-03	0.99	2.84E-05	0.97
2R(6-0.04)		0.05	7.16E-04	3.22E-02	0.98	3.77E-04	1.00
3R(6-1.00)		1.33	8.06E-06	3.63E-04	0.93	1.26E-05	0.98
4R(6-0.15)		0.20	2.21E-04	9.95E-03	1.00	8.05E-05	1.00
5R(6-3.20)		5.00	1.10E-06	4.95E-05	0.80	-2.83E-06	0.05
6R(6-0.50)		0.75	1.85E-05	8.33E-04	0.96	1.05E-05	0.99
7R(8.5-0.30)	8.5	0.33	3.72E-04	1.67E-02	0.98	1.82E-05	0.98
8R(8.5-0.04)		0.05	4.94E-04	2.22E-02	0.64	2.22E-03	1.00
9R(8.5-1.00)		1.33	3.22E-06	1.45E-04	0.79	1.78E-05	0.98
10R(8.5-0.15)		0.20	1.96E-04	8.82E-03	1.00	3.30E-05	0.96
11R(8.5-3.20)		5.00	1.36E-06	6.12E-05	0.92	5.22E-06	0.31
12R(8.5-0.50)		0.75	5.28E-05	2.38E-03	1.00	1.29E-05	1.00

The reactors 5R(6-3.20) and 11R(8.5-3.20) both had the highest sorbate/sorbent ratio with 1.9 Bq/mL of Pu concentration and 27 mg of HESR-II(57). The low correlation factor for 5R and 11R using Ho's second order shows that the model is not suitable for higher sorbate to sorbent ratio measurements. The assumption of initial diffusion of Pu across the external membrane, further diffusion into the pores and finally sorption to the actives sites does not hold true for 5R and 11R.

Table E.2. *Langmuir and Freundlich isotherm calculation*

Reactor	$V.C_o$	$V.C_o$	$V.C_e$	$V.C_e$	V	m	C_o	C_e	q_e	C_e/q_e
	Bq	**mg**	**Bq**	**mg**	**L**	**g**	**mg/L**	**mg/L**	**mg/g**	**g/L**
1R(6-0.30)	7.52	1.20E-08	3.55	5.64E-09	0.045	0.027	2.66E-07	1.25E-07	2.34E-07	0.54
2R(6-0.04)	7.52	1.20E-08	0.46	7.25E-10	0.045	0.18	2.66E-07	1.61E-08	6.24E-08	0.26
3R(6-1.00)	26.32	4.18E-08	14.92	2.37E-08	0.045	0.027	9.30E-07	5.27E-07	6.72E-07	0.78
4R(6-0.15)	26.32	4.18E-08	1.43	2.27E-09	0.045	0.18	9.30E-07	5.04E-08	2.20E-07	0.23
5R(6-3.20)	85.82	1.36E-07	70.03	1.11E-07	0.045	0.027	3.03E-06	2.47E-06	9.30E-07	2.66
6R(6-0.50)	85.82	1.36E-07	15.81	2.51E-08	0.045	0.18	3.03E-06	5.58E-07	6.18E-07	0.90
7R(8.5-0.30)	6.64	1.06E-08	0.77	1.23E-09	0.045	0.027	2.35E-07	2.72E-08	3.46E-07	0.08
8R(8.5-0.04)	6.64	1.06E-08	0.50	7.88E-10	0.045	0.18	2.35E-07	1.75E-08	5.43E-08	0.32
9R(8.5-1.00)	24.76	3.94E-08	19.38	3.08E-08	0.045	0.027	8.75E-07	6.85E-07	3.17E-07	2.16
10R(8.5-0.15)	24.76	3.94E-08	1.64	2.61E-09	0.045	0.18	8.75E-07	5.80E-08	2.04E-07	0.28
11R(8.5-3.20)	85.88	1.37E-07	64.00	1.02E-07	0.045	0.027	3.03E-06	2.26E-06	1.29E-06	1.76
12R(8.5-0.50)	85.88	1.37E-07	5.99	9.53E-09	0.045	0.18	3.03E-06	2.12E-07	7.06E-07	0.30

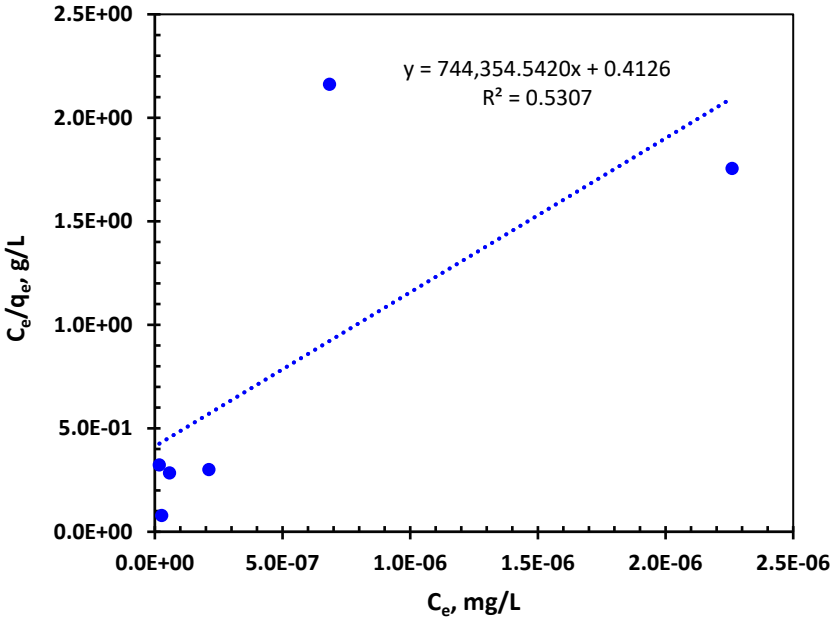

Figure E.3 Linear form of Langmuir isotherm at pH 8.5 for HESR-II(57)at contact duration of 2880 mins

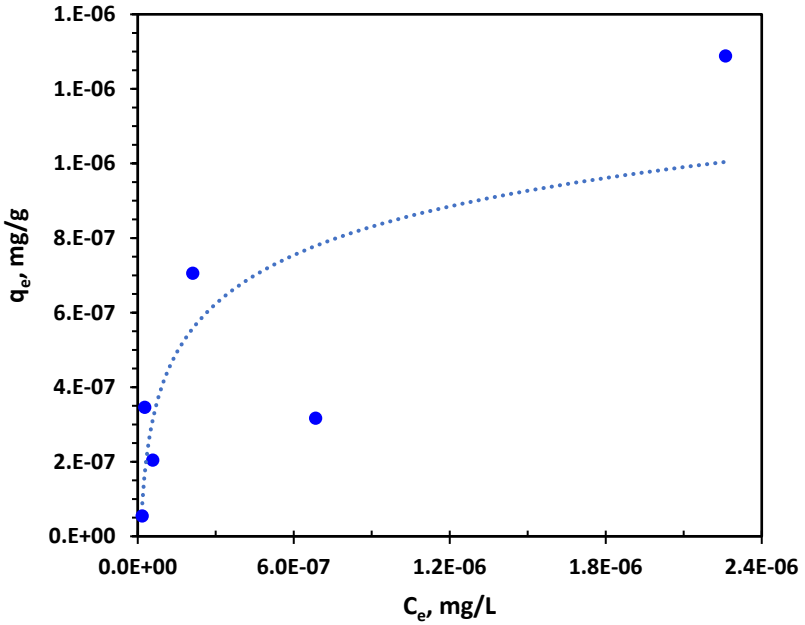

Figure E.4 Langmuir isotherm for the same data as Figure E.3.

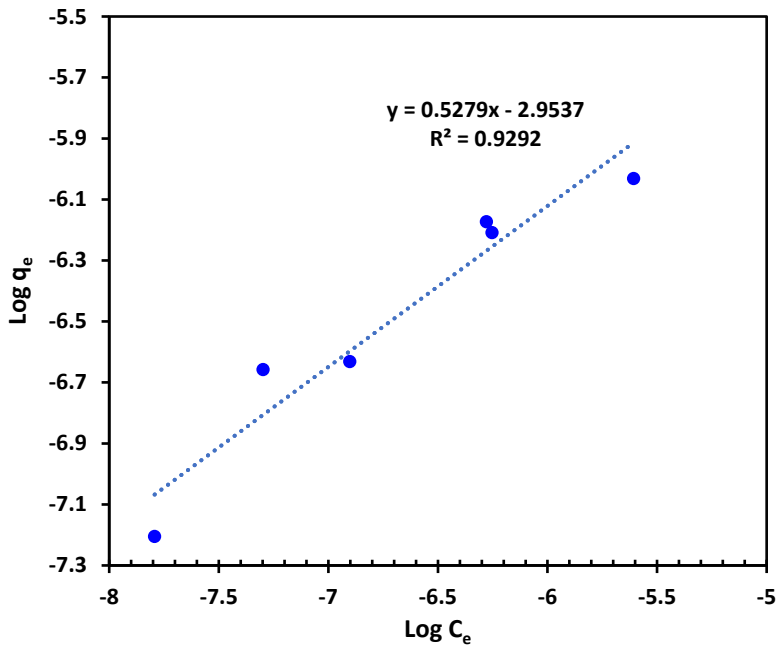

Figure E.5 Freundlich isotherm for data in Table E.2 at pH 6

n= 1.69, K_f= 1.12×10^{-3} mg/g

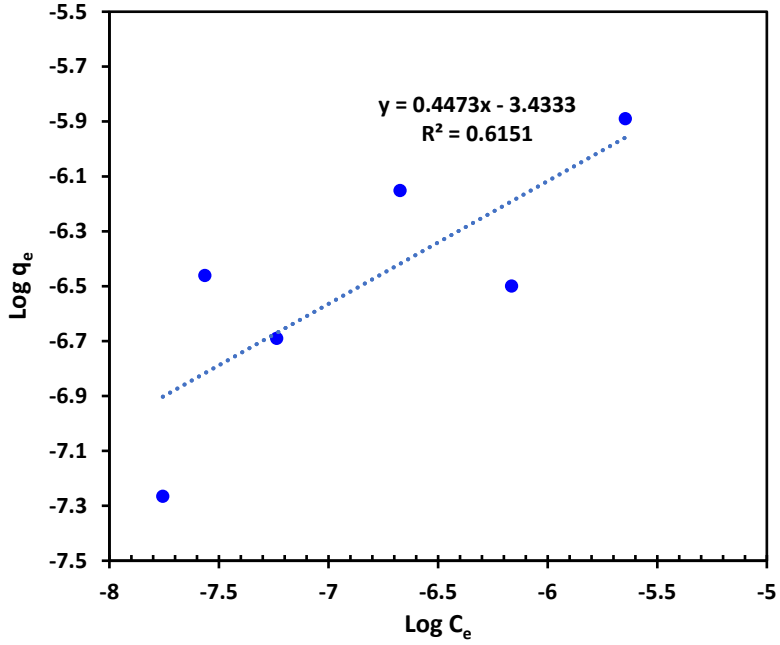

Figure E.6 Freundlich isotherm for data in Table E.2 at pH 8.5

n= 2.24, K_f= 3.72×10^{-4} mg/g

Freundlich isotherm constants were calculated using the **Equation 4.13**. The correlation coefficient for Langmuir isotherm was higher compared to Freundlich isotherm implying a better fit of kinetic data to Langmuir model.

APPENDIX F

Permissions to Reprint Figures

Permission was received to reprint selected figures in Chapters 1 and 2 through the Copy Right Clearance Center (www.copyright.com) and creative commons. All documentation of the approvals is listed on the following pages.

Creative Commons License Deed

Attribution-NonCommercial 3.0 Unported (CC BY-NC 3.0)

This is a human-readable summary of (and not a substitute for) the license.

You are free to:

Share — copy and redistribute the material in any medium or format

Adapt — remix, transform, and build upon the material

The licensor cannot revoke these freedoms as long as you follow the license terms.

Under the following terms:

Attribution — You must give appropriate credit, provide a link to the license, and indicate if changes were made. You may do so in any reasonable manner, but not in any way that suggests the licensor endorses you or your use.

NonCommercial — You may not use the material for commercial purposes.

No additional restrictions — You may not apply legal terms or technological measures that legally restrict others from doing anything the license permits.

Notices:

You do not have to comply with the license for elements of the material in the public domain or where your use is permitted by an applicable exception or limitation.

No warranties are given. The license may not give you all of the permissions necessary for your intended use. For example, other rights such as publicity, privacy, or moral rights may limit how you use the material.

www.creativecommons.org/licenses/by-nc/3.0

Title: Radionuclide Sensors for Environmental Monitoring: From Flow Injection Solid-Phase Absorptiometry to Equilibration-Based Preconcentrating Minicolumn Sensors with Radiometric Detection

Author: Jay W. Grate, Oleg B. Egorov, Matthew J. O'Hara, et al

Publication: Chemical Reviews

Publisher: American Chemical Society

Date: Feb 1, 2008

Logged in as:
Amruta Pujari
Clemson University
Account #:
3001234264
LOGOUT

PERMISSION/LICENSE IS GRANTED FOR YOUR ORDER AT NO CHARGE

This type of permission/license, instead of the standard Terms & Conditions, is sent to you because no fee is being charged for your order. Please note the following:

- Permission is granted for your request in both print and electronic formats, and translations.
- If figures and/or tables were requested, they may be adapted or used in part.
- Please print this page for your records and send a copy of it to your publisher/graduate school.
- Appropriate credit for the requested material should be given as follows: "Reprinted (adapted) with permission from (COMPLETE REFERENCE CITATION). Copyright (YEAR) American Chemical Society." Insert appropriate information in place of the capitalized words.
- One-time permission is granted only for the use specified in your request. No additional uses are granted (such as derivative works or other editions). For any other uses, please submit a new request.

If credit is given to another source for the material you requested, permission must be obtained from that source.

BACK CLOSE WINDOW

RightsLink®

Home | Account Info | Help

Title:	Pu(V) and Pu(IV) Sorption to Montmorillonite
Author:	James D. Begg, Mavrik Zavarin, Pihong Zhao, et al
Publication:	Environmental Science & Technology
Publisher:	American Chemical Society
Date:	May 1, 2013

Logged in as:
Amruta Pujari
Clemson Univesity
Account #:
3001234264

LOGOUT

PERMISSION/LICENSE IS GRANTED FOR YOUR ORDER AT NO CHARGE

This type of permission/license, instead of the standard Terms & Conditions, is sent to you because no fee is being charged for your order. Please note the following:

- Permission is granted for your request in both print and electronic formats, and translations.
- If figures and/or tables were requested, they may be adapted or used in part.
- Please print this page for your records and send a copy of it to your publisher/graduate school.
- Appropriate credit for the requested material should be given as follows: "Reprinted (adapted) with permission from (COMPLETE REFERENCE CITATION). Copyright (YEAR) American Chemical Society." Insert appropriate information in place of the capitalized words.
- One-time permission is granted only for the use specified in your request. No additional uses are granted (such as derivative works or other editions). For any other uses, please submit a new request.

If credit is given to another source for the material you requested, permission must be obtained from that source.

BACK | CLOSE WINDOW

SPRINGER NATURE

Thank you for your order!

Dear Ms. Amruta Pujari,

Thank you for placing your order through Copyright Clearance Center's RightsLink® service.

Order Summary

Licensee:	Clemson Univesity
Order Date:	Jan 4, 2018
Order Number:	4261960840149
Publication:	Springer eBook
Title:	Plutonium
Type of Use:	Thesis/Dissertation
Order Total:	0.00 USD

View or print complete details of your order and the publisher's terms and conditions.

Sincerely,

Copyright Clearance Center

How was your experience? Fill out this survey to let us know.

Tel: +1-855-239-3415 / +1-978-646-2777
customercare@copyright.com
https://myaccount.copyright.com

Copyright Clearance Center RightsLink®

SPRINGER NATURE

Thank you for your order!

Dear Ms. Amruta Pujari,

Thank you for placing your order through Copyright Clearance Center's RightsLink® service.

Order Summary

Licensee:	Clemson Univesity
Order Date:	Jan 4, 2018
Order Number:	4261970061784
Publication:	Metallurgical and Materials Transactions A
Title:	Phase stability and phase transformations in plutonium and plutonium-gallium alloys
Type of Use:	Thesis/Dissertation
Order Total:	0.00 USD

View or print complete details of your order and the publisher's terms and conditions.

Sincerely,

Copyright Clearance Center

How was your experience? Fill out this survey to let us know.

Tel: +1-855-239-3415 / +1-978-646-2777
customercare@copyright.com
https://myaccount.copyright.com

Copyright Clearance Center RightsLink®

SPRINGER NATURE

Thank you for your order!

Dear Ms. Amruta Pujari,

Thank you for placing your order through Copyright Clearance Center's RightsLink® service.

Order Summary

Licensee:	Clemson Univesity
Order Date:	Jan 4, 2018
Order Number:	4262010184834
Publication:	Nature Materials
Title:	Long-term storage of spent nuclear fuel
Type of Use:	Thesis/Dissertation
Order Total:	0.00 USD

View or print complete details of your order and the publisher's terms and conditions.

Sincerely,

Copyright Clearance Center

How was your experience? Fill out this survey to let us know.

Tel: +1-855-239-3415 / +1-978-646-2777
customercare@copyright.com
https://myaccount.copyright.com

Copyright Clearance Center RightsLink®

SPRINGER NATURE

Thank you for your order!

Dear Ms. Amruta Pujari,

Thank you for placing your order through Copyright Clearance Center's RightsLink® service.

Order Summary

Licensee:	Clemson Univesity
Order Date:	Jan 4, 2018
Order Number:	4262030727497
Publication:	Journal of Radioanalytical and Nuclear Chemistry
Title:	Removal of plutonium from carbonate medium using titania microspheres prepared by sol-gel route
Type of Use:	Thesis/Dissertation
Order Total:	0.00 USD

View or print complete details of your order and the publisher's terms and conditions.

Sincerely,

Copyright Clearance Center

How was your experience? Fill out this survey to let us know.

Tel: +1-855-239-3415 / +1-978-646-2777
customercare@copyright.com
https://myaccount.copyright.com

Copyright Clearance Center RightsLink®

Thank you for your order!

Dear Ms. Amruta Pujari,

Thank you for placing your order through Copyright Clearance Center's RightsLink® service.

Order Summary

Licensee:	Clemson Univesity
Order Date:	Jan 4, 2018
Order Number:	4262020954323
Publication:	Separation and Purification Technology
Title:	Studies on BenzoDODA encapsulated polymeric beads for separation of plutonium from acidic solution
Type of Use:	reuse in a thesis/dissertation
Order Total:	0.00 USD

View or print complete details of your order and the publisher's terms and conditions.

Sincerely,

Copyright Clearance Center

How was your experience? Fill out this survey to let us know.

Tel: +1-855-239-3415 / +1-978-646-2777
customercare@copyright.com
https://myaccount.copyright.com

Thank you for your order!

Dear Ms. Amruta Pujari,

Thank you for placing your order through Copyright Clearance Center's RightsLink® service.

Order Summary

Licensee:	Clemson Univesity
Order Date:	Jan 4, 2018
Order Number:	4262030084162
Publication:	Surface Science Reports
Title:	The surface science of titanium dioxide
Type of Use:	reuse in a thesis/dissertation
Order Total:	0.00 USD

View or print complete details of your order and the publisher's terms and conditions.

Sincerely,

Copyright Clearance Center

How was your experience? Fill out this survey to let us know.

Tel: +1-855-239-3415 / +1-978-646-2777
customercare@copyright.com
https://myaccount.copyright.com

Thank you for your order!

Dear Ms. Amruta Pujari,

Thank you for placing your order through Copyright Clearance Center's RightsLink® service.

Order Summary

Licensee:	Clemson Univesity
Order Date:	Jan 4, 2018
Order Number:	4262031148746
Publication:	Applied Clay Science
Title:	Properties and applications of halloysite nanotubes: recent research advances and future prospects
Type of Use:	reuse in a thesis/dissertation
Order Total:	0.00 USD

View or print complete details of your order and the publisher's terms and conditions.

Sincerely,

Copyright Clearance Center

How was your experience? Fill out this survey to let us know.

Tel: +1-855-239-3415 / +1-978-646-2777
customercare@copyright.com
https://myaccount.copyright.com

REFERENCES

Balakrishnan, T., & Ford, W. T. **(1982)**. Particle size control in suspension copolymerization of styrene, chloromethylstyrene, and divinylbenzene. *Journal of Applied Polymer Science*, *27*(1), 133–138.

Begg, J. D., Zavarin, M., Tumey, S. J., & Kersting, A. B. **(2014)**. Plutonium Adsorption and Desorption from Bentonite, *Progress Report*, Distributed by the Office of Scientific and Technical Information, U.S. Dept. of Energy, FT-14LL0807071.

Begg, J. D., Zavarin, M., Zhao, P., Tumey, S. J., Powell, B., & Kersting, A. B. **(2013)**. Pu(V) and Pu(IV) sorption to montmorillonite. *Environmental Science and Technology*, *47*(10), 5146–5153.

Bhagyashree, K., Mishra, R. K., Shukla, R., Kasar, S., Kar, A., Kumar, S., Tomar, B. S. **(2013)**. Sorption of plutonium from low level liquid waste using nano MnO2. *Journal of Radioanalytical and Nuclear Chemistry*, *295*(2), 1561–1566.

Bliznyuk, V. N., Duval, C. E., Apul, O. G., Seliman, A. F., Husson, S. M., & DeVol, T. A. **(2015)**. High porosity scintillating polymer resins for ionizing radiation sensor applications. *Polymer*, *56*(Supplement C), 271–279.

Cember, H., Johnson, T. E., & Alaei, P. **(2008)**. Introduction to Health Physics: Fourth Edition. Medical Physics, *35(12)*, *McGraw Hill Companies, Inc. ISBN: 9780071423083*.

Conroy, N. A., Wylie, E. M., & Powell, B. A. **(2016)**. A Novel Method for Tracer Concentration Plutonium(V) Solution Preparation. *Analytical Chemistry*, *88*(8), 4196–4199.

Cowan, G. A. **(1976)**. A natural fission reactor. *Scientific American*, *235*(1), 36–47.

Crane, R. A., Dickinson, M., & Scott, T. B. **(2015)**. Nanoscale zero-valent iron particles for the remediation of plutonium and uranium contaminated solutions. *Chemical Engineering Journal*, *262*, 319–325.

Crowley, K. D., & Ahearne, J. F. **(2002)**. Managing the Environmental Legacy of U. S. Nuclear-Weapons Production. *American Scientist*, *90*(6), 514–523.

Diebold, U. **(2003)**. The surface science of titanium dioxide. *Surface Science Reports*, *48*(5), 53–229.

Duval, C. E., DeVol, T. A., & Husson, S. M. **(2016)**. Extractive scintillating polymer sensors for trace-level detection of uranium in contaminated ground water. *Analytica Chimica Acta*, *947*, 1–8.

EPA, **(2000)**. Radionuclides Rule 66, National Primary Drinking Water Regulations for Radionuclides, *Federal Register*, *Vol. 65*(No. 236.).

Ewing, R. C. **(2015)**. Long-term storage of spent nuclear fuel. *Nature Materials*, *14*(3), 252–257.

Gauthier-Lafaye, F., Holliger, P., & Blanc, P.L. **(1996)**. Natural fission reactors in the Franceville basin, Gabon: A review of the conditions and results of a critical event in a geologic system. *Geochimica et Cosmochimica Acta*, *60*(23), 4831–4852.

Gokmen, M. T., & Du Prez, F. E. **(2012)**. Porous polymer particles: A comprehensive guide to synthesis, characterization, functionalization and applications. *Progress in Polymer Science (Oxford)*, *37*(3), 365–405.

Goldman, M., Nelson, R. C., Bollinger, L., Hoover, M. D., Templeton, W., & Anspaugh, L. (1991). Potential health risks from postulated accidents involving the Pu-238 RTG on the Ulysses solar exploration mission. *AIP Conference Proceedings*, *217*, 152–164.

Grate, J. W., Egorov, O. B., O'Hara, M. J., & DeVol, T. A. **(2008)**. Radionuclide sensors for environmental monitoring: from flow injection solid-phase absorptiometry to equilibration-based preconcentrating minicolumn sensors with radiometric detection. *Chemical Reviews*, *108*(2), 543–562.

Hanson W, E. **(1980)**. Quantities of transuranic elements in the environment from operations relating to nuclear weapons. *Transuranic Elements in the Environments*, (DOE/TIC-22800), 86–91.

Ho, Y. S. **(2006)**. Review of second-order models for adsorption systems. *Journal of Hazardous Materials*, *136*(3), 681–689.

Hughes, L. D., & DeVol, T. A. **(2006)**. Evaluation of flow cell detector configurations combining simultaneous preconcentration and scintillation detection for monitoring of pertechnetate in aqueous media. *Analytical Chemistry*, *78*(7), 2254–2261.

Kaplan, D. I., Powell, B. A., Demirkanli, D. I., Fjeld, R. A., Molz, F. J., Serkiz, S. M., & Coates, J. T. **(2004)**. Influence of oxidation states on plutonium mobility during long-term transport through an unsaturated subsurface environment. *Environmental Science and Technology*, *38*(19), 5053–5058.

Katz, J. J. **(2006)**. The Chemistry of the Actinide and Transactinide Elements (Volumes 1-5), *1*, *Springer Science & Business Media*, ISBN:978-1-4020-3598-2

Keeney-Kennicutt, W. L., & Morse, J. W. **(1985)**. The redox chemistry of $Pu(V)O^{2+}$ interaction with common mineral surfaces in dilute solutions and seawater. *Geochimica et Cosmochimica Acta*, *49*(12), 2577–2588.

Keith, D. W. **(2010)**. Toxicological Profile for Plutonium. Agency for Toxic Substances and Disease Registry, *Toxicological Profiles*, CAS#: 7440-07-5.

Kessler, M. J. **(1989)**. *Liquid Scintillation Analysis: Science and Technology*. Packard Instrument, PerkinElmer, Inc., lsabooklet-012129-01.

Kilislioglu, A., & Bilgin, B. **(2002)**. Adsorption of uranium on halloysite. *Radiochimica Acta*, *90*(3), 155–160.

Knoll G. F. **(2010)** *Radiation detection and measurement.* John Wiley & Sons. ISBN: 978-0-470-13148-0.

Kosmulski, M. **(2002)**. The significance of the difference in the point of zero charge between rutile and anatase. *Advances in Colloid and Interface Science*, *99*(3), 255–64.

Kosmulski, M. **(2011)**. The pH-dependent surface charging and points of zero charge. V. Update. *Journal of Colloid and Interface Science*, *353*(1), 1–15.

Krey, P. W. **(1967)**. Atmospheric Burnup of a Plutonium-238 Generator. *Science*, *158*(3802), 769–771.

Li, D., & Kaplan, D. I. **(2012)**. Sorption coefficients and molecular mechanisms of Pu, U, Np, Am and Tc to Fe (hydr) oxides: A review. *Journal of Hazardous Materials*, *243*, 1–18.

Liu, B., Shi, K., Ye, G., Guo, Z., & Wu, W. **(2015)**. Rapid determination of plutonium in environmental water samples using vacuum box TEVA resin microextraction chromatography system and detection by low background liquid scintillation counter. *Microchemical Journal*, *124*, 824–830.

Lok, K. P., & Ober, C. K. **(1985)**. Particle size control in dispersion polymerization of polystyrene. *Canadian Journal of Chemistry*, *63*(1), 209–216.

Mahara, Y., & Kudo, A. **(1995)**. Plutonium released by the Nagasaki A-bomb: Mobility in the environment. *Applied Radiation and Isotopes*, *46*(11), 1191–1201.

Mark, J. E. **(1999)**. *Polymer data handbook*. Oxford University Press. ISBN: 978-0-1951-8101-2.

Marsac, R., Banik, N. L., Lützenkirchen, J., Buda, R. A., Kratz, J. V, & Marquardt, C. M. **(2015)**. Modeling plutonium sorption to kaolinite: Accounting for redox equilibria and the stability of surface species. *Chemical Geology*, *400*, 1–10.

Mian, Z., & Glaser, A. **(2015)**. Global Fissile Material Report, 2015. The International Panel on Fissile Materials (IPFM), Nuclear weapons and fissile material stockpiles and production, Eighth annual report of the International Panel on Fissile Materials, *NPT Review Conference*, Vol. *8*. Creative Commons Attribution-Noncommercial License.

Mitchell, J. N., Schwartz, D. S., Stan, M., & Boehlert, C. J. **(2004)**. Phase stability and phase transformations in plutonium and plutonium-gallium alloys. *Metallurgical and Materials Transactions A*, *35*(8), 2267–2278.

Olsson, M., Jakobsson, A. M., & Albinsson, Y. **(2003)**. Sorption of Pu(VI) onto TiO_2. *Journal of Colloid and Interface Science*, *266*(2), 269–275.

Orlandini, K. A., Penrose, W. R., & Nelson, D. M. **(1986)**. Pu(V) as the stable form of oxidized plutonium in natural waters. *Marine Chemistry*, *18*(1), 49–57.

Pius, I. C., Bhanushali, R. D., Bamankar, Y. R., Mukerjee, S. K., & Vaidya, V. N. **(2004)**. Removal of plutonium from carbonate medium using titania microspheres prepared by sol-gel route. *Journal of Radioanalytical and Nuclear Chemistry*, *261*(3), 547–550.

Powell, B. A., Fjeld, R. A., Kaplan, D. I., Coates, J. T., & Serkiz, S. M. **(2004)**. Pu (V) O^{2+} adsorption and reduction by synthetic magnetite (Fe_3O_4). *Environmental Science & Technology*, *38*(22), 6016–6024.

Powell, B. A., Fjeld, R. A., Kaplan, D. I., Coates, J. T., & Serkiz, S. M. **(2005)**. Pu (V) O^{2+} adsorption and reduction by synthetic hematite and goethite. *Environmental Science & Technology*, *39*(7), 2107–2114.

Powell, B. A., Kersting, A., Zavarin, M., & Zhao, P. **(2008)**. Development of a Composite Non-Electrostatic Surface Complexation Model Describing Plutonium Sorption to Aluminosilicates, U.S. Department of Energy by Lawrence Livermore National Laboratory, LLNL-TR-408276.

Qiu, H., Lv, L., Pan, B., Zhang, Q., Zhang, W., & Zhang, Q. **(2009)**. Critical review in adsorption kinetic models. *Journal of Zhejiang University-Science A*, *10*(5), 716–724.

Rinehart, G. H. (2001). Design characteristics and fabrication of radioisotope heat sources

for space missions. *Progress in Nuclear Energy*, *39*(3–4), 305–319.

Romanchuk, A. Y., Kalmykov, S. N., Egorov, A. V, Zubavichus, Y. V, Shiryaev, A. A., Smirnov, E. A., & Garshev, A. V. **(2016)**. Photoreduction of Pu (V, VI) by TiO_2. *Radiochimica Acta*, *104*(12), 843–851.

Ruhela, R., Panja, S., Singh, A. K., Dhami, P. S., & Gandhi, P. M. **(2016)**. BenzoDODA grafted polymeric resin- Plutonium selective solid sorbent. *Journal of Hazardous Materials*, *318*, 186–193.

Sanchez, A. L., Murray, J. W., & Sibley, T. H. **(1985)**. The adsorption of plutonium IV and V on goethite. *Geochimica et Cosmochimica Acta*, *49*(11), 2297–2307.

Seliman, A. F., Bliznyuk, V. N., Husson, S. M., & DeVol, T. A. **(2015)**. Development of polymerizable 2-(1-naphthyl)-5-phenyloxazole scintillators for ionizing radiation detection. *Journal of Materials Chemistry C*, *3*(27), 7053–7061.

Shang, J., Chai, M., & Zhu, Y. **(2003)**. Photocatalytic degradation of polystyrene plastic under fluorescent light. *Environmental Science and Technology*, *37*(19), 4494–4499.

Silva, R. J., & Nitsche, H. **(1995)**. Actinide environmental chemistry. *Radiochimica Acta*, *70*(s1), 377–396.

Singh, K. K., Panja, S., Ruhela, R., Kumar, M., Tripathi, S. C., Singh, A. K., Bajaj, P. N. **(2015)**. Studies on BenzoDODA encapsulated polymeric beads for separation of plutonium from acidic solution. *Separation and Purification Technology*, *154*, 186–192.

Suslick, K. S., & Price, G. J. **(1999)**. Applications of Ultrasound to Materials Chemistry. *Annual Review of Materials Science*, *29*(1), 295–326.

Wu, F. C., Tseng, R. L., Huang, S. C., & Juang, R. S. **(2009)**. Characteristics of pseudo-second-order kinetic model for liquid-phase adsorption: A mini-review. *Chemical Engineering Journal*. *151*, 1-9.

Yuan, P., Tan, D., & Annabi-Bergaya, F. **(2015)**. Properties and applications of halloysite nanotubes: recent research advances and future prospects. *Applied Clay Science*, *112*, 75–93.

Zavarin, M., Powell, B. A., Bourbin, M., Zhao, P., & Kersting, A. B. **(2012)**. Np(V) and Pu(V) ion exchange and surface-mediated reduction mechanisms on montmorillonite. *Environmental Science and Technology*, *46*(5), 2692–2698.

Zavarin, M., Roberts, S. K., Hakem, N., Sawvel, A. M., & Kersting, A. B. **(2005)**. Eu(III),

Sim(III), Np(V), Pu(V), and Pu(IV) sorption to calcite. *Radiochimica Acta*, *93*(2), 93–102.